Cobalt supported on carbon nanofibers as catalysts for the Fischer-Tropsch synthesis

Leendert Bezemer

ISBN 90-393-4133-8

Drukkerij Ponsen & Looijen

Cobalt supported on carbon nanofibers as catalysts for the Fischer-Tropsch synthesis

Kobaltkatalysatoren voor de Fischer-Tropsch synthese met koolstofvezels als dragermateriaal

(met een samenvatting in het Nederlands)

Proefschrift

ter verkrijging van de graad van doctor aan de Universiteit Utrecht
op gezag van de Rector Magnificus, Prof. Dr. W.H. Gispen, ingevolge het
besluit van het College voor Promoties in het openbaar te verdedigen op
maandag 23 januari 2006 des middags te 4.15 uur

door

Gerrit Leendert Bezemer

geboren op 4 mei 1979 te Bleskensgraaf en Hofwegen

Promoter: Prof. dr. ir. K.P. de Jong
Faculteit Scheikunde, Universiteit Utrecht

Co-promoter: Dr. A.J. van Dillen
Faculteit Scheikunde, Universiteit Utrecht

The research described in this thesis was financially supported by Shell Global Solutions.

Sol Iustitiae Illustra Nos

†

Zon der Gerechtigheid ga op over ons

CONTENTS

I

GENERAL INTRODUCTION

Catalysis

A catalyst can be described as a substance that increases the rate of a reaction without being consumed itself and that often permits reactions to take place more effectively or under milder conditions. Catalysis, although probably not recognized as such, has been used for thousands of years in the production of wine [1]. Compared to that, industrial production of chemicals using catalysts started rather late, just a few hundred years ago [2]. The concept of 'catalysis' was discovered in 1835 and the operation of a catalytic force in chemical reactions was mentioned for the first time [3]. Since that time both the scientific insight in the functioning of catalysts and their industrial use has grown tremendously. Nowadays catalysts have a large impact on society, as they are used for the efficient and clean production of many valuable consumer products.

The catalysts studied most often are heterogeneous catalysts in which catalyst and reactants/products are in a different phase. These catalysts generally consist of very small particles of an active phase, *e.g.* a metal oxide, deposited on oxidic support materials. The main role of the support is the anchoring of the catalytically active particles and thus the prevention of sintering during activation and operation. Generally, small amounts of promoting elements are added to enhance activity, selectivity or stability. In the Fischer-Tropsch synthesis supported cobalt, iron or ruthenium catalysts are used, promoted with a range of other elements.

History of the Fischer-Tropsch synthesis

The Fischer-Tropsch (FT) process is named after Franz Fischer and Hans Tropsch (figure 1) who discovered in 1923 that synthesis gas (CO/H_2) can be converted over a catalyst into hydrocarbons and water [4-6]. Using the FT process liquid transportation

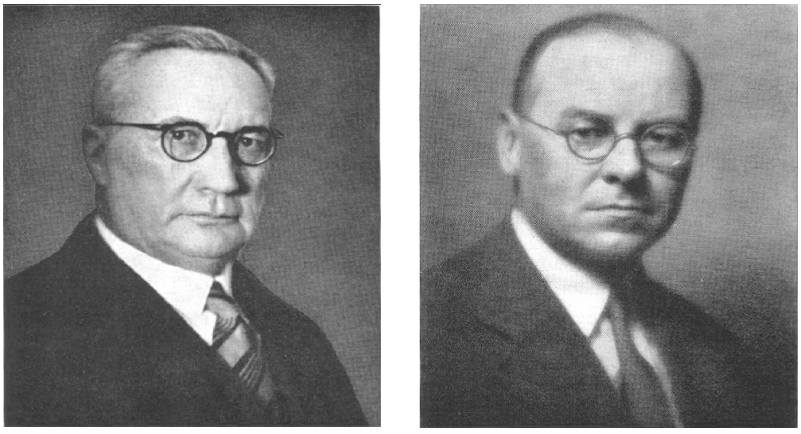

Figure 1. Franz Fischer (left) and Hans Tropsch (right).

fuels of superior quality can be produced from other carbon sources than crude oil. This was of strategic importance for Germany before World War II as the country had virtually no oil supply, but availed of abundant coal reserves and wanted to be energy independent. Together with the coal hydrogenation process of Bergius, the FT synthesis could be used to ensure a supply of liquid fuels [7-9]. Already in 1935 Ruhrchemie started the commercial application of the FT process and constructed the first out of nine plants. The maximum production of the fuels peaked in 1944 at 4.1 million barrels per year [7]. The FT plants were operated at atmospheric or at medium pressure (5-15 bar) and a cobalt catalyst was used. In the standard catalyst the mineral Kieselguhr (mainly SiO_2) was used as support material which was loaded with 31 wt% cobalt [8]. The addition of thoria (1.6 wt%) and magnesia (2.6 wt%) was found to be crucial to shift the product distribution towards the desired heavier hydrocarbons and to protect the catalyst against impurities [8]. After World War II the production of synthetic fuels was no longer economically viable and all plants were dismantled [9].

Although the German plants ceased to operate in 1945, interest in the FT process continued as reserves of crude oil were thought at that time to be rather limited [10,11]. However, after the discovery of the huge oil fields in the Middle East around 1955, the oil price sharply decreased and most research activities were abandoned. Only in South Africa scientific and industrial interest remained. In that country with large reserves of very cheap coal, the government wanted to become energy independent − as was the case in pre-war Germany − and stimulated the development of an own FT industry. The Sasol Company constructed several large FT plants from 1955 onwards and is currently the largest player in the synthetic fuel industry. In the seventies of the last century the oil embargo by major oil producing countries and the forecasts about fading oil reserves renewed global interest in the FT process. Oil companies like Shell, ExxonMobil, Gulf/Chevron and Statoil started research programs and all have now their own position defended with a patents portfolio [12].

Prospects of the Fischer-Tropsch synthesis

The current interest in the FT synthesis is driven by several factors: environmental demands, changes in fossil energy reserves, geopolitical reasons and the high oil prices. The environmental constraints are present at the site of oil recovery where the flaring of associated natural gas has to be reduced as much as possible [11]. Using the FT synthesis this natural gas can be converted into liquid fuels that don't contain any sulfur or nitrogen (Gas-to-Liquids, GtL). These ultra clean FT fuels can be blended in traditional fuels to

help it meet strict fuel specifications. Changes in the estimation of fossil energy reserves are the second driver for interest in the FT synthesis. The currently known reserves of natural gas outnumber that of crude oil, but are often located too far from the markets. The conversion of gas to liquids enables their transport and adds economical value. Also geopolitical aspects are important for the current interest in the FT reaction. Using the FT process transportation fuels can be obtained from other carbon sources than crude oil, like coal (CtL) and also biomass (BtL) thus lowering the dependency on the oil exporting countries. The last driver for current interest in the FT synthesis is the oil price at values above 20$/barrel, which makes the production of synthetic fuels economically viable.

Nowadays, Sasol and Shell commercially operate the Fischer-Tropsch process with a combined production of 0.2 million barrels per day [11]. Although this seems to be a lot, it is rather a small amount compared to the plans announced by Shell, Sasol, ExxonMobil and ConocoPhilips to build natural gas-based FT plants in Qatar with a total capacity of 0.8 million barrels per day in 2011 [13]. Apart from these huge projects in Qatar the construction of smaller plants in Australia, China, Nigeria and other countries is considered. This shows that the Fischer-Tropsch process more than 70 years after its introduction is of growing importance.

Key parameters of FT catalysts

The FT process can be performed on cobalt, iron and ruthenium catalysts. Ruthenium catalysts are reported to be the most active ones, but due to the very limited ruthenium reserves they cannot be used on a commercial scale. FT catalysts based on iron are very cheap, but not very active, and as they can be active in the water-gas shift reaction, they are mainly attractive for coal-based FT plants. Cobalt catalysts are well known for their activity and stability and they are the catalysts of choice for natural gas based FT plants. Currently, most research is dedicated to these catalysts and also this thesis will focus on cobalt catalysts, supported on carbon nanofibers.

In the FT reaction CO and H_2 are converted on the cobalt surface into water and hydrocarbons. In the generally accepted mechanism both CO and H_2 dissociate on the surface and oxygen is removed by reaction with hydrogen to water. Subsequently, carbon becomes partially hydrogenated, which is followed by a polymerization reaction resulting in hydrocarbon chains [14]. These chains can be terminated by either hydrogen addition, forming paraffins or by hydrogen abstraction forming olefins. In this way hydrocarbons with different chain lengths result. The chain growth probability (α) is a key parameter in FT synthesis and a value between 0.9 and 1 is desired in order to limit the formation of

light hydrocarbons. Next to the α value generally the weight selectivities towards methane (C_1) and towards products with a chain length of 5 and higher (C_{5+}) are mentioned. Low methane selectivity and high C_{5+} selectivity are preferred in order to minimize gas recycling. Besides the catalyst selectivity, the activity of the catalyst is an important issue. Activities are generally reported as activities normalized to the weight of cobalt in the catalyst (Cobalt Time Yield, CTY) or as specific activities normalized to the number of cobalt surface atoms in the catalyst (turn-over frequency, TOF).

Cobalt particle size effects in FT catalysis

More than 70 years of FT research has brought tremendous improvement in catalyst activity and stability [12]. A rational strategy in the quest for even more active catalysts is to improve the cobalt dispersion by decreasing the average cobalt particle size. In this way the available cobalt surface area per unit of weight is increased and a higher cobalt time yield can be expected. Most FT catalysts have a rather low cobalt dispersion with average cobalt particle sizes of about 20 nm and consequently 95% of the cobalt atoms are not located at the surface and hence are catalytically inactive [12]. If catalysts could be prepared with an average cobalt particle size of 5 nm this would result in a four times more efficient use of cobalt. As cobalt is not a cheap metal, a 75% reduction of cobalt usage for commercial FT catalysts would significantly decrease their costs. However, although the preparation of catalysts with smaller cobalt particle sizes is possible, these catalysts are often not as active as expected from the higher surface area, as it is reported that the TOF decreases for particles smaller than ~10 nm. The phenomenon of lower TOF values for smaller particles has been referred to as the cobalt particle size effect [15].

For cobalt particles larger than 10 nm the particle size effect seems to be absent. The most conclusive studies in this range have been performed by Iglesia *et al.* who showed that in the range of 9-200 nm the TOF was not systematically influenced by the cobalt particle size [16-18]. The absence of the cobalt particle size effect for catalysts with particles larger than 10 nm has been confirmed by several other authors [19-21]. However, going to catalysts with even smaller particle sizes the results reported in literature are more scattered. Some groups observed lower activities for smaller cobalt particles [15,22-30], while others reported the opposite [31-34]. This confusion is mainly caused by problems to synthesize fully reduced small cobalt particles on oxidic support materials. CoO can react with these supports both during synthesis and during the reduction treatment resulting in mixed compounds like $CoAl_2O_4$, $CoSiO_3$ or $CoTiO_3$. These mixed compounds require far too high reduction temperatures to extract the metal,

so in this way cobalt metal is lost, resulting in catalysts with lower activity. Moreover, the formation of mixed compounds has been observed also during FT operation even further lowering the activity [35,36]. Small particles have a relative large specific surface area and are therefore more susceptible for reaction with the support, resulting in a lower degree of reduction of cobalt in the reduced catalysts. This explanation for the lower activity of small cobalt particles supported on oxidic support materials is referred to as a secondary particle size effect [33]. In contrast to this are primary particle size effects not caused by the support material but by the particle size dependent exposure of specific active cobalt sites [37].

In order to study the influence of cobalt particle size on the FT reaction without the interference of the effects caused by the support material, inert carbon supports could be beneficial. Preliminary studies report on the use of activated carbon support materials [15,31,32]. Activated carbon often contains impurities as well as micropores with limited accessibility. Therefore, we decided to fundamentally study cobalt particle size effects using the pure and well-defined carbon nanofibers (CNF) as a support material. CNF is a new graphitic support with an attractive meso- and macroporous structure and with potential in many (catalytic) applications [38,39]. In figure 2, a TEM image of a fiber is shown in which the individual graphitic planes are visible. The fibers are interwoven, see the SEM image in figure 3, resulting in strong macroscopic bodies that are easy to handle and only contain meso- and macropores between the fibers.

CNF is not only a very suitable support to study cobalt particle size effects in FT catalysis, but it also provides a way to study promotion effects without interference of the support material. Promoters that are added to enhance selectivity towards C_{5+} products are most often metal oxides. Therefore, it can be understood that the oxidic support

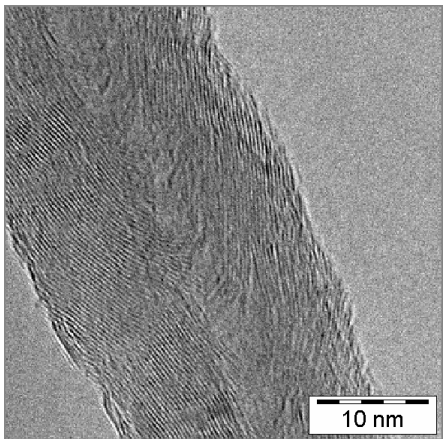

Figure 2. TEM image of CNF.

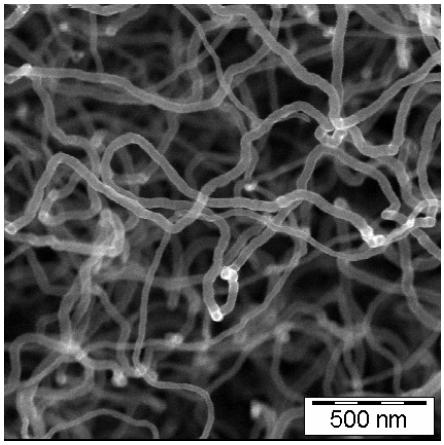

Figure 3. SEM image of CNF showing the open structure at the surface of a particle.

materials also increase selectivity towards longer chains, thus acting as a promoter itself [40,41]. In this way promotion effects induced by a support could mask the effect of the added promoter. Furthermore, the added promoter is stabilized on the oxidic support and is therefore at best not only present in contact with the cobalt metal, but also separately on the support surface, resulting in less pronounced promoting effects. On CNF the support does not promote the selectivity and, moreover, the inert support does not stabilize the added metal oxides, so it can be expected that promoter effects on CNF will be more pronounced as compared to studies using traditional oxidic supports.

Scope and outline of this thesis

Aim of the work described in this thesis is to investigate carbon nanofibers as support for the Fischer-Tropsch reaction both in the study of the influence of cobalt particle size on catalytic performance and in the study of promoter effects. Since use of well-defined systems is crucial, special care has been given to the preparation and characterization of the catalysts.

In **chapter 2** the preparation of highly loaded cobalt catalysts on CNF and on SiO_2 using homogeneous deposition precipitation (HDP) is studied. It is shown that with the traditionally applied HDP method, which uses urea hydrolysis to achieve a slow and homogeneous pH increase, catalysts with unsatisfactory cobalt dispersions are obtained. An alternative HDP method in which ammonia evaporation is used to achieve a slow and homogeneous pH decrease is developed, which results in better-dispersed catalysts. In **chapter 3** the synthesis and characterization of Co/CNF catalysts with average cobalt particle sizes varying from 2.6 to 27 nm is described. It is shown that the catalysts have quite narrow cobalt particle size distributions and are fully metallic after an *in situ* reduction treatment. Using catalytic data obtained at atmospheric pressure the pronounced influence of the cobalt particle size in the FT reaction is shown for catalysts with cobalt sizes smaller than 6 nm. At industrially relevant pressure (35 bar) the cobalt particle size turned out to be even more critical for performance than at atmospheric pressure. X-ray absorption spectroscopy results show that the observed cobalt particle size effects cannot be explained by the presence of bulk or surface oxides, or by classical structure sensitivity. It is argued that lower catalytic performances activities are caused by CO-induced, non-classical structure sensitivity of cobalt particles. In **chapter 4** our study on the preparation and catalytic performance of MnO promoted Co/CNF catalysts is presented. It is demonstrated that the promoter is only present associated with the cobalt phase and not separately on the support, both in the dried and in the reduced samples.

Moreover, it is proven that the addition of minor amounts of the promoter results in increased activities and selectivities in catalytic tests at 1 bar, while in experiments at 20 bar the TOF increased largely whereas the selectivity increased only slightly. In **chapter 5** it is shown that the inner tubes of carbon nanofibers are opened during the activation treatment (oxidation in boiling HNO_3) and are now accessible, resulting in the deposition of metal particles inside the fibers. It is shown that the weight fraction of metal deposited in the inner tube is related to the fraction of surface area or pore volume related with this tube. Finally, in **chapter 6** a summary of the results of the previous chapters is given. In this chapter also some concluding remarks and suggestions for further research are presented.

References

1. Mozes, Genesis 9:20, in: Bible, Jongbloed, Leeuwarden, 1991, p. 15.
2. A.P. Kieboom, J.A. Moulijn, P.W.N.M. van Leeuwen, R.A. van Santen, in: J. A. Moulijn, P. W. N. M. van Leeuwen, R. A. van Santen (Eds.), Catalysis: an integrated approach to homogeneous, heterogeneous and industrial catalysis, Elsevier, Amsterdam, 1993, p. 3.
3. J.J. Berzelius, Jahresberichte 15 (1835) 237.
4. F. Fischer, H. Tropsch, Brennstoff-Chemie 4 (1923) 276.
5. F. Fischer, H. Tropsch, Brennstoff-Chemie 5 (1924) 201.
6. F. Fischer, H. Tropsch, Brennstoff-Chemie 7 (1926) 97.
7. A.N. Stranges, Proc. 3rd Top. Conf. Nat. Gas Utilization (2003) 635.
8. H.H. Storch, N. Golumbic, R.B. Anderson, The Fischer-Tropsch and Related Syntheses, Wiley, New York, 1951.
9. J.E. Lesch, The German Chemical Industry in the Twentieth Century, Kluwer Academic, Dordrecht, 2000.
10. M.E. Dry, Catal. Today 71 (2002) 227.
11. H. Schulz, Appl. Catal. A 186 (1999) 3.
12. R. Oukaci, A.H. Singleton, J.G. Goodwin, Appl. Catal. A 186 (1999) 129.
13. R. Heydenrich, Howard Weil Energy Conference (april 2005).
14. H. Schulz, Catal. Today 84 (2003) 67.
15. R.C. Reuel, C.H. Bartholomew, J. Catal. 85 (1984) 78.
16. E. Iglesia, S.L. Soled, R.A. Fiato, J. Catal. 137 (1992) 212.
17. E. Iglesia, S.L. Soled, R.A. Fiato, G.H. Via, Stud. Surf. Sci. Catal. 81 (1994) 433.
18. E. Iglesia, Appl. Catal. A 161 (1997) 59.

19. A.Y. Khodakov, A. Griboval-Constant, R. Bechara, V.L. Zholobenko, J. Catal. 206 (2002) 230.
20. W.P. Ma, Y.J. Ding, L.W. Lin, Ind. Eng. Chem. Res. 43 (2004) 2391.
21. S. Storsaeter, O. Borg, E.A. Blekkan, A. Holmen, J. Catal. 231 (2005) 405.
22. A.S. Lisitsyn, A.V. Golovin, V.L. Kuznetsov, Y.I. Yermakov, C1 Mol. Chem. 1 (1984) 115.
23. L. Fu, C.H. Bartholomew, J. Catal. 92 (1985) 376.
24. A.S. Lisitsyn, A.V. Golovin, V.L. Kuznetsov, Y.I. Yermakov, J. Catal. 95 (1985) 527.
25. S.W. Ho, M. Houalla, D.M. Hercules, J. Phys. Chem. 94 (1990) 6396.
26. L. van de Loosdrecht, M. Van der Haar, A.M. van der Kraan, A.J. Van Dillen, J.W. Geus, Appl. Catal. A 150 (1997) 365.
27. A. Barbier, A. Tuel, I. Arcon, A. Kodre, G.A. Martin, J. Catal. 200 (2001) 106.
28. G. Jacobs, T.K. Das, Y.Q. Zhang, J.L. Li, G. Racoillet, B.H. Davis, Appl. Catal. A 233 (2002) 263.
29. S. Sun, K. Fujimoto, Y. Yoneyama, N. Tsubaki, Fuel 81 (2002) 1583.
30. A. Martinez, C. Lopez, F. Marquez, I. Diaz, J. Catal. 220 (2003) 486.
31. I. Fernandez-Morales, A. Guerrero-Ruiz, F.J. Lopez-Garzon, I. Rodriguez-Ramos, C. Moreno-Castilla, Appl. Catal. 14 (1985) 159.
32. C. Moreno-Castilla, F. Carrasco-Marin, J. Chem. Soc., Faraday Trans. 91 (1995) 3519.
33. B.G. Johnson, C.H. Bartholomew, D.W. Goodman, J. Catal. 128 (1991) 231.
34. C.M. Lok, Stud. Surf. Sci. Catal. 147 (2004) 283.
35. G. Jacobs, P.M. Patterson, T.K. Das, M.S. Luo, B.H. Davis, Appl. Catal. A 270 (2004) 65.
36. P.J. van Berge, J. van de Loosdrecht, S. Barradas, A.M. van der Kraan, Catal. Today 58 (2000) 321.
37. R. van Hardeveld, F. Hartog, Surf. Sci. 15 (1969) 189.
38. K.P. de Jong, J.W. Geus, Catal. Rev.-Sci. Eng. 42 (2000) 481.
39. P. Serp, M. Corrias, P. Kalck, Appl. Catal. A 253 (2003) 337.
40. K.J. Williams, A.B. Boffa, J. Lahtinen, M. Salmeron, A.T. Bell, G.A. Somorjai, Catal. Lett. 5 (1990) 385.
41. A. Boffa, C. Lin, A.T. Bell, G.A. Somorjai, J. Catal. 149 (1994) 149.

II

PREPARATION OF FISCHER-TROPSCH COBALT CATALYSTS SUPPORTED ON CARBON NANOFIBERS AND SILICA USING HOMOGENEOUS DEPOSITION-PRECIPITATION

Homogeneous deposition-precipitation on either a silica or a carbon nanofibers (CNF) support of cobalt from basic solution using ammonia evaporation has been studied and compared to conventional deposition from acidic solution using urea hydrolysis. In the low-pH experiment the interaction between precipitate and silica was too high as cobalt hydrosilicates were formed that needed a reduction temperature of 600 ºC resulting in low cobalt dispersion. Lower interaction in experiments performed in basic environment yielded a well-dispersed Co_3O_4 phase on silica and after reduction at only 500 ºC a catalyst with 13 nm cobalt particles was obtained. On CNF from acidic solution cobalt hydroxy carbonate precipitated, which displayed a low interaction with the support resulting in a catalyst with 25 nm-sized particles after reduction at 350 ºC. Probably related to a higher extent of ion adsorption from basic solution we obtained high dispersion of cobalt on the CNF. After drying Co_3O_4 crystallites were obtained that after reduction at 350 ºC resulted in a catalyst with 8 nm Co particles. Samples prepared from high pH showed 2-4 times higher cobalt-specific activities in the Fischer-Tropsch reaction than their low pH counterparts. Both the carbon nanofibers support and the high pH deposition-precipitation technique hold considerable potential for cobalt-based Fischer-Tropsch catalysts.

Introduction

Research on Fischer-Tropsch cobalt catalysts is largely confined to cobalt on oxidic supports, generally prepared via an impregnation technique. Drawback of these support materials is their reactivity towards CoO, which during preparation or catalysis results in the formation of mixed compounds that are only reducible at high reduction temperatures [1,2]. To avoid these problems the use of carbon as support has been explored [3,4]. However, the carbon materials used up to now, *i.e.* activated carbons, were ill-defined and not very pure. Therefore, we decided to use well-defined carbon nanofibers (CNF) as a support. CNF is a novel support material with an attractive meso- and macroporous structure with high potential in many (catalytic) applications [5-9]. It consists of interwoven fibers of graphitic carbon with a high purity, a high mechanical strength and a high chemical inertness. This latter feature, however, makes the application of a dispersed cobalt phase a challenging task. In this chapter we investigate the deposition precipitation of cobalt on carbon nanofibers supports.

Commonly, for loading pre-shaped support bodies with a precursor of a catalytically active metal, ion-adsorption or incipient-wetness impregnation techniques are utilized [10-15]. Although these routes excel because of their practical simplicity, general drawbacks are the low maximum loadings and the sometimes unsatisfactory distribution and low dispersion of the active phase in the ultimate catalysts [16,17].

For the preparation of highly loaded and highly dispersed oxide supported metal catalysts, *e.g.* Cu or Ni on silica, the homogeneous deposition-precipitation (HDP) technique has been developed [18-23]. With HDP a solvated metal precursor is deposited exclusively onto the surface of a suspended support by slow and homogeneous introduction of a precipitating agent, generally hydroxyl ions, in such a way that nucleation of a solid precursor compound in the bulk solution is avoided. Generally, the hydrolysis of urea at 90 °C is used to achieve the required slow and homogeneous raise of the pH.

In the deposition process the adsorption of the metal ions onto the support coincides with nucleation and growth of a surface compound. With oxidic supports this compound mainly consists of a mixed (hydr)oxide of the metal ion and the support [18-21]. Its formation and growth prevents nucleation in the solution and upon its reduction, generally by hydrogen, the desired small and thermostable supported metal particles are generated [18,23]. Only few articles have been published on the preparation of carbon supported metal catalysts with the HDP method. Prinsloo *et al.* published on the preparation of cobalt and iron Fischer-Tropsch catalysts, unfortunately without providing

details on metal dispersion and catalytic performances [24,25]. The preparation of nickel on CNF catalysts has been described by Bitter *et al.* who succeeded in the preparation of well-dispersed Ni up to at least 45 wt%, which is remarkable as the formation of a mixed compound with the support is not possible [26]. We, therefore, extended their work with a detailed study on the deposition of Co^{2+} ions on CNF by HDP. In many respects the chemistry of Co^{2+} resembles that of Ni^{2+} and it could be expected that highly loaded Co/CNF catalysts can be prepared using this HDP method.

Hydrolysis of urea at 90 ºC was used to achieve the homogeneous production of hydroxyl ions to increase the pH from acidic to around neutral, *i.e.* at this temperature to a pH of around 6. Besides this traditionally employed HDP procedure we used a method developed by Lok *et al.* [27,28] in which the pH is homogeneously decreased from moderately basic to neutral values by controlled evaporation of ammonia from an ammonia/carbonate buffer solution at 90 ºC. To follow the precipitation processes the course of the pH was monitored as a function of time. From the difference between the pH curves with and without support conclusions can be drawn concerning the nucleation and precipitation process. Additional information on the precipitation processes was obtained from the development of the Co loading with time. Precipitations were performed both on activated carbon nanofibers and on an oxidic silica support. The precipitates were characterized after drying and after reduction by H_2 chemisorption TEM, TGA-MS, TPR, XRD and XRF, while Fischer-Tropsch catalysis experiments were carried out at atmospheric pressure.

Experimental

Carbon nanofibers of the fishbone-type with a diameter of about 30 nm were grown from synthesis gas and purified using an earlier described method [29]. These 'as synthesized' CNF were activated by refluxing in concentrated HNO_3 as described by Toebes *et al.* [30]. After washing and drying at 120 ºC this resulted in samples with a BET surface area of 180 m^2/g. Silica with a surface area of 196 m^2/g was used as obtained from Degussa (Aerosil 200).

Deposition-precipitations starting at low pH

Deposition-precipitation to prepare catalysts with intended cobalt loadings of 15 wt% using urea hydrolysis at 90 ºC was performed under a nitrogen atmosphere using double-walled glass equipment described elsewhere [18,19]. Typically 5 g of powdered support (CNF or SiO_2) was suspended in 220 ml of demineralized water to which 4.35 g

Table 1. Samples prepared.

Codes	Precursor	Co loading[a] (wt%)	Dispersion (%)
L-un	$Co(NO_3)_2{\cdot}6H_2O$	-	-
H-un	$Co(CO_3)_2{\cdot}4H_2O$	-	-
L-CNF	$Co(NO_3)_2{\cdot}6H_2O$	10.8	3.9
H-CNF	$Co(CO_3)_2{\cdot}4H_2O$	15.0	12.2
L-SiO_2	$Co(NO_3)_2{\cdot}6H_2O$	15.0	2.5[b]
H-SiO_2	$Co(CO_3)_2{\cdot}4H_2O$	15.0	7.3[b]

[a] Loading as measured by XRF and AAS

[b] Highest dispersion as measured by H_2 chemisorption

$Co(NO_3)_2{\cdot}6H_2O$ (Acros *p.a.*) was added. For deposition using urea decomposition, the pH of the suspension was adjusted at room temperature to 3.0 by addition of HNO_3 (Merck *p.a.*). Then the temperature was increased to 90 ºC, after which 2.70 g urea (Acros *p.a.*) in 30 ml was added. The pH of the slurry was monitored in course of time. After at most 23 h, when the pH had reached a value close to neutral, the suspension was cooled to room temperature and filtered. The solid was washed with demineralized water dried at 120 ºC in air. Catalyst precursors were reduced in He/H_2 (3/1 v/v) at 600 ºC (Co/SiO_2) or 350 ºC (Co/CNF) for 2 h. In order to investigate the role of the support during precipitation of cobalt, experiments were performed also without a support being present. Samples summarized in table 1 are coded L-un (precipitated from acidic solution without support), L-CNF (precipitated from acidic solution in the presence of CNF), and L-SiO_2 (precipitated from acidic solution with silica present).

Deposition-precipitations starting at high pH

Preparations from high pH were done in the same double-walled glass equipment, the only difference being that a polypropylene vessel of 120 ml was inserted in the glass vessel to suppress deposition of solid material on the walls. Typically 0.74 g $Co(CO_3){\cdot}0.1H_2O$ (Acros) was dissolved in 27.70 g 25 wt% ammonia (Merck pure) to which 77.30 g demineralized water and 5.47 g $(NH_4)_2CO_3$ (Acros *p.a.*) were added (pH ~11). After filtration of this dark-red solution 2.0 g of support was added. Nitrogen was flushed through the system with a rate of 200 $ml{\cdot}min^{-1}$. The system was provided with a cooler to minimize the evaporation of water. The temperature of the suspension was raised from room temperature to around 90 ºC and kept at this value during the precipitation process. During the whole process the pH was recorded. After the reaction was completed, indicated by the colourlessness of the supernatant and a pH value of about 8, the mixture was cooled to room temperature and filtered. The solid was washed three times with

demineralized water and dried at 120 ºC in air. Catalyst precursors were reduced in He/H_2 (3/1 v/v) at 500 ºC (Co/SiO_2) or 350 ºC (Co/CNF) for 2 h. In order to investigate the role of the support during precipitation of cobalt, also experiments were performed without any support being present. Samples were coded H-un, H-CNF and H-SiO_2, referring to the high pH from which the deposition process started (table 1).

Analysis and characterization

During each of the preparations described above, samples of the liquid phase were collected in order to determine the development of the cobalt-ion concentration in time. Samples were diluted to concentrations of 30-150 ppm cobalt using 0.1 M HNO_3. Cobalt concentrations were measured with flame atomic absorption spectroscopy (AAS) on a Varian spectrAA-10 at 346.6 nm.

Cobalt-ion adsorption on the supports prior to addition of urea was determined in separate experiments in which the solid phase was analysed. Now 1 g of support was slurried for 1 h in 50 ml of the cobalt solutions described above. To prevent the start of deposition due to ammonia evaporation the temperature was restricted to RT for the high pH preparations. Adsorptions in acidic solutions were done both at RT and at 90 ºC. The support was collected by filtration followed by thoroughly washing. A portion of the support was re-suspended in a known volume of 0.1 M HNO_3. After filtration the cobalt concentration in this solution was determined using AAS as described above. The cobalt loading on the carbon nanofibers supported catalysts was also determined using this method.

X-ray Fluorescence, used to determine the cobalt loading on the silica support, was measured on a Goffin Meyvis spectro X-lab 2000.

The dried catalyst precursors and the reduced catalysts were examined with transmission electron microscopy (TEM) in a FEI Tecnai12 or in a FEI Technai20F. TEM samples were crushed and suspended in ethanol under ultrasonic vibration. A drop of this suspension was brought onto a holey carbon film on a copper TEM grid.

Powder X-ray diffraction (XRD) patterns were measured using an Enraf-Nonius CPS 120 powder diffraction apparatus with Co K_α radiation (λ=1.789 Å).

Thermo gravimetric analysis (TGA) on a Netzsch STA-429 thermo balance was used to study the dried unsupported samples. The gases evolved were monitored by a Fisons Thermolab quadropole mass spectrometer, through a capillary situated directly above the sample cup. Temperature programmed reductions (TPR) were executed with an Autochem 2920 instrument from Micromeritics using a heating rate of 5 ºC/min and a H_2/Ar flow (1/19 v/v).

Hydrogen chemisorption measurements were carried out using a Micromeritics ASAP 2010C. Before each measurement a sample was dried in vacuum at 120 ºC overnight, and reduced for 2 h in flowing H_2 at 350 ºC (CNF) or at 400, 500, 600, 700 and 800 ºC (SiO_2), with a heating rate of 5 ºC/min. After reduction the samples were evacuated at this temperature for 30 min. The H_2-adsorption isotherms were measured at 150 ºC. The H/Co atomic ratios at zero pressure were found by extrapolation of the linear part of the isotherm of the total amount of hydrogen adsorbed. Particle size estimations are based on cobalt particles with hemi-spherical geometry, assuming complete reduction and an H/Co adsorption stoichiometry of 1, using the following formula: d = 81.6 * W/X, where d is the cobalt particle diameter (nm), W the weight percentage of cobalt and X the total hydrogen uptake in micromoles per gram of catalyst [31].

Catalytic testing

The Fischer-Tropsch measurements were carried out at 220 ºC and at 1 bar CO/H_2 (1:2 v/v). Typically 50 mg of catalyst particles (0.5-1.0 mm) was diluted with 200 mg SiC (0.2 mm) to achieve isothermal plug-flow conditions. Catalyst precursors were reduced for 2 h at 350 ºC (L-CNF, H-CNF), 500 ºC (H-SiO_2) or 600 ºC (L-SiO_2). Hydrocarbon products (C_1-C_{16}) were analyzed with an FID on a Varian 3800 GC with a fused silica CP-Sil 5CB column. Selectivities of the catalysts were compared at the same CO-conversion (2%), which was achieved by adjusting the flow. Reported catalytic performances are stabilized values after 2 days of operation.

Results and Discussion

Precipitation starting from low pH

Analysis of pH curves and cobalt deposition

The first 6 hours of the pH-time curves monitored during the precipitation with and without support are shown in figure 1A. In figure 1B the corresponding fraction of cobalt deposited as measured with AAS is shown. For unsupported cobalt (L-un, figure 1) the onset of precipitation was observed at a pH of about 6.6 after 0.5 h. At this pH the solution obviously had become sufficiently supersaturated to enforce nucleation and growth of a precipitate. Equilibrium was re-established by enhanced consumption of hydroxyl ions as indicated by a small and rapid drop of the pH to a value of 6.3 [18,19]. Next, the pH was virtually constant and finally increased to reach a value of 6.4 after 18 h. From the equilibrium pH of 6.3 and the starting Co^{2+} concentration, *i.e.* $60 \cdot 10^{-3}$ mol·l^{-1}, a solubility product for $Co(OH)_2$ can be calculated of roughly $3.0 \cdot 10^{-15}$ mol^3·l^{-1} which is

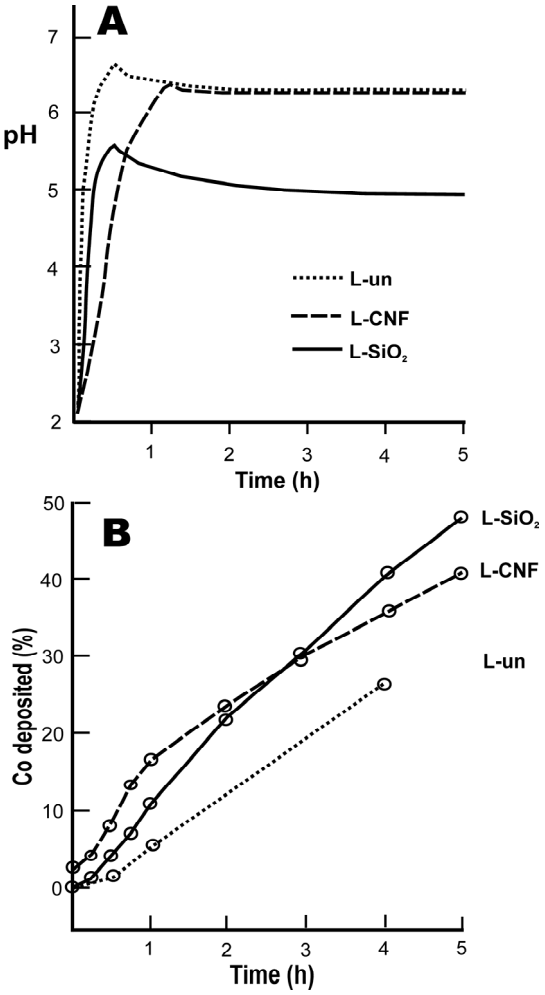

Figure 1. pH curves during precipitation from low pH (A) with corresponding cobalt deposition as function of deposition time (B).

close to the value of $1.6 \cdot 10^{-15}$ $mol^3 \cdot l^{-1}$ at 20 ºC for β-$Co(OH)_2$ as reported in the literature [32]. The difference observed is probably due to the fact that we measured at a higher temperature and in our case, no β-$Co(OH)_2$ had precipitated but Co hydroxide with intercalated anions, *viz.* α-$Co(OH)_2$. From the AAS data we found that with L-un only a limited amount of cobalt had deposited before the maximum in pH had been reached, which could also reflect the experimental error in our method. Four hours after the addition of urea 27% of cobalt had deposited, which amount increased to a final value of 68%. This incomplete deposition was also indicated by the pinkish color of the solution, and it reflects the solubility of cobalt hydroxide at the prevailing pH. Visual inspection showed that most cobalt hydroxide was deposited on the wall of the vessel and on the pH electrode.

For L-SiO_2 the onset of precipitation already was reached at a pH of 5.6, also after ~0.5 h. Next, the pH decreased rapidly, then more gradually to reach a value of 4.9 after about 3 h. Around 13 h after addition of urea the pH started to increase to reach a value of 6.0 after 23 h. This increase of the pH indicated that precipitation of cobalt had come

to completeness, which was confirmed by the colorless filtrate. Interesting information comes from the corresponding AAS measurements (figure 1B). Ion adsorption for 1 h at the starting pH did not result in uptake of any cobalt by the support, independent of the temperature, and also in the first 15 min of reaction no cobalt was found on the support. After 0.5 h the cobalt loading was measured to be 0.6 wt% and this loading increased rapidly to 7.2 wt% (48%) at 5 h. The deposition rate slowly decreased in the next three hours, accompanying the decrease of pH from 5.6 to 4.9 and reflecting the lowering of the hydroxyl concentration. From the deposition rate between 4 and 5 hours we calculated that deposition would be completed after 12 h, which nicely coincided with the onset of pH increase (data not shown).

From these pH curves and the AAS data it may be concluded that the presence of the silica support highly influenced the precipitation process. Precipitation was faster on the silica support, as is clear from the higher extent of deposition after 4 h. The considerable shift of the pH to lower values demonstrated the strong interaction of the cobalt precipitate with silica and the difference in equilibrium pH values indicated a difference in nature of the precipitates.

For L-CNF 1.25 h was needed to reach the onset of precipitation at a pH of 6.4. Shortly afterwards, the pH decreased to 6.3, the quasi-equilibrium also found for L-un. Next, the pH was virtually constant and finally increased to reach a value of 6.4 after 23 h. The AAS measurements showed that at the starting pH already 0.45 wt% cobalt was loaded on the CNF support. The amount of cobalt loaded increased rapidly and at the precipitation onset, after 1.25 h, approximately 17% of cobalt had deposited, amounting a 2.5 wt% loading. Once the maximum pH was reached, the deposition rate slowed down and even after 23 h not all cobalt had deposited, but around 20% remained in solution, which was also indicated by the pink color of the solution. The deposited cobalt was not solely present on the CNF, but also on the glass parts of the set-up. With AAS the real cobalt loading on the support was determined to be 10.8 wt%, showing that the large majority of the precipitated cobalt was present on the support.

The longer time needed for L-CNF compared to L-un (1.25 h *vs.* 0.5 h) to start the precipitation could be due to the presence of acid sites on the activated CNF support which already from the start adsorb Co^{2+} and $CoOH^{+}$ ions. Using the AAS data we found a substantial amount of cobalt deposited (2.5 wt%) before the precipitation onset was reached. From the number of acidic oxygen groups on the surface (0.42 mmol/g) we calculated a loading of 2.5 wt% based on a one-to-one exchange ratio, so it is possible that indeed the retarded pH increase is caused by the ion exchange of Co^{2+} in combination with or followed by hydroxylation. It is also possible that already in this

stage small cobalt hydroxide clusters are growing on the CNF support. This growth of metal hydroxide clusters before the precipitation onset was observed by Van der Lee *et al.* in the preparation of Ni/CNF using similar techniques [33]. The gradual growth of such small clusters can retard the pH increase, meanwhile loading cobalt on the support.

Shortly after the onset of precipitation at pH 6.4 the pH dropped to 6.3, the quasi-equilibrium also found for L-un. Obviously, due to a lack of sufficient interaction with the CNF support a cobalt precipitate was formed at pH values where also bulk precipitation is possible. We show below that these precipitates have the same composition.

Investigation of dried samples

The bulk precipitate L-un consisted of ordered rectangular shaped rods with lengths up to 2 μm, and aspect ratios of about 10 (figure 2A). The high resolution TEM image in figure 2B shows that the rods comprised of ordered stacked layers with an average lattice spacing of 0.94 nm, a value characteristic for intercalated α-$Co(OH)_2$ [34,35]. In our case the intercalation of carbonate and/or ammonium ions was likely as they are formed during the hydrolysis of urea [36]. The intercalation of carbonate in $Ni(OH)_2$ during precipitation by means of urea hydrolysis was observed before by Hermans *et al.* [19]. With TGA-MS we proved the presence of carbonate and small amounts of ammonia in L-un (data not shown).

A TEM image of dried L-CNF is given in figure 3. Cobalt has precipitated in rectangular shaped rods smaller in size than obtained with L-un and often partly connected with the support. This suggests a rapid growth of the precipitate, hereby growing disconnected from the CNF. This could reveal that not enough nucleation sites were available at the start of the growth process. In some cases a cobalt precipitate was

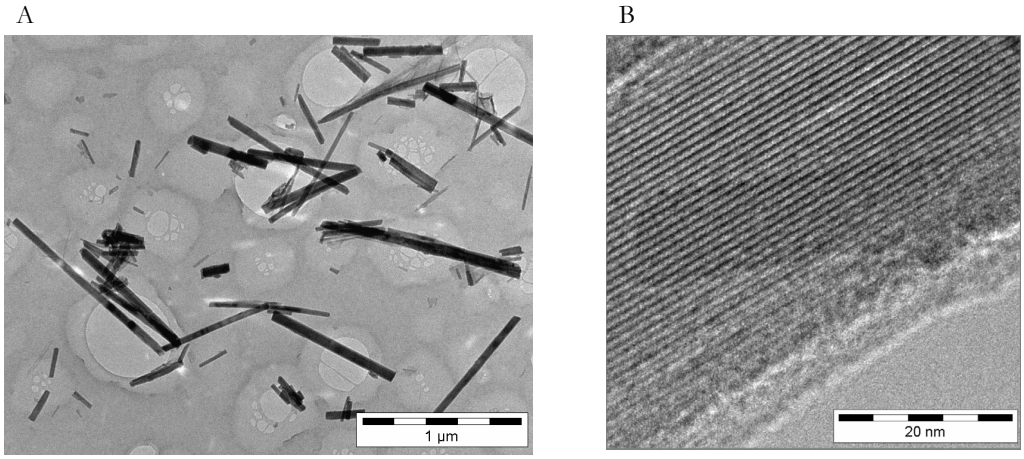

Figure 2. TEM image of dried L-un with different sized rectangular rods (A) that consist of ordered stacked layers with a lattice spacing indicative of intercalated α-Co(OH)2 (B).

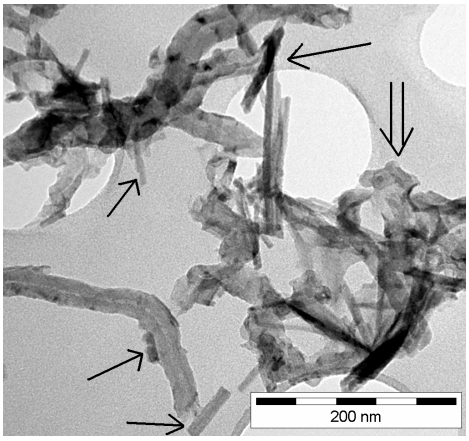

Figure 3. TEM image of dried L-CNF with cobalt precipitated on the support (single arrows) and also unsupported cobalt (open arrow).

found next to the CNF support. From figure 3 it is also apparent that considerable parts of the fibers are found without cobalt precipitate detectable, pointing to the limited nucleation on the support.

A TEM image of dried L-SiO_2, depicted in figure 4A, shows aerosil particles (~20 nm) and claylike structures (8 to 80 nm), typical for phyllo-silicates [18-21]. Obviously, silica has reacted to a large extent with cobalt during the precipitation process. However, TEM shows that in some parts of the sample small particles with sizes varying from 2 to 5 nm were present in close contact with the support (figure 4B). With TEM EDX we verified that these particles contain cobalt indeed, but that only a small part of cobalt is present in this form. Most likely these particles consist of some type of cobalt (hydroxy)carbonate, precipitated as small particles. Both types of cobalt species observed are in close contact with the support, which is in line with the conclusion drawn from the pH-time curve.

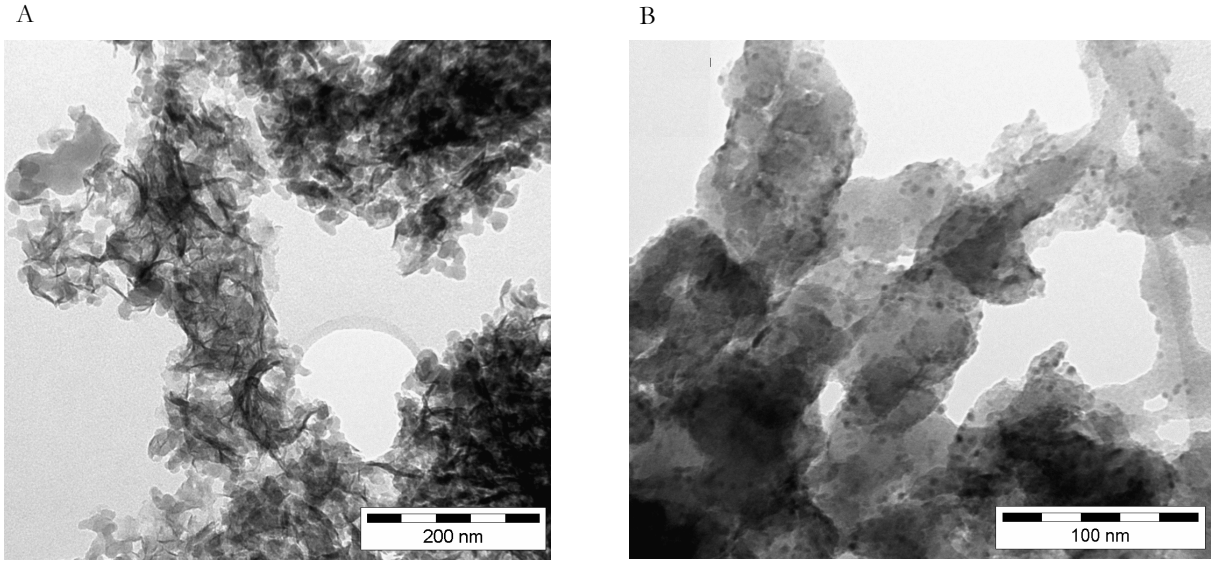

Figure 4. TEM images of dried L-SiO_2 showing clay-like structures typical for phyllo-silicates (A). In some parts of the sample small cobalt particles can be observed (B).

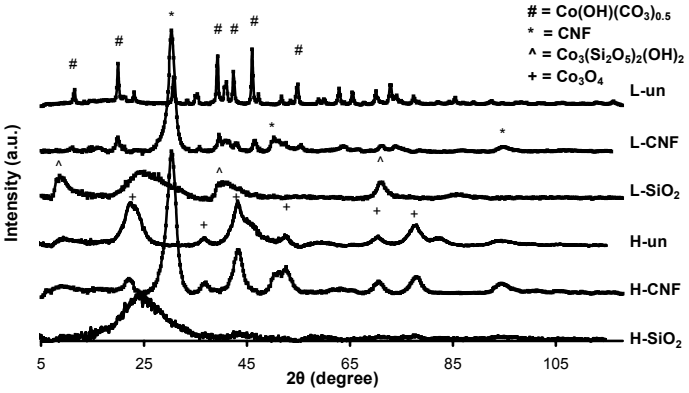

Figure 5. XRD patterns of dried samples with strongest diffraction lines of main components indicated.

XRD patterns of the dried samples are shown in figure 5 with the most pronounced diffraction lines of the main components indicated. The narrow line of L-un, indicative of large crystallites, can be attributed to a cobalt hydroxy carbonate: $Co(OH)(CO_3)_{0.5}{\cdot}0.11H_2O$ [37]. The precipitation of mixed carbonate hydroxides is thermodynamically more likely than the precipitation of pure cobalt hydroxide as was calculated by Mostafa *et al.*[38]. For L-CNF, in addition to the graphite lines the three most intense diffraction lines of L-un are observed as well, although somewhat broadened. During the precipitation probably a similar type of cobalt compound was formed in the unsupported sample as with the CNF sample. The diffraction lines of L-SiO_2 are characteristic for the presence of cobalt hydrosilicates [39], while the absence of other diffraction lines also indicates that the largest fraction of cobalt is present as hydrosilicates and not as small cobalt hydroxy carbonate particles.

Temperature programmed reduction profiles given in figure 6 show that the narrow reduction peak of L-un is located at 280 ºC. Around 200 ºC a small reduction peak is present, probably originating from reduction of some urea contamination in the sample. Reduction of L-CNF started at the same temperature as L-un. Due to the smaller particles of the precipitate the reduction rate increased less steeply with temperature and the peak

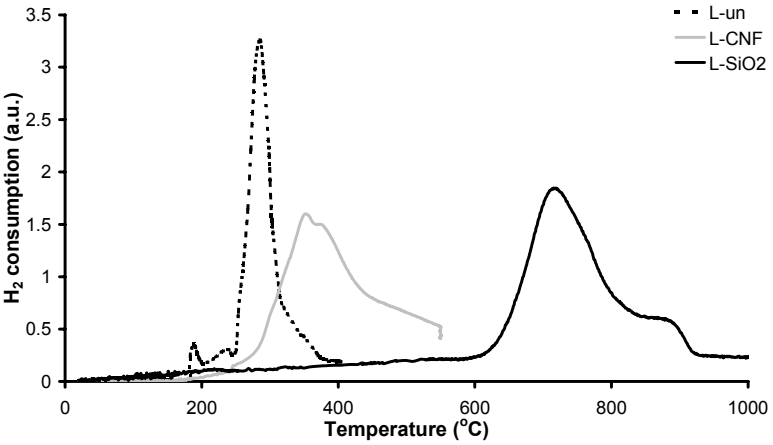

Figure 6. TPR profiles normalized to the amount of cobalt for samples prepared from low pH.

position shifted to a somewhat higher temperature (350 ºC). Furthermore, as GC analysis demonstrated, the broad shoulder at temperatures beyond 350ºC has to be ascribed to gasification of CNF to methane. For L-SiO_2 a high temperature reduction peak at 650 and a shoulder at 800 ºC are found, that can be ascribed to the presence of cobalt (II) silicates [39]. From the hydrogen consumption we calculated that cobalt was fully reduced at 900 ºC.

Investigation of reduced samples

TEM analysis of L-CNF reduced at 350 ºC showed cobalt particles with sizes varying from 4 to 100 nm (figure 7). The smaller particles are found throughout the whole sample and are always in close contact with the support (figure 7A/B). The largest particles, probably formed out of the large rods, have only limited interaction with the support. These large cobalt particles are black, surrounded with a greyish layer (figure 7B, arrows). This indicates that some re-oxidation of metallic cobalt took place when the sample was transferred from the reactor to the microscope. The thickness of the cobalt oxide layer is about 3 nm, so particles smaller than 6 nm would be completely re-oxidized by air after the reduction treatment. We estimated the average cobalt particle size to be around 30 nm, with a broad size distribution. The dispersion obtained from hydrogen chemisorption was 3.9%, which is equivalent to an average particle size of 25 nm. The XRD pattern of reduced and passivated L-CNF depicted in figure 9 shows not only characteristic diffractions of hexagonal metallic cobalt but also broad diffraction lines of CoO.

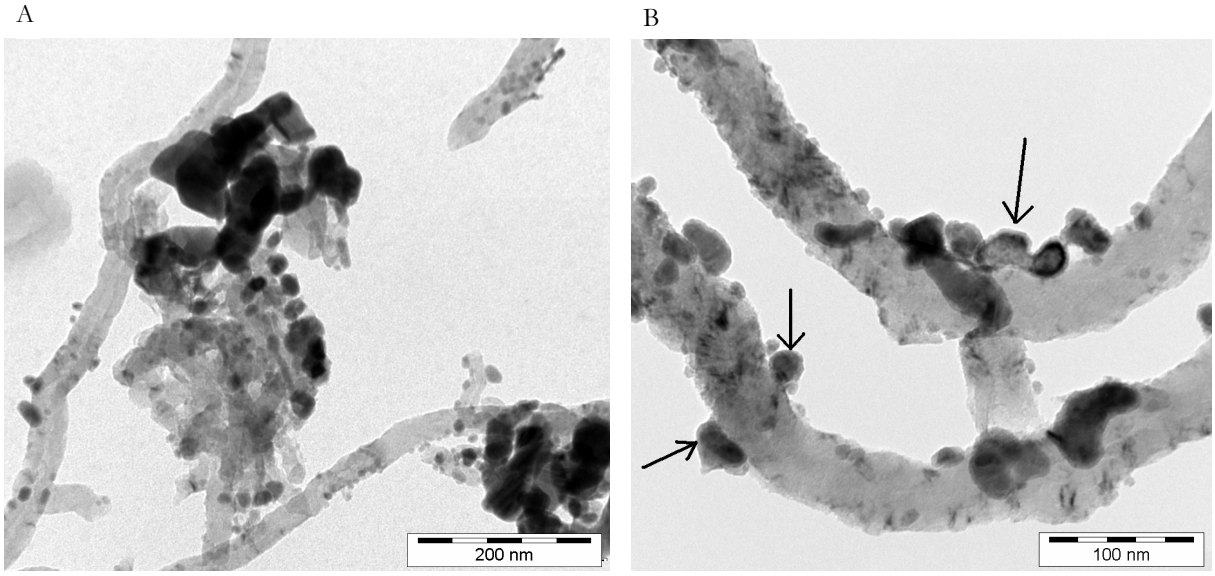

Figure 7. TEM images of reduced L-CNF showing small supported cobalt particles together with larger particles with limited interaction with the support (A). Using a higher magnification around the black metallic core a greyish layer of CoO (arrows) can be observed (B).

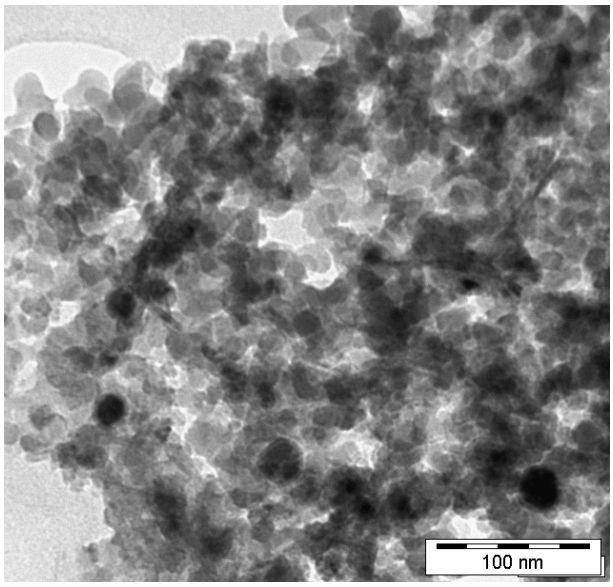

Figure 8. TEM image of reduced L-SiO_2 with spherical cobalt particles of 10-40 nm.

TEM images of L-SiO_2 reduced at 600 ºC show the presence of cobalt particles with sizes varying from 10 to 40 nm (figure 8). The average particle size, calculated by averaging over 150 particles, turned out to be 35 nm. These results demonstrate that cobalt at the high reduction temperature is prone to sintering. Sintering was also evident from the difference in hydrogen uptake, measured with H_2 chemisorption, after reductions at different temperatures. Data presented in table 2 are apparent cobalt dispersions, assuming total reduction. Reduction at 400 and 500 ºC showed only minimal hydrogen uptake, but reduction at 600 ºC resulted in the highest uptake. Reduction at 700 or 900 ºC resulted in slightly lower dispersions, indicating the modest sintering of cobalt at these high temperatures. The highest dispersion of 2.5% after reduction at 600 ºC corresponds to cobalt particles of 40 nm, which confirms the TEM data. The XRD pattern of the reduced and passivated L-SiO_2 sample displayed in figure 9 exhibits a weak and broad diffraction of SiO_2 around 30 º2θ together with cobalt oxide lines and stronger diffraction lines of metallic cobalt. The peaks at 49, 52 and 56 º2θ are indicative of the

Table 2. Influence of reduction temperature on apparent cobalt dispersion of L-SiO_2 and H-SiO_2.

Temperature (ºC)	**L-SiO_2 (%)**	**H-SiO_2 (%)**
400	0.07	5.7
500	0.43	7.3
600	2.50	5.5
700	2.11	5.4
900	2.05	5.0

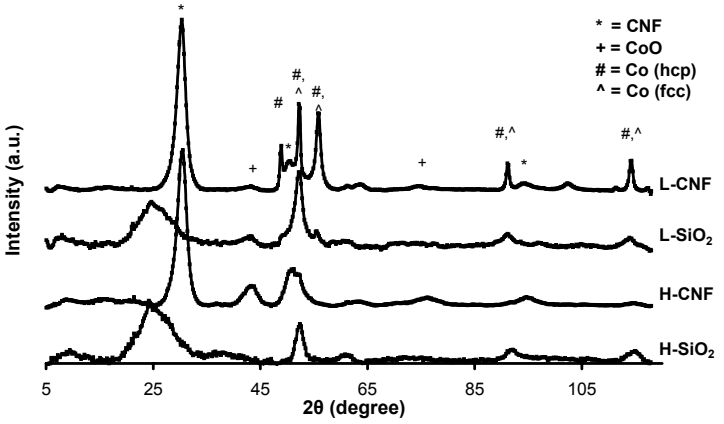

Figure 9. XRD patterns of reduced and passivated samples with the strongest diffraction lines of the main components indicated.

presence of hexagonal closed packed cobalt, but the diffraction line at 60 º2θ in combination with a far higher intensity of the 52 º2θ line than expected for hcp, indicates that also face centered cubic cobalt is present. Although hcp is the most stable structure for bulk cobalt at room temperature the fcc structure is reported to be the main phase in some cases, especially on oxidic supports [31].

Precipitation starting from high pH

Observations during preparation and analysis of pH curves

The solutions were transparent dark-red at the starting pH (~11) due to the presence of $Co(NH_3)_6^{2+}$. During the process the color of the solutions changed first to orange before becoming purple. Next, the solutions gradually de-colorized, indicating that cobalt had completely precipitated. Unsupported and silica-supported precipitates were dark brown. During the first half hour with all systems the pH dropped rapidly, which is related to both the temperature increase and the fast evaporation of ammonia. As shown in figure 10A the course of the pH curves were rather similar with some discontinuities that reflect the influence of the precipitation process. The most unambiguous observation with the pH-time experiments is that at corresponding times the pH is significantly lower when a support is present. This could indicate that cobalt did not precipitate on the support, as for the formation of a precipitate in strong interaction with the support, precipitation at higher pH values than for bulk precipitation is expected. However, from the analysis of the precipitates it will become clear that cobalt precipitated exclusively on the support for both H-CNF and H-SiO_2. This indicates that pH measurements during precipitation starting from basic solution are not conclusive with respect to the nature of the precipitation process. Evaluation of the precipitation could be done only when the information of the pH-curves was combined with information from the Co deposition measured with AAS.

Extent of cobalt deposition in time

In figure 10B the cobalt fraction deposited as a function of time is shown for the three experiments. With H-un the deposited cobalt fraction remained negligible up to at least 5 h and most likely nucleation started after the shallow pH overshoot at that time (figure 10A). With H-SiO_2 and H-CNF cobalt had adsorbed already at the start and during the experiment the amounts precipitated on the supports remained larger, indicating the facilitated surface-precipitation. At the start of the experiment 8 to 10% of the total amount of cobalt was adsorbed on the support, which coincided nicely with the loadings measured with samples separately prepared by ion adsorption.

An increased rate of Co deposition on CNF was measured after 2 h, at a pH of 8.5, indicated by the steeper slope of the deposition curve. A further acceleration of the rate of precipitation was measured after 4 h resulting in almost complete removal of Co from the solution in the next two hours. With silica as the support a small enhancement of the

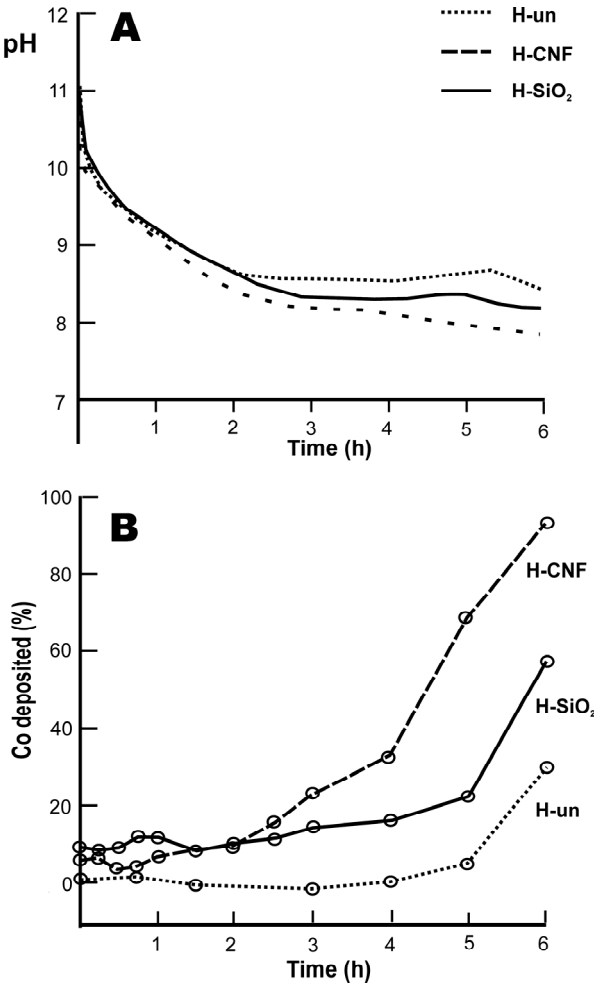

Figure 10. pH curves during precipitation from high pH (A) with corresponding cobalt deposition as function of deposition time (B).

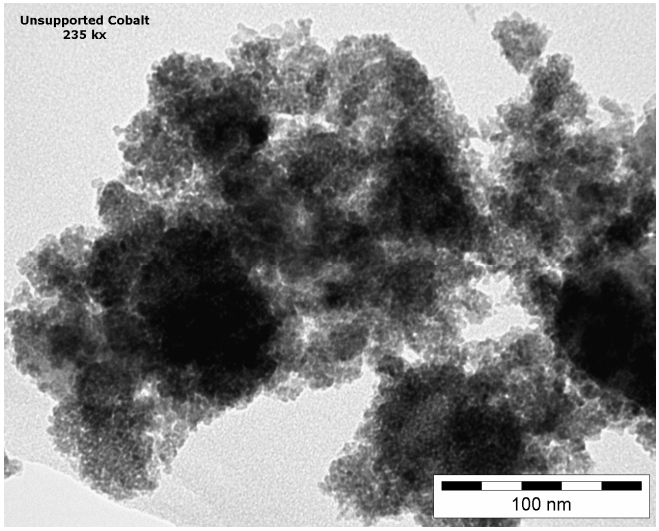

Figure 11. TEM image of dried H-un showing that cobalt precipitated in clusters of a few hundred nm that consist of subunits of 5 nm.

rate of precipitation was observed after around 3 h, while a more significant acceleration proceeded after around 4 h. In both cases this was first accompanied with a stabilization of the pH followed by a further decrease of the pH. Probably this pH stabilization was brought about by the production of NH_3 from the ligand exchange in the ammonia complex.

Investigation of dried samples

With H-un cobalt had precipitated in particles with a size of about 5 nm, clustered together to units up to a few hundred nm (figure 11). The XRD pattern of dried H-un, depicted in figure 5, is typical for Co_3O_4 with line shapes broadened, indicating the presence of particles of around 5 nm. As the direct deposition of Co_3O_4 is not feasible from the Co^{2+} solution, this compound was either formed during aging in the solution or in the drying step. In experiments that were stopped before the final pH was reached (data not shown) we observed very distinct patterns from $(NH_4)_2Co_8(CO_3)_6(OH)_6(H_2O)_4$ [40], although super positioned on broad diffraction lines of Co_3O_4. We propose that the initial cobalt phase deposited was largely $(NH_4)_2Co_8(CO_3)_6(OH)_6(H_2O)_4$ which was further oxidized to Co_3O_4 during aging and drying.

The initial $(NH_4)_2Co_8(CO_3)_6(OH)_6(H_2O)_4$ phase in H-un is different from that obtained with L-un, *viz.* $Co(OH)(CO_3)_{0.5}{\cdot}0.11H_2O$. When comparing the TEM images the difference in crystallite size of H-un and L-un catches the eye. Clearly, upon super saturation at high pH more nuclei are formed and/or growth of the nuclei is slower. An explanation could be the higher ionic strength with H-un, which decreases the activation energy for nuclei formation [41,42].

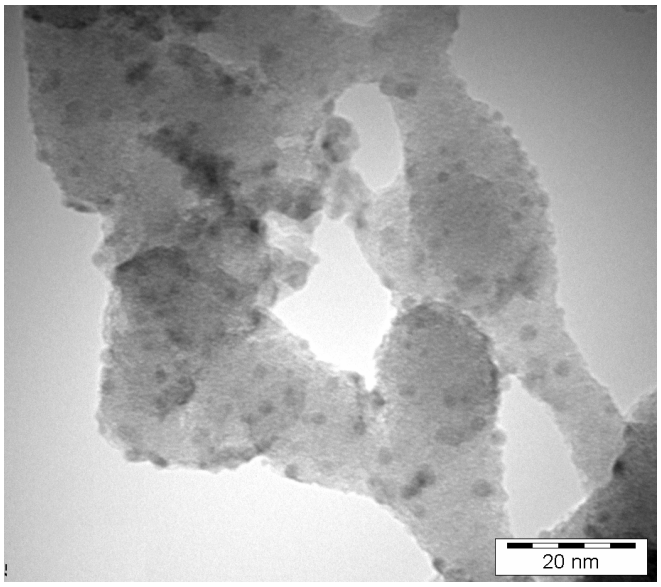

Figure 12. TEM image of dried H-SiO_2 with small, evenly distributed cobalt particles.

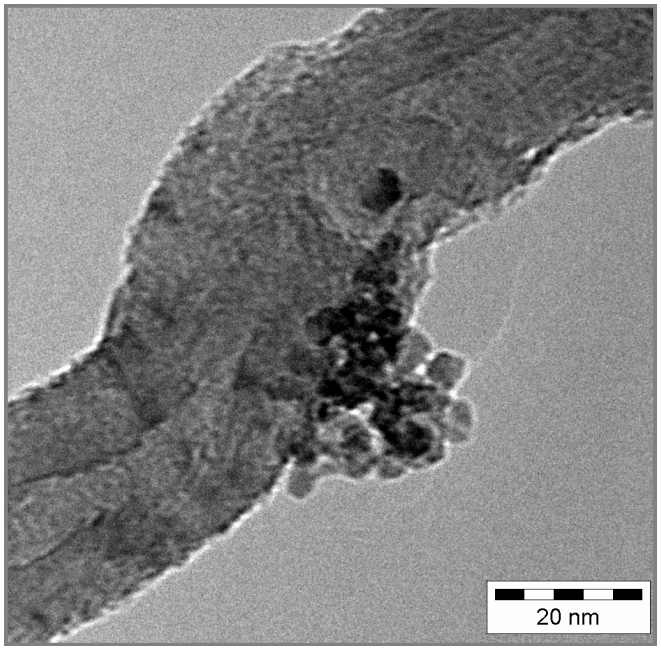

Figure 13. TEM image of dried H-CNF showing an individual carbon nanofiber with a bunch-like cobalt precipitate.

In figures 12 and 13 supported cobalt particles are apparent on both H-SiO_2 and H-CNF. As we concluded from the AAS measurements and the pH-time curves, not only with H-SiO_2 but also with H-CNF no precipitation separate from the support was found. For H-SiO_2 the cobalt particles have sizes of around 5 nm (figure 12). With TEM we found no indication of plate-like hydrosilicates dissimilar to L-SiO_2. XRD of H-SiO_2 shows broad diffraction lines, which complicated assignment (figure 5). Apart from the silica band weak and broad contributions are present from Co_3O_4 in line with the 5 nm particles that we observed with TEM. A TEM image of dried H-CNF revealed that cobalt had deposited onto the surface of the fiber as clusters consisting of

5 nm particles (figure 13). The bunch-like shape of the precipitate in both H-un and H-CNF indicates that the precipitation was not a single nucleation followed by growth process, but rather that at the surface of particles new nuclei were formed.

However, TEM analysis (figure 13) also showed that a considerable part of the fibers was not covered with particles. This suggests that only in certain places on the fibers nucleation had occurred, *i.e.* the critical density of adsorbed cobalt ions had been reached. Toebes *et al.* showed that after reflux in nitric acid for 2 h the density of carboxylic groups on CNF was about 0.42 mmol/g [30]. However, it is rather likely that these groups are not evenly distributed over the surface. In regions with a high density of carboxylic groups the concentration of adsorbed cobalt ions might become high enough to facilitate nucleation at the surface. Subsequent growth of the nuclei and formation of new nuclei on the fresh crystals finally results in the grape-like morphology of the precipitate. This can also explain why H-CNF showed a better cobalt dispersion than L-CNF. Due to the 2.5 times higher concentration of adsorbed cobalt ions for H-CNF more nucleation sites are available, resulting in a smaller cobalt particle size after reduction. XRD of dried H-CNF, see figure 5, shows the characteristic graphite diffraction lines and cobalt diffraction lines at positions typical for Co_3O_4.

Temperature programmed reduction profiles are shown in figure 14. H-un exhibited a reduction peak at 330 ºC, which is somewhat higher than that obtained with L-un. This shift to higher temperature might be related to the smaller size of the H-un crystallites. The peak around 180-210 ºC can be ascribed to the reduction of Co_3O_4 to CoO.

H-SiO_2 shows an early reduction peak at 200 ºC, probably being the reduction of cobalt Co^{3+} to Co^{2+} and a very broad reduction peak starting at 410 ºC to above 700 ºC, which can be ascribed to the reduction of small CoO particles and cobalt(II)silicates. Although platelets of hydro-silicates were not indicated from XRD and TEM *in situ* formation of cobalt silicates during the reduction is possible. When compared to L-SiO_2,

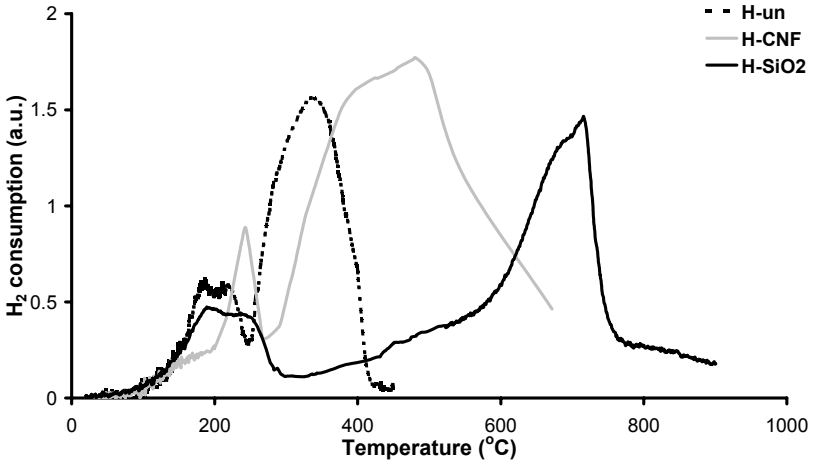

Figure 14. TPR profiles normalized to the amount of cobalt for samples prepared from high pH.

H-SiO_2 has the main reduction peak at the same temperature (700 ºC), but has the reduction onset 150 ºC earlier and also returns more steeply to the baseline. The degree of reduction for H-SiO_2 calculated from the amount of H_2 consumed during the TPR experiment was 95%.

In the reduction profile of H-CNF two distinct stages exist: the reduction of Co^{3+} to Co^{2+} with a peak at 240 ºC and the reduction of Co^{2+} to Co^0 beyond 270 ºC with a maximum at 400 ºC, that overlaps with the gasification of the carbon fibers. As soon as metal was formed in close contact with the support, gasification started. With H-CNF more metal particles than with L-CNF were in close contact with the support, due to which gasification proceeded faster. Taking into account the cobalt loading and oxidation state we calculated that one third of the area of the second peak can be attributed to the consumption of hydrogen in this gasification step.

Investigation of reduced samples

With TEM metallic cobalt clusters of around 20 nm were found with H-SiO_2 reduced at 500 ºC (data not shown). Apparently some sintering had taken place during reduction, but not as much as observed with L-SiO_2. The XRD pattern of reduced and passivated H-SiO_2, depicted in figure 9, also shows diffraction lines similar to that of L-SiO_2, stemming from a mixture of CoO and fcc and hcp metallic cobalt. The dispersion of the catalyst was also measured with H_2 chemisorption. In table 2 the cobalt dispersions (assuming complete reduction) as a function of reduction temperature are shown. Already after reduction at 400 ºC a large fraction of the cobalt had been reduced. With H-SiO_2 the

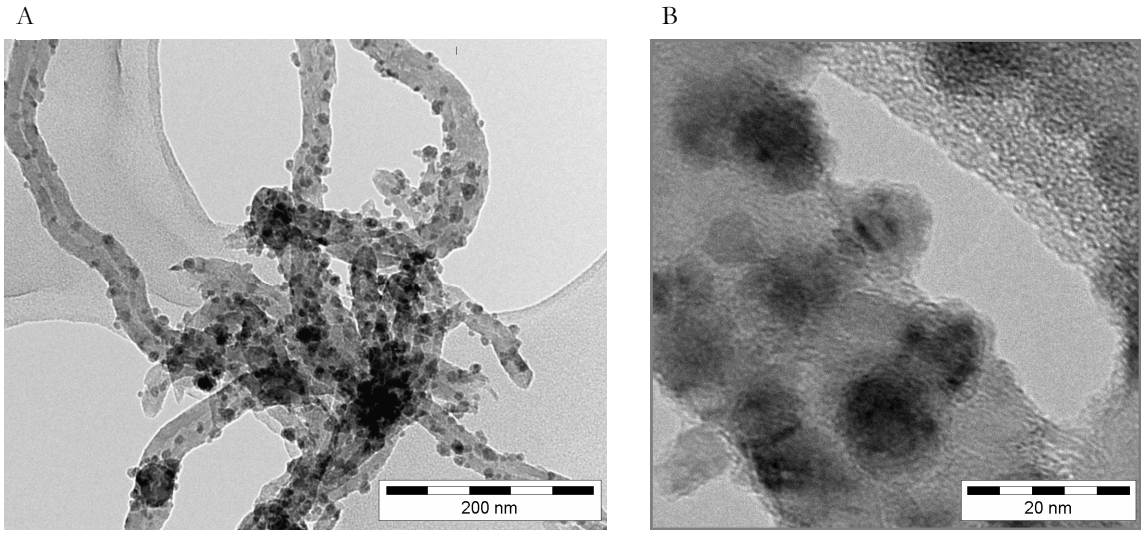

Figure 15. TEM images of reduced and passivated H-CNF showing almost spherical, partly re-oxidized cobalt particles distributed over the carbon nanofibers at (A) medium resolution and (B) high resolution.

highest dispersion of 7.3%, found after reduction at 500 ºC, is equivalent to a cobalt particle size of 13 nm. Higher reduction temperatures resulted in modest sintering, as was observed before for L-SiO_2.

Two representative TEM images of reduced H-CNF are shown in figure 15A/B. From the first figure it is clear that cobalt is nicely dispersed over the CNF surface. The particle size is around 10 nm with a narrow size distribution. The high-resolution image in figure 15B shows that the particles are almost spherical with a dark core and a more greyish shell. The dark core is metallic cobalt, while the outer layer of about 4 nm is oxidized by air forming an expanded and amorphous CoO layer with lower contrast. An XRD pattern of reduced and passivated H-CNF is given in figure 9 showing strong CoO diffraction lines and broad metal lines for fcc cobalt.

The cobalt particle size as obtained with H_2 chemisorption of H-CNF was 8 nm (table 1). This is in close agreement with the 10 nm found with TEM if the contraction of CoO to Co (25%) during reduction is taken into account.

Catalytic data

The different catalysts were tested for their performance in the Fischer-Tropsch reaction (table 3). The catalysts prepared using precipitation starting from high pH outperformed the catalysts prepared in acidic solution. For the silica-supported catalysts the activity increased fourfold going from L-SiO_2 to H-SiO_2, while the selectivity was virtually the same. Also for the CNF supported catalysts a two times higher activity was found for H-CNF as compared to L-CNF. The methane selectivity of H-CNF was only 20 wt%, while the C_{5+} selectivity was as high as 53 wt%, values characteristic for promoted catalysts [8]. Probably related to this high selectivity was the quite low specific activity (TOF) of this catalyst, but more research is needed before we can explain this observation.

Table 3. Performance of catalysts in the FT reaction after reduction for 2 h at 350 ºC (L-CNF, H-CNF), 500 ºC (H-SiO_2) or 600 ºC (L-SiO_2).

Sample	Cobalt size (nm)	Activity[a]	TOF[b]	C_1 (wt%)	C_{5+} (wt%)
L-CNF	25	0.64	9.7	40	23
H-CNF	7.9	1.24	6.0	20	53
L-SiO_2	40	0.35	8.3	40	23
H-SiO_2	13	1.31	10.6	42	21

Conditions: 1 bar, H_2/CO=2, 220 ºC, 2% conversion of CO

[a] Normalized activity: 10^{-5} mol_{CO} $\cdot g_{Co}^{-1}$ $\cdot s^{-1}$

[b] TOF: 10^{-3} s^{-1} based on dispersion H_2 chemisorption

Conclusions

With the classical homogeneous deposition precipitation (HDP) method, using urea decomposition to slowly increase the pH from acidic to neutral, a 15 wt% catalyst on silica was prepared. A strong interaction between the cobalt species and the silica was found, resulting in a sample mainly consisting of cobalt hydrosilicates. The stability of the formed compound was high and it turned out to be fully reducible only at around 600 ºC due to which the formed metal particles sintered to 35 nm. Using an HDP method with ammonia evaporation to lower the pH, a cobalt compound precipitated with less interaction with the silica, present as 4 nm Co_3O_4 particles in the dried sample. A lower reduction temperature of 500 ºC was sufficient to attain complete reduction, resulting in a silica-supported catalyst with cobalt particles of 13 nm.

With CNF as the support material, activated by treatment in nitric acid, adsorption of Co species in acidic solution on the mainly carboxylic groups appeared too small to achieve nucleation selectively on the support. Due to this too low interaction a catalyst with a cobalt metal dispersion of only 3.9% was obtained. A stronger interaction was found for the sample prepared from high pH. Now the cobalt precursor precipitated on the support selectively, resulting in a catalyst after reduction at 350 ºC with a cobalt metal dispersion of 12%. By precipitation at high pH a 2.3 times higher cobalt ion adsorption was observed on the CNF surface. For the H-CNF sample now both prerequisites are fulfilled to enable preparation of highly dispersed catalysts with HDP. The first is a sufficient interaction in the aqueous phase in order to achieve nucleation exclusively on the support surface. The second is the modest interaction in the solid phase to facilitate reduction of the catalyst at low temperatures. The cobalt hydroxy carbonate precipitate turned out to be reducible already at a relatively low temperature, due to which sintering could be avoided indeed, thus killing two birds with one stone.

Catalytic tests showed that catalysts prepared from high pH outperformed the catalysts prepared from low pH. Depending on the support material the activity increased with a factor 2-4. Remarkable high and stable C_{5+} selectivity of around 53 wt% was found for H-CNF, showing the good prospect for Fischer-Tropsch both of the synthesis route and the support material.

References

1. P.J. van Berge, J. van de Loosdrecht, S. Barradas, A.M. van der Kraan, Catal. Today 58 (2000) 321.
2. J.L. Li, G. Jacobs, T. Das, Y.Q. Zhang, B. Davis, Appl. Catal. A 236 (2002) 67.

3. C. Moreno-Castilla, F. Carrasco-Marin, J. Chem. Soc., Faraday Trans. 91 (1995) 3519.
4. R.C. Reuel, C.H. Bartholomew, J. Catal. 85 (1984) 78.
5. K.P. de Jong, J.W. Geus, Catal. Rev.-Sci. Eng. 42 (2000) 481.
6. P. Serp, M. Corrias, P. Kalck, Appl. Catal. A 253 (2003) 337.
7. G.L. Bezemer, A. van Laak, A.J. van Dillen, K.P. de Jong, Stud. Surf. Sci. Catal. 147 (2004) 259.
8. G.L. Bezemer, U. Falke, A.J. van Dillen, K.P. de Jong, Chem. Commun. (2005) 701, chapter 4 of this thesis.
9. M.L. Toebes, F.F. Prinsloo, J.H. Bitter, A.J. van Dillen, K.P. de Jong, J. Catal. 214 (2003) 78.
10. N. Spanos, L. Vordonis, C. Kordulis, A. Lycourghiotis, J. Catal. 124 (1990) 301.
11. O. Clause, M. Kermarec, L. Bonneviot, F. Villain, M. Che, J. Am. Chem. Soc. 114 (1992) 4709.
12. W.A. Spieker, J.R. Regalbuto, Chem. Eng. Sci. 56 (2001) 3491.
13. J.R. Regalbuto, M. Schrier, X. Hao, W.A. Spieker, J.G. Kim, J.T. Miller, A.J. Kropf, Stud. Surf. Sci. Catal. (2002) 45.
14. A.J. van Dillen, R. Terorde, D.J. Lensveld, J.W. Geus, K.P. de Jong, J. Catal. 216 (2003) 257.
15. J.A. Bergwerff, T. Visser, B.R.G. Leliveld, B.D. Rossenaar, K.P. de Jong, B.M. Weckhuysen, J. Am. Chem. Soc. 126 (2004) 14548.
16. A. Lekhal, B.J. Glasser, J.G. Khinast, Chem. Eng. Sci. 56 (2001) 4473.
17. E. Iglesia, Appl. Catal. A-Gen. 161 (1997) 59.
18. A.J. Van Dillen, J.W. Geus, L.A.M. Hermans, J. Van der Meijden, Proc. 6th Int. Congr. Catal. 2 (1977) 677.
19. L.A.M. Hermans, J.W. Geus, Stud. Surf. Sci. Catal. 3 (1979) 113.
20. P. Burattin, M. Che, C. Louis, J. Phys. Chem. B 102 (1998) 2722.
21. P. Burattin, M. Che, C. Louis, J. Phys. Chem. B 101 (1997) 7060.
22. K.P. de Jong, Stud. Surf. Sci. Catal. 63 (1991) 19.
23. P. Burattin, M. Che, C. Louis, J. Phys. Chem. B 103 (1999) 6171.
24. M. Keyser, F.F. Prinsloo, Carbon'01, Int. Conf. on Carbon, Lexington (2001) 1206.
25. F.F. Prinsloo, D. Hauman, R. Slabbert, Carbon'01, Int. Conf. on Carbon, Lexington (2001) 940.
26. J.H. Bitter, M.K. van der Lee, A.G.T. Slotboom, A.J. van Dillen, K.P. de Jong, Catal. Lett. 89 (2003) 139.
27. R.L.C. Bonne, C.M. Lok, WO Patent 9604072 (1996), to Crosfield Joseph & Sons.
28. C.M. Lok, Stud. Surf. Sci. Catal. 147 (2004) 283.

29. M.L. Toebes, J.H. Bitter, A.J. van Dillen, K.P. de Jong, Catal. Today 76 (2002) 33.
30. M.L. Toebes, J.M.P. van Heeswijk, J.H. Bitter, A.J. van Dillen, K.P. de Jong, Carbon 42 (2004) 307.
31. R.C. Reuel, C.H. Bartholomew, J. Catal. 85 (1984) 63.
32. C.F. Baes, R.E. Mesmer, The Hydrolysis of Cations, John Wiley & Sons, Inc., New York, USA, 1976, p. 240.
33. M.K. van der Lee, A.J. van Dillen, J.H. Bitter, K.P. de Jong, J. Am. Chem. Soc. 127 (2005) 13573.
34. M. Dixit, G.N. Subbanna, P.V. Kamath, J. Mater. Chem. 6 (1996) 1429.
35. J. Ismail, M.F. Ahmed, P.V. Kamath, G.N. Subbanna, S. Uma, J. Gopalakrishnan, J. Solid State Chem. 114 (1995) 550.
36. H.H. Willard, N.K. Tang, J. Am. Chem. Soc. 59 (1937) 1190.
37. P. Porta, R. Dragone, G. Fierro, M. Inversi, M. Lo Jacono, G. Moretti, J. Chem. Soc., Faraday Trans. 88 (1992) 311.
38. M.G. Mostafa, A. Matsumoto, K. Wase, Y. Kishi, Hydrometallurgy 57 (2000) 97.
39. A.A. Khassin, T.M. Yurieva, G.N. Kustova, L.M. Plyasova, T.A. Krieger, I.S. Itenberg, M.P. Demeshkina, T.V. Larina, V.F. Anufrienko, V.N. Parmon, Mater. Res. Innovations 4 (2001) 251.
40. K. Petrov, E. Deleva, O. Garcia-Martinez, Solid State Ion. 92 (1996) 303.
41. D. Mealor, A. Townshend, Talanta 13 (1966) 1069.
42. J.W. Geus, A.J. Van Dillen, Preparation of Solid Catalysts (1999) 460.

III

COBALT PARTICLE SIZE EFFECTS IN THE FISCHER-TROPSCH REACTION STUDIED WITH CARBON NANOFIBERS SUPPORTED CATALYSTS

The large influence of cobalt particle size on the performance of Fischer-Tropsch catalysts has been investigated for the first time on an inert support material in the full range of 2.6 to 27 nm using well-defined catalysts. X-ray Absorption Spectroscopy revealed that cobalt was metallic after the *in situ* reduction treatment, which is a prerequisite for catalytic operation and is difficult on traditional oxidic supports. The turn-over frequency (TOF) for CO-hydrogenation was independent of cobalt particle size for catalysts with sizes larger than 6 nm (1 bar) or 8 nm (35 bar), while both the selectivity and the activity changed for catalysts with smaller particles. At 35 bar the TOF decreased from $23 \cdot 10^{-3}$ s^{-1} to $1.4 \cdot 10^{-3}$ s^{-1} while the C_{5+} selectivity decreased from 85 to 51 wt% when the cobalt particle size was reduced from 16 to 2.6 nm. This demonstrates that the minimal required cobalt particle size for Fischer-Tropsch catalysis is larger (6-8 nm) than can be explained by classical structure sensitivity. Other explanations raised in literature, *viz.* formation of CoO or Co carbide species on small particles during catalytic testing, were not substantiated by experimental evidence with X-ray Absorption Spectroscopy. Interestingly, we found with EXAFS a decrease of the cobalt coordination number under reaction conditions, which points to reconstruction of the cobalt surface. Consequently, it is argued that the cobalt particle size effects can be attributed to CO-induced non-classical structure sensitivity. The profound influence of particle size may be important for the design of new Fischer-Tropsch catalysts.

Introduction

In the Fischer-Tropsch (FT) reaction CO and H_2 are catalytically converted into hydrocarbons via surface polymerization. Using this process clean transportation fuels can be produced from non-crude oil feedstocks, and therefore, the FT process receives much attention both in academia and industry [1-6].

Supported cobalt is well known for its catalytic activity and selectivity in the FT reaction, however, improvements in activity can be envisaged as commercial FT catalysts have cobalt particle sizes around 20 nm [7]. In the quest for the development of more active catalysts a rational strategy is to improve the cobalt dispersion by decreasing the average particle size. Bartholomew [8] and Yermakov [9,10] pioneered this field in 1984 and later on Iglesia and co-workers reported a large increase of activity when the cobalt particle size was decreased from 200 to 9 nm [11-13]. They showed that the surface-specific activity, often referred to as turn-over frequency (TOF), was not influenced by the cobalt particle size as such. However, going to even smaller cobalt particle sizes the results reported in the literature are more scattered. Several research groups have reported that the TOF suddenly decreased for catalysts with cobalt particle sizes smaller than 10 nm [8-10,14-22]. Other research groups did not observe this so-called cobalt particle size effect, while measuring catalysts with similar sizes [11-13,23-27]. This controversy points to the need of a systematic study on the influence of size on FT performance, in particular in the range below 10 nm using well-defined catalysts.

The chemical background of these cobalt particle size effects has remained largely unclear. Most authors assume the lower reducibility of small cobalt clusters to be responsible for the lower activity, but also carbide formation and structure sensitivity have been suggested as causes for the cobalt particle size effect [8,25,28-30]. It is likely that indeed in most of the studies the lower activities of catalysts with small particles were caused by low degrees of reduction as oxidic support materials were mainly used. With oxidic supports irreducible mixed oxides like cobalt aluminate or cobalt silicate can be formed during preparation and testing, especially when using highly dispersed catalysts [30-32]. However, this implies that the support material may have masked the cobalt particle size effects. This suggests that research focused on intrinsic cobalt particle size effects is advantageously performed using an inert support material, *viz.* graphitic carbon.

In order to study the intrinsic cobalt particle size effects on an inert support material we made use of graphitic carbon nanofibers (CNF), a pure and structured material with a large pore volume and surface area [33,34]. Recently, we showed the promising performance of Co/CNF catalysts for the FT reaction [14,35]. Here, we present a

comprehensive study of the preparation and FT performance of a series of catalysts with cobalt particle sizes varying from 2.6 to 27 nm. Characterization was done with TEM, TPR, H_2 chemisorption, XPS, X-ray Absorption Spectroscopy (XAS) and XRF. Catalytic performances for the FT reaction were measured both at 1 bar and at 35 bar in fixed bed reactors, while *in situ* XAS was done at the former pressure.

Experimental session

Support material

Carbon nanofibers of the fishbone-type with a diameter of about 30 nm were grown from synthesis gas (CO and H_2) using a 5 wt% Ni/SiO_2 growth catalyst. The preparation of the growth catalyst and the experimental growth conditions were previously described by Toebes *et al.* [36]. Treatments of these 'as synthesized' CNF for 2 h in 1M KOH and in concentrated HNO_3 resulted in purified and surface-oxidized CNF [37].

Catalyst preparation

Different preparation methods, *viz.* incipient-wetness impregnation (IWI), ion adsorption (IA) and homogeneous deposition-precipitation (HDP) were used in order to obtain a broad range of particle sizes with a relatively narrow particle-size distribution. Ion adsorption and incipient-wetness impregnation were used for the synthesis of highly dispersed catalysts with low cobalt loading, while HDP and impregnation were used for the preparation of highly loaded catalysts with intermediate dispersion.

Two samples with 9 and 11 wt% cobalt were prepared by homogeneous deposition-precipitation (HDP). In a double-wall vessel 0.41 g $Co(CO_3)\cdot 0.1H_2O$ (Acros) was dissolved in 12.5 g 25 wt% ammonia (Merck pure) to which 35.4 g demineralized water and 2.55 g $(NH_4)_2CO_3$ (Acros *p.a.*) were added (pH~10.9). After filtration 2.0 g support was suspended in the solution and nitrogen flushing (200 ml·min^{-1}) was started meanwhile the temperature was raised from room temperature to 90 ºC. After 18 h, the mixture was cooled to room temperature (pH=8) and subsequently filtered. The solid was washed three times with demineralized water and dried at 120 ºC in air and was coded HDP9. The other sample (HDP11) was prepared from 5 g CNF suspended in 220 ml demineralized water to which 4.35 g $Co(NO_3)_2\cdot 6H_2O$ was added. The temperature was increased to 90 ºC, after which 2.70 g urea (Acros *p.a.*) in 30 ml was added. After 18 h the reaction was complete, the sample was collected as described above for HDP9.

Nine samples were prepared by incipient-wetness impregnation (IWI) for which we first determined the total pore volume of the CNF by adding demineralized water to de-

gassed CNF with a syringe until the support had a sticky appearance. Typically, 3 g of de-gassed CNF was impregnated with 2.34 ml aqueous solution containing either cobalt nitrate or cobalt acetate. Five catalysts were prepared using ethanol (Merck p.a.) as solvent and $Co(NO_3)_2 \cdot 6H_2O$ as precursor. Special care was taken in the latter case to prevent boiling of ethanol by working at 25 mbar and 5 ºC, while for aqueous impregnations 7 mbar and 25 ºC were used. Samples prepared by incipient-wetness impregnation were coded with three letters indicating method, solvent and precursor followed by the cobalt loading, *e.g.* IEN5 referring to a 5 wt% catalyst prepared by impregnation with cobalt nitrate dissolved in ethanol. A survey of all the catalysts with their designations and cobalt loadings is given in table 1 in the results and discussion section.

One sample was prepared using an ion adsorption method. The cobalt solution was prepared by dissolving 0.32 g $CoCO_3 \cdot 0.1H_2O$ and 2.46 g $(NH_4)_2CO_3$ in 250 ml of a diluted aqueous ammonia solution (pH 11.2). In this dark-red solution 3 g of CNF was suspended and stirred for 24 h at room temperature. After filtration the sample encoded IOC1 was obtained.

All catalyst precursors were dried overnight in air at 120 ºC. Catalysts were obtained after a 2 h reduction treatment at 350 ºC using 10% H_2/N_2. This reduction temperature was selected from TPR experiments (data not shown) where reduction onsets of cobalt(II) oxide were apparent around 300 ºC. Reduction of the catalysts was followed by a passivation treatment at room temperature using a diluted (0.1%) oxygen flow.

Catalyst characterization

X-ray fluorescence experiments to determine the cobalt loading on the support were carried out on a Goffin Meyvis spectro X-lab 2000.

N_2 physisorption measurements were performed using a Micromeritics Tristar Surface Area and Porosity analyzer with samples previously out-gassed at 393 K.

Reduced and passivated samples were examined with transmission electron microscopy (TEM) in an FEI Tecnai12 or in an FEI Technai20F. TEM samples were crushed and suspended in ethanol under ultrasonic vibration. A drop of this suspension was brought onto a holey carbon film on a copper TEM grid. Metal particle sizes from TEM reported in table 1 are surface-area averaged values (~200 particles) that have been corrected for the presence of a ~3 nm CoO layer on the passivated Co particles.

The XPS data for passivated sample were obtained with a Vacuum Generators XPS system using Al-K_α radiation. Shirley backgrounds were subtracted from the raw data to obtain the areas of the C_{1s} and the Co_{2p} peaks. The C_{1s} peak at 284.2 eV was used to correct for charging effects (max. 0.2 eV). The inelastic mean free path of photoelectrons

generated inside cobalt oxide is only 1.4 nm, so the intensity ratio I_{Co}/I_C can be used to calculate the metal(oxide) dispersion. Calculations to determine the cobalt dispersion of the catalysts were based on the papers by Kuipers *et al.* [38,39] and performed with XPSCAT [40] assuming hemi-spherical cobalt oxide particles. In a previous paper we showed that cobalt present in the inner tubes of the CNF (<15%) does not contribute to the Co signal, so we corrected for either the pore volume or the surface area of the inner tubes [41]. Particle sizes from XPS reported in table 1 have also been corrected for the contraction of CoO to Co that occurs upon reduction to enable comparison with values obtained with H_2 chemisorption.

Hydrogen chemisorption measurements were carried out using a Micromeritics ASAP 2010C. Before each measurement the sample was dried in vacuum at 120 ºC overnight. Samples were subsequently heated in flowing H_2 with a heating rate of 5 ºC/min to the reduction temperature of 350 ºC. A reduction time of 2 h was used, after which the samples were evacuated at that temperature for 30 minutes. The H_2-adsorption isotherms were measured at 150 ºC. The H/Co ratios at zero pressure were found by extrapolation of the linear part of the isotherm. Particle size estimations are based on hemi-spherical geometry, assuming complete reduction and an H/Co_s adsorption stoichiometry of 1, using the formula: $d = 81.6 * W/X$, with d the cobalt particle diameter (nm), W the weight percentage of cobalt and X the total H_2 uptake in micromoles per gram of catalyst [42].

X-ray Absorption Spectroscopy (XAS) data were measured in transmission at beam-line E4 of HASYLAB synchrotron in Hamburg. The beam-line was equipped with a Si(111) double crystal monochromator which was detuned to 60% of the maximum intensity to avoid higher harmonics. A cobalt foil was simultaneously measured as a reference with a third ionization chamber. Samples were reduced *in situ* in N_2/H_2 (2/1 v/v) in a dedicated cell and cooled down to liquid-nitrogen temperature to measure the EXAFS. Subsequently the temperature was slowly raised to 220 ºC and the gasses were switched to CO/H_2 (1/2 v/v) while measuring XANES. After 1 h of FT reaction the gas was changed to He and cooled down to liquid nitrogen to record the EXAFS spectra.

Spectra of cobalt foil, CoO and Co_3O_4 were measured as references. Extraction of the EXAFS data from the measured absorption spectra was performed with the XDAP code using standard procedures, averaging over three scans [43,44]. Normalization was done at 50 eV after the absorption edge using cubic spline routines for the background subtraction. Data for phase shifts and backscattering amplitudes for Co-Co and Co-O were obtained from FEFF8 calculations and calibrated by the experimental data of Co foil and CoO. Data analysis of the Co/CNF catalysts was performed by multiple shell fitting

of the data applying k^1 and k^3 weighting using the difference file technique in R space (1.8 to 2.6 Å) with the XDAP code [43,44].

Catalytic testing

Catalysts were tested at atmospheric pressure and at 35 bar. The measurements at 1 bar were carried out at 220 ºC using CO/H_2 (1/2 v/v) after a reduction treatment at 350 ºC for 2 h in H_2 flow. Typically 50 mg of catalyst particles (0.5-1.0 mm) was diluted with 200 mg SiC particles (0.2 mm) to achieve isothermal plug-flow conditions. Gas chromatography (GC) was used for online product analysis and to establish weight selectivities towards methane (C_1) and towards products with chain length of 5 and higher (C_{5+}). Catalysts were measured atmospherically at a CO-conversion of 2%, which was achieved by tailoring the space velocity. For the high-pressure measurements 0.25 g catalyst (150-212 μm) was diluted with 0.5-0.7 g SiC. Catalytic data were obtained at 210 ºC and a pressure of 35 bar using a flow of $CO/H_2/N_2$ (33/66/6). The space velocity was adjusted to maximize CO conversions at around 60%. Both online and offline product analysis was performed with GC. Reported catalytic data were obtained after at least three days of operation.

Results and Discussion

Characterization of the support

The CNF were fishbone type with the graphene sheets oriented in a angle to the main axis of the fiber [33]. The fibers possessed an average external diameter of 30 nm and an inner core with a diameter of 7 nm (*cf.* figure 1). From nitrogen physisorption a total BET surface area of 161 m^2/g was found. The samples did not contain micropores and the total mesopore volume was 0.68 ml/g. A pore volume of 0.78 ml/g was found when demineralized water was added to the support until they had a sticky appearance. The microscopic fibers were interwoven and had grown into macroscopic particles with an average size of 2 mm. The density of a packed bed of this support material amounted to 0.47 g/ml.

Cobalt particle size

The cobalt metal loadings (XRF) varied from 0.77 to 22.0 wt% in the final catalysts. For the impregnated catalysts the loading measured with XRF was very close to the value calculated from the cobalt intake.

Table 1. Sample codes, preparation methods, cobalt loadings and metallic cobalt particle sizes as determined by H_2 chemisorption, XPS and TEM of the various CNF-supported catalysts after reduction at 350 ºC.

Sample	Method, solvent	Precursor	Co (wt%)	H_2 ads.	Co/C (at/at)	H_2 (nm)	XPS (nm)	TEM (nm)
HDP11	HDP	Nitrate	11	36	0.010	25	27	~30
HDP9	HDP	Carbonate	9.0	53	0.021	12.5	12.8	14
IWN22	IWI, water	Nitrate	22	111	0.047	16	16	-
IWN13	IWI, water	Nitrate	13	124	0.031	8.5	8.5	7.5
IWN10	IWI, water	Nitrate	9.9	82	0.022	9.8	10	-
IEN8	IWI, ethanol	Nitrate	7.5	89	0.023	6.9	5.9	-
IEN5	IWI, ethanol	Nitrate	5.4	91	0.017	4.9	5.3	-
IEN4	IWI, ethanol	Nitrate	3.7	69	0.013	4.4	4.7	3.6
IEN1	IWI, ethanol	Nitrate	1.1	20	0.0036	4.3	4.5	-
IWA4	IWI, water	Acetate	4.2	54	0.015	6.1	4.1	3.7
IWA1	IWI, water	Acetate	1.0	2.5	0.0073	n.a.	2.6	2.5
IOC1	IA, water	Carbonate	0.8	13	0.0034	5.5	3.0	-

H_2 ads.: $\mu mol_{H2} \cdot g_{Cat}^{-1}$ Co/C obtained from XPS

Four techniques were used to determine the cobalt particle sizes of the catalysts, because all have their limitations. The cobalt particle size calculated from the hydrogen chemisorption varied from 4.3 to 25 nm (table 1). In addition to chemisorption we used quantitative XPS to measure the cobalt dispersion. The Co/C atomic ratios varied from 0.0034-0.047 from which cobalt particle sizes varying from 2.6 to 27 nm were obtained (table 1). Catalysts prepared by HDP possessed the largest cobalt particle sizes, followed by samples obtained with impregnation. Cobalt size for impregnated catalysts decreased with cobalt weight loading and was even lower when ethanol was used as solvent, as in this case better wetting with the CNF surface was achieved. Very small cobalt particles of around 3 nm were obtained with cobalt acetate as precursor, which is a chelating ligand that often favors dispersion [45] and with ion adsorption.

With TEM we found that the particle-size distributions in the catalysts were rather narrow with standard deviations of at most 20% of the average size. In the figures 1 to 4 representative TEM images are shown for HDP9, IEN8, IEN4 and IWA1 after reduction and passivation. In figure 1 rather long fibers are visible that have been decorated with cobalt particles. In the HR-TEM image of IEN8, depicted in figure 2, apart from the graphite layers with lattice distance of 0.34 nm the smaller lattice distance of CoO (0.21 nm) is visible, pointing towards reoxidation during the passivation treatment. In figure 3 cobalt particles with uniform diameters are found for IEN4 both at medium and at high

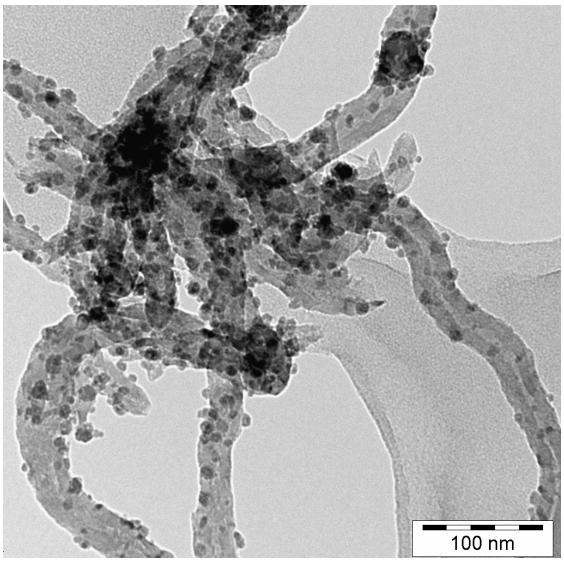

Figure 1. TEM image of HDP9 showing particles with sizes of around 14 nm distributed over the fibers.

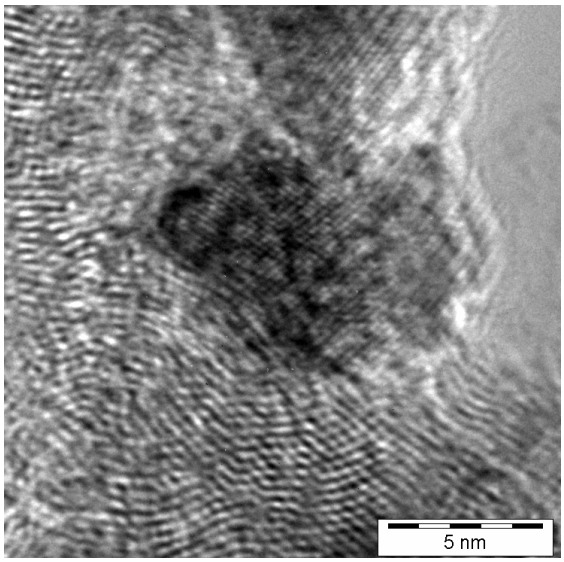

Figure 2. HR-TEM image of reduced and passivated IEN8 showing the graphite lattice (0.34 nm) and lattice planes of CoO (0.21 nm).

A

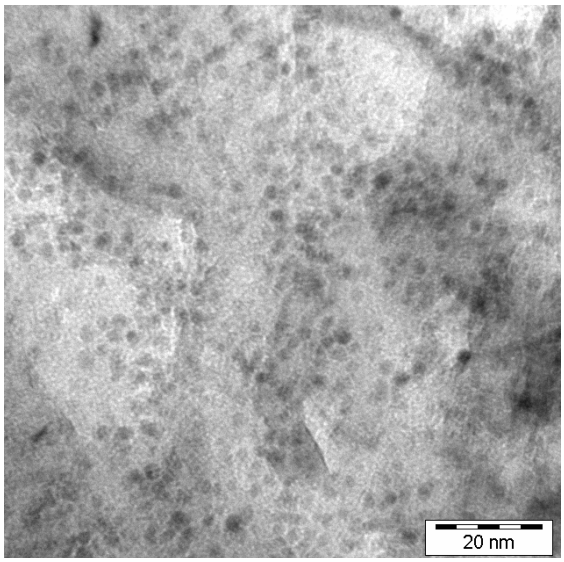

B

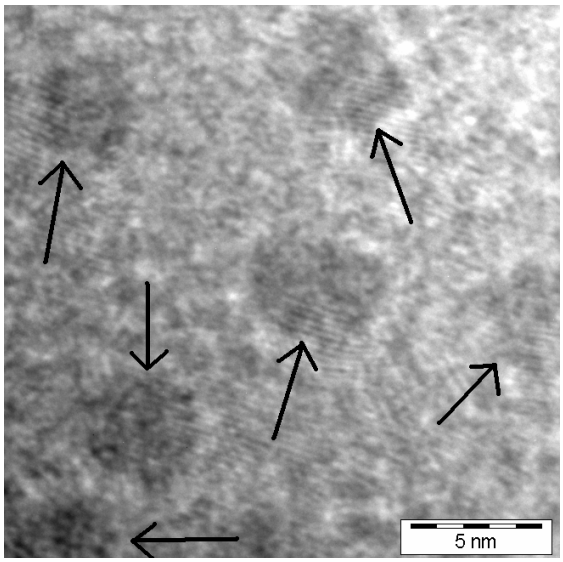

Figure 3. TEM images of reduced and passivated IEN4 showing spherical cobalt oxide particles distributed over the support at (A) medium resolution and (B) high resolution; particles of ~4 nm indicated by arrows.

resolution. Very small particles are found in IWA1 (figure 4) with limited contrast in the TEM because the particles had been re-oxidized completely.

Also from the EXAFS data of the *in situ* reduced IWA1 and IEN4 (table 2) we could obtain cobalt particle sizes. The obtained Co-Co coordination numbers were 9.5 (IWA1) and 10.1 (IEN4) that correspond to particle sizes of 1.7 and 2.7 nm respectively [46]. The

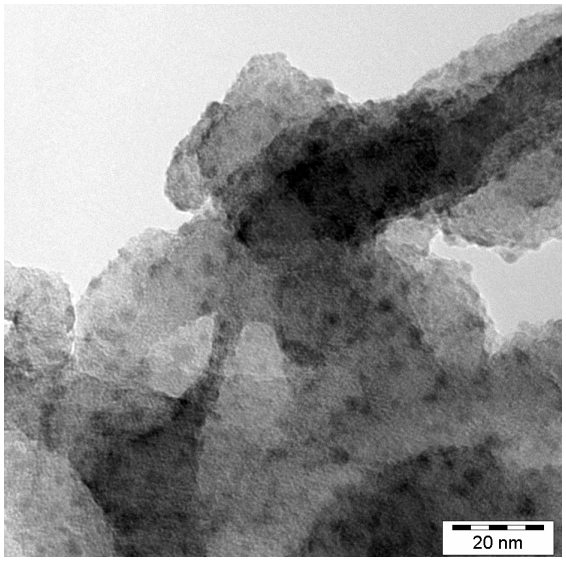

Figure 4. TEM image of IWA1 showing the presence of small cobalt oxide particles distributed over the support.

error in the coordination number found with EXAFS is estimated to be around 10% [47]. For our catalysts, with rather high coordination numbers, this results in a particle size range from 1.2 to 3 nm for IWA1 and from 1.3 to 5 nm for IEN4.

For catalysts with moderate to large XPS particle sizes (4.5-27 nm) a close agreement with the results of hydrogen chemisorption was found, which was further supported by TEM (table 1). For the catalysts with sizes smaller than 4.5 nm a discrepancy with the results obtained with hydrogen chemisorption was found. Since the TEM results coincide with the XPS the latter values can be used for all catalysts. Hydrogen chemisorption uptake depends on temperature [42], and the low uptake for samples with small cobalt particles might indicate that they require a different measurement temperature. The particle sizes found with EXAFS for IWA1 and IEN4 display considerable uncertainty but are in agreement with sizes from XPS. In the remaining of this paper particle sizes reported have been based on XPS unless stated otherwise.

Table 2. Fit parameters of the first Co-Co shell of IEN4 and IWA1 after *in situ* reduction ('Red') and after 1 h *in situ* catalysis ('FT') (Δk:3.3-12 Å^{-1}, ΔR: 1.8-2.6 Å). The cobalt particle size and size range have been derived from N and N$\pm\Delta$N, respectively.

Catalyst	N	R (Å)	$\Delta\sigma_2$ (Å^2)	ΔE_0 (eV)	k^3-variance		Size (nm)
					Im.	Abs.	
IEN4 Red	10.1	2.48	$9.9\cdot10^{-4}$	-0.78	0.0042	0.0150	2.7 (1.3-5)
IEN4 FT	9.5	2.48	$1.3\cdot10^{-3}$	0.92	0.0048	0.0120	
IWA1 Red	9.5	2.48	$7.7\cdot10^{-4}$	-1.00	0.0025	0.0051	1.7 (1.2-3)
IWA1 FT	8.8	2.48	$8.8\cdot10^{-4}$	-1.01	0.0077	0.0125	

Chemical state of cobalt prior to catalytic testing

The Fischer-Tropsch reaction proceeds only on metallic cobalt, however, incomplete reduction is often the case, especially with small cobalt precursor particles, resulting in Co^{2+} still being present after the reduction treatment [48]. Therefore, we studied the bulk oxidation state of cobalt of two highly dispersed catalysts with XAS. In figure 5 the XANES spectra of IWA1 and IEN4 measured after *in situ* reduction are plotted together with reference spectra of CoO and Co foil. The reference compounds are markedly different from each other with a far more intense absorption around 7725 eV for CoO as compared to Co. The XANES spectra of IEN4 and IWA1 (sizes: 4.7 and 2.6 nm) closely resembled the cobalt foil, with only a small difference in the 7725-7735 eV region. The foil showed here two peaks that were well resolved with a higher intensity for the second one, while for the catalysts these peaks were flattened and had similar heights. This difference can be related to different crystal structures in catalysts and foil. The cobalt foil displays the characteristics of the hcp structure, while the pattern of the catalysts can be explained by the presence of a mixture of fcc (stable only for small particles) and hcp or bcc cobalt [42,49]. If these catalysts contain some CoO it was estimated to be less than 3% using linear combinations of CoO and Co foil.

The EXAFS results in table 2 show a Co-Co bond distance of 2.48 Å, which is slightly lower than the bulk distance of 2.49 Å we measured for the cobalt foil. From the Fourier

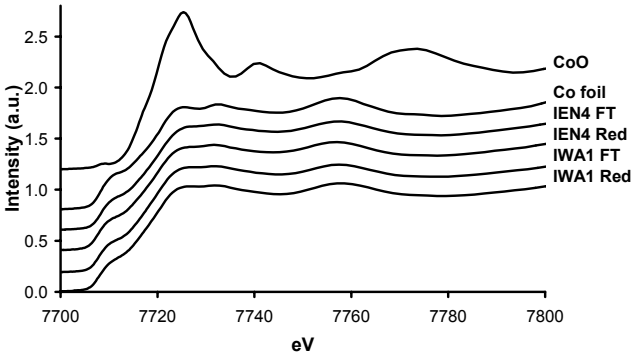

Figure 5. Normalized XANES spectra after *in situ* reduction ('Red') and after *in situ* FT ('FT') synthesis for IEN 4 and IWA1 plotted together with spectra of CoO and Co foil.

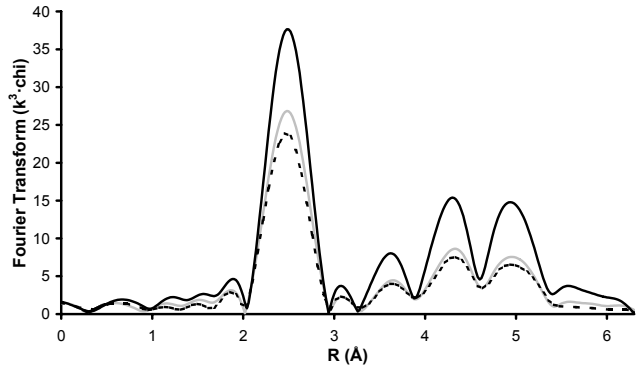

Figure 6. Fourier transform magnitude of the phase-corrected EXAFS data of the cobalt foil (black), IEN4 after *in situ* reduction (grey) and IEN4 after 1 h of catalytic testing (dashed).

transform magnitudes of cobalt foil and IEN4 (figure 6) it can be seen that IEN4 has a lower intensity at the first Co-Co shell at 2.5 Å. The ratio of peak intensity between foil and IEN4 is even larger at higher R values, indicative for small particles. Using the difference file technique no Co-O or Co-C contributions were found in the data, showing that, within the experimental error of 10%, the samples were metallic.

Chemical state of cobalt during and after catalytic testing

The cobalt oxidation state of the catalysts IEN4 and IWA1 was measured with XANES under reaction conditions at 1 bar, 220 °C. With this technique we did not detect any changes during the first hour of operation (data not shown). Spectra with better quality were obtained measuring at liquid nitrogen temperature. These spectra before and after catalytic testing are shown in figure 5 and also don't exhibit a change. However, the fourier transform of the k^3 weighted spectra (figure 6) did change considerably as the intensity of the peaks decreased significantly, indicating the decrease of coordination number of the cobalt atoms. The full EXAFS analysis revealed that the coordination number of the first Co-Co shell decreased with 6-7% after the FT synthesis and the Debye Waller factor increased, while other parameters were not influenced (table 2). These changes indicate a reconstruction of the cobalt surface during FT synthesis (see General Discussion).

In IWA1 and IEN4 the fraction of cobalt present at the surface can be calculated to be 36 and 21% respectively, which implies that surface oxidation during FT synthesis would give rise to a substantial increase of the peak at 7725 eV and the formation of Co-O contributions in the EXAFS spectra. The absence of these changes indicates that neither bulk oxidation nor substantial surface oxidation occurs during FT operation.

Catalytic performance at 1 bar

Activity and selectivity were measured at 2% CO conversion (except IWA1 and IOC1) and values of the catalysts are listed in table 3. In Figure 7 the cobalt-specific activity is plotted versus the cobalt particle size. Going from 27 nm (HDP11) to about 6 nm (IEN8) the activity increases from 0.64 to $3.51 \cdot 10^{-5}$ $mol_{CO} \cdot g_{Co}^{-1} \cdot s^{-1}$. This increase in activity correlates well with the higher specific cobalt surface areas. For catalysts with cobalt particle sizes smaller than 6 nm the activity decreases quite rapidly to $0.80 \cdot 10^{-5}$ $mol_{CO} \cdot g_{Co}^{-1} \cdot s^{-1}$ for IWA1. The surface specific activities (TOF) were calculated using both the dispersion obtained from H_2 chemisorption (HTOF) and that from XPS (XTOF) and are given in table 4. The TOF data based on the XPS dispersion have been plotted in figure 8 from which it becomes clear that the TOF is rather constant with a value around 10^{-2} s^{-1}

Table 3. Catalytic properties measured at 220 °C, $H_2/CO=2$, 1 bar.

Sample	Activity (CTY)	HTOF (10^{-3} s^{-1})	XTOF (10^{-3} s^{-1})	C_1 (wt%)	C_{5+} (wt%)	P/O_8 (mol/mol)
HDP11	0.64	9.6	10.6	42	23	13
HDP9	1.27	10.5	9.7	22	50	2.0
IWN22	1.21	12.0	11.5	41	24	13
IWN13	2.17	11.4	11.3	39	28	11
IWN10	1.74	10.5	10.7	40	28	11
IEN8	3.51	14.9	12.2	40	30	13
IEN5	2.51	7.5	8.0	41	30	21
IEN4	2.19	5.9	6.6	49	25	27
IEN1	0.96	2.5	2.7	51	20	51
IWA4	1.46	5.4	3.8	47	24	55
IWA1	0.80	15.2	1.3	53	18	40
IOC1	0.79	2.3	1.5			52

CTY = 10^{-5} mol_{CO} g_{Co}^{-1} s^{-1}
HTOF is based on dispersion H_2 chemisorption
XTOF is based on dispersion XPS

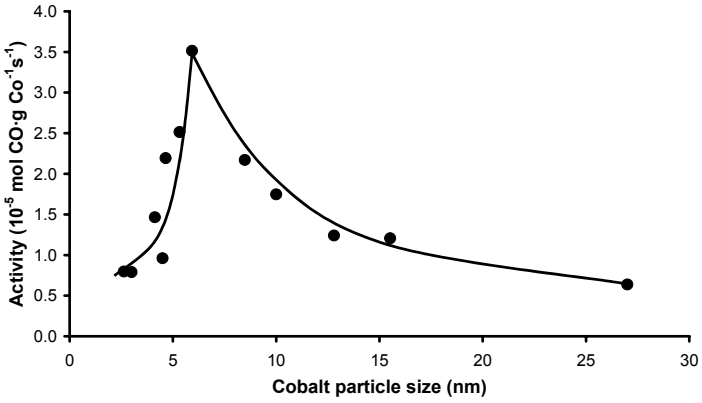

Figure 7. The influence of cobalt particle size on activity normalized to the cobalt loading (220 ºC, $H_2/CO=2$, 1 bar).

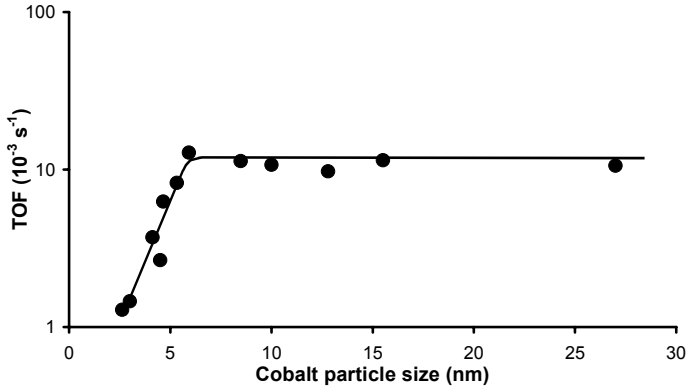

Figure 8. The influence of cobalt particle size on the TOF (220 ºC, $H_2/CO=2$, 1 bar).

for cobalt particles ranging from 6 to 27 nm. For smaller particle sizes the TOF steeply decreases to a value close to 10^{-3} s^{-1} for IWA1.

At 1 bar total pressure a methane selectivity of around 41 wt% and a C_{5+} selectivity of around 25 wt% were observed (table 3). The catalyst HDP9 exhibited a superior selectivity compared to all the other catalysts, with a methane selectivity of only 22 wt% and a C_{5+} selectivity of 50 wt%, which are typical for promoted catalysts [35]. Catalysts prepared with this method are currently under investigation to explain this behavior. In figure 9 the methane selectivity is plotted as a function of cobalt particle size, excluding HDP9. It is clear that all catalysts with sizes smaller than 5 nm have progressively higher methane selectivity. For catalysts with high methane selectivities also lower chain growth probabilities were found, resulting in an even lower selectivity to heavy weight hydrocarbons. The formation of methane indicates that dissociated hydrogen is abundantly present on the catalyst surface. The higher selectivity to methane might also indicate a lower abundance of sites active for chain growth, resulting in more carbon species at the surface that become fully hydrogenated to methane.

Another difference in the catalytic performance of the catalysts is the selectivity to olefins and paraffins. In table 3 and in figure 10 the relation between cobalt particle size and the octane/octene ratio is given. The paraffin/olefin ratio at C_8 was found to be

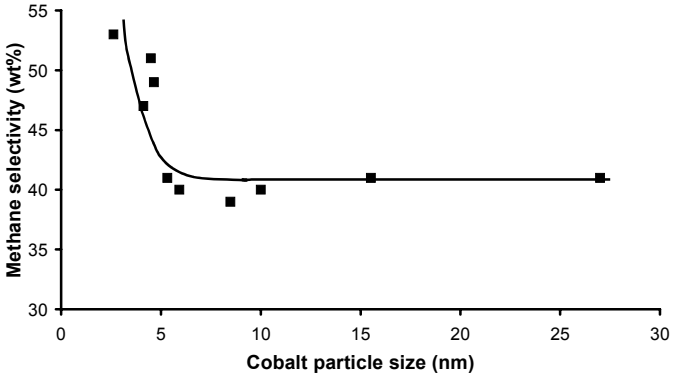

Figure 9. The influence of cobalt particle size on methane selectivity (220 ºC, H_2/CO=2, 1 bar).

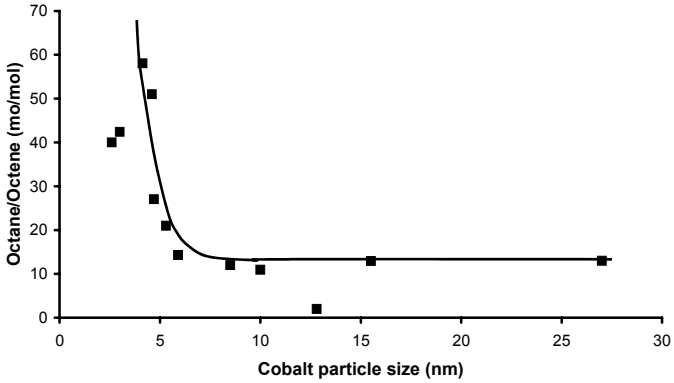

Figure 10. The influence of cobalt particle size on hydrogenation (220 ºC, H_2/CO=2, 1 bar).

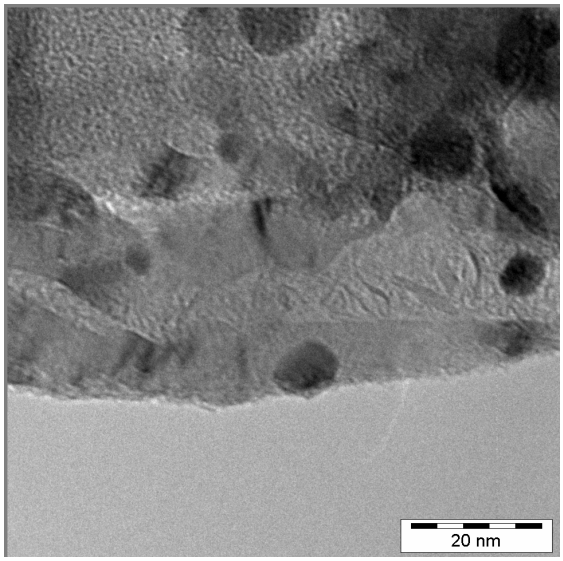

Figure 11. TEM image of spent HDP9 indicating the absence of sintering.

representative for other carbon numbers too. Catalysts with a high C_{5+} selectivity like HDP9 had a much lower octane/octene ratio than the average value of 11 in this study. The general trend valid for all samples is that catalysts with cobalt particles smaller than 8 nm show a substantial increase of the paraffin over olefin ratio. The shift towards paraffins might indicate higher primary hydrogenation activities as it parallels the higher methane selectivity. However, part of the higher paraffin over olefin ratio could stem from different degrees of secondary hydrogenation caused by differences in space velocity in the catalytic tests [13]. Other possible causes for differences in secondary hydrogenation, like diffusional limitations [50] can be excluded.

Spent catalysts contained SiC, making analysis with XPS, XRD and H_2 chemisorption cumbersome. Therefore, we used transmission electron microscopy to get an impression of cobalt dispersion after catalytic testing. In figure 11 an image of HDP9 is shown obtained after 2 days of catalytic testing. The cobalt particles are similarly sized as in the fresh sample (figure 1) indicating the absence of sintering during catalytic operation. Also for other catalysts we did not find larger cobalt particles in the spent catalyst, which indicates that the differences in catalytic performance are not induced by a particle-size dependent sintering under reaction conditions.

Catalytic performance at 35 bar

Five catalysts with particle sizes ranging from 2.6 to 13 nm were also studied at industrially relevant conditions (35 bar). We aimed for CO-conversions of around 60%, however, this was not possible for IWA1 and IEN4, catalysts with both small cobalt particle sizes and low metal loadings. Slight deactivation was found with IWN22, while this was absent for the other catalysts. Table 4 lists the performances obtained at 210 °C

Table 4. Catalytic properties measured at 210 °C and at 250 °C, $H_2/CO=2$, 35 bar.

Sample	Temp. (ºC)	% CO Conv.	Activity (CTY)	XTOF (10^{-3} s^{-1})	C_{5+} (wt%)	CO_2 (%)	WTY
IWN22	210	61	14.0	22.6	84.6	2.7	268
IWN13	210	66	25.6	22.5	81.7	1.7	290
IEN8	210	65	21.8	13.5	76.1	1.8	145
IEN8	250	84	56.3	34.8	74.0	4.9	723
IEN4	210	10	7.0	3.4	-	23.7	21
IEN4	250	67	45.3	22.0	60.9	8.5	151
IWA1	210	4.3	5.2	1.4	-	11.0	6
IWA1	250	13	33.8	9.4	50.7	5.1	26

CTY = 10^{-5} mol_{CO} $\cdot g_{Co}^{-1}$ $\cdot s^{-1}$
XTOF is based on dispersion from XPS
WTY= g_{CH2} $\cdot kg_{cat}^{-1}$ $\cdot h^{-1}$
CO_2 = % of CO-conversion

for all five catalysts, and also at 250 °C for IWA1, IEN4 and IEN8. The activities at 210 ºC varied from 5.2 to 25.6·10^{-5} mol_{CO} $\cdot g_{Co}^{-1}$ $\cdot s^{-1}$ and were dependent on cobalt particle size. In figure 12 the TOF values at 210 ºC have been plotted versus the cobalt particle size. The TOF was constant for the samples with cobalt particle sizes larger than ~8 nm, whereas it started to decrease for catalysts with smaller sizes. We have added in figure 12 data from Iglesia *et al.* [13], which nicely coincide with our data for larger particles. Exploiting the benefits of an inert support material we succeeded to study smaller particles that, however, revealed the far lower activities. Using these results we comment on recent claims concerning the performance of Co/Al_2O_3 catalysts with 3-5 nm cobalt crystallites [24]. As the author did not report a particle size effect, we expect that his actual cobalt particle sizes were larger, around 8 nm. With this value, the reported activities and results from hydrogen chemisorption can be rationalized [24].

It can be seen by comparison of figures 8 and 12, that the catalytic data at 1 bar and at

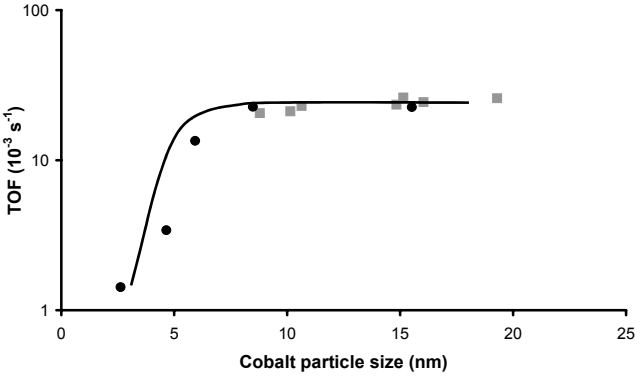

Figure 12. The influence of cobalt particle size on the TOF at 35 bar, 210 ºC in black, data obtained from ref. 13 are plotted in grey for comparison.

35 bar of pressure show the same general trend, with constant TOF for larger Co particles and size dependency for smaller crystallites. However, the catalyst with the optimum particle size at 1 bar (IEN8, 6 nm) showed a lower TOF at 35 bar, which might indicate that the influence of particle size on performance is somewhat different at elevated pressure.

All the catalysts displayed some activity towards formation of CO_2 via the water-gas-shift reaction. The selectivity varied from 1.7 to 24 % of CO converted and was larger for the catalysts with lower activity, although no relation with particle size could be derived. The C_{5+} selectivity (figure 13) was also clearly dependent on cobalt particle size and varied from 76 to 84 wt% at 210 ºC and from 51 to 74 wt% at 250 ºC with higher selectivities for larger particles. Furthermore, the product distribution of IWN22 (16 nm) was more shifted towards the heavy hydrocarbons than IWN13 (~8 nm), i.e. a larger chain growth probability α, as becomes clear from figure 14. Note that the differences in selectivity are apparent for cobalt sizes larger than ~8 nm, where the activity was not influenced by size (compare figure 12 and 13). One of the possible explanations of part of these differences is the four-fold variation of the cobalt site density in the catalysts, which has been reported to affect the C_{5+} selectivity [51]. Based on these literature data the differences in cobalt site density can account for at most 10% change in C_{5+} selectivity, which is about

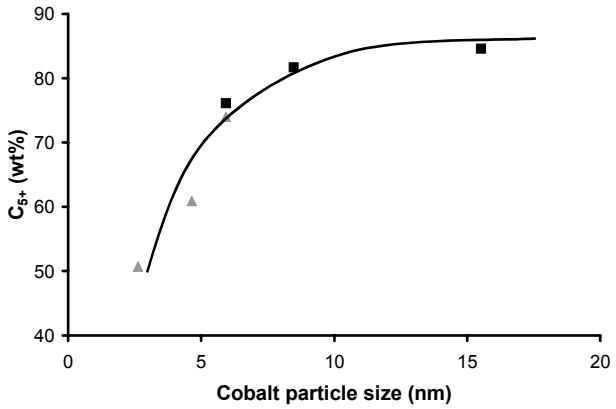

Figure 13. The influence of cobalt particle size on the C_{5+} selectivity measured at 35 bar; data markers in black at 210 ºC and in grey at 250 ºC.

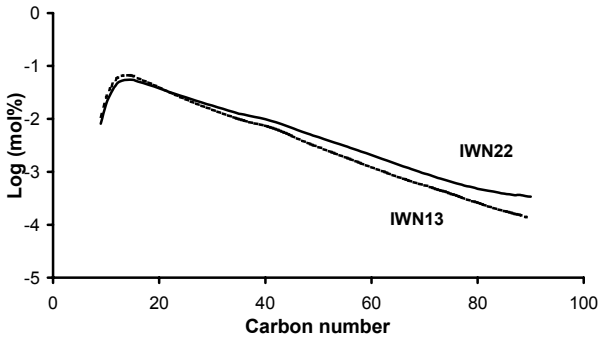

Figure 14. Product distribution of hydrocarbons collected in hot trap of IWN13 (dashed line) and IWN22 (solid line) after operation at 35 bar, 210 ºC.

half of the current observation. The CO conversion level may have serious impact on selectivity too, but it was possible for all but one (IWA1) catalysts to reach similar CO conversions. Therefore, we ascribe the large differences in selectivity predominantly to the variation in the cobalt particle sizes of the catalysts.

General Discussion

In the literature the change of the catalyst structure during FT reaction has been mentioned, resulting in the formation of either cobalt oxides or cobalt carbides [13,25,28-31,52-55]. Small particles seem to be more susceptible to oxidation than larger particles and oxidation during high pressure catalytic testing has been reported to occur for catalysts with cobalt sizes smaller than 6 nm [13]. Recent thermodynamic calculations for a p_{H2O}/p_{H2} ratio of 1.5 (75% CO conversion) have shown that cobalt particles smaller than 4 nm can be oxidized during FT operation [53]. In our measurements at high pressure, oxidation of cobalt could proceed for the two catalysts with smallest sizes. The catalytic tests at 1 bar and 2% CO conversion, resulted in p_{H2O}/p_{H2} ratios (0.03) that do not enable the oxidation of cobalt. More importantly, during our *in situ* XAS experiments no formation of CoO was observed for catalysts with small particle sizes.

Also the formation of cobalt carbide species is a possible deactivation mechanism. For example XPS studies after *in situ* catalytic testing have shown the presence of carbides on cobalt single crystals [25,28]. However, carbide formation with (small) cobalt crystals was not observed in our *in situ* XAS measurements.

To rationalize particle size effects, the influence of surface structure has been treated by Van Hardeveld and Hartog [56]. Using models the authors evaluated the fraction and type of surface atoms formed as a function of crystal size. They conclude that for metal particles with sizes below about 4 nm differences in specific activity can arise because different sites are exposed. The observed cobalt particle size effect in our work was present for catalysts with sizes up to ~8 nm, and hence cannot be explained by conventional structure sensitivity.

We ascribe the influence of cobalt particle size on FT performance to non-classical particle size effects, caused by the invasive character [57] of CO during catalytic testing. Wilson and De Groot [58] demonstrated by scanning tunneling microscopy the strong impact of synthesis gas on cobalt surfaces. Exposure of Co(0001) single crystals to synthesis gas at 4 bar caused severe surface reconstruction. Cobalt islands of about 1.75 nm size and with a single-atom height were formed on the surface, which were subsequently converted into larger triangular-shaped islands. In our EXAFS analysis we

measured a decreased CO coordination number due to synthesis gas feeding to Co/CNF, pointing towards catalyst reconstruction, and which is probably related to a change in particle shape. This is comparable to flattening of copper particles supported on ZnO upon reduction [59,60]. Our results show that also with supported Co particles the actual catalyst is created *in situ*. However, a certain cobalt particle size is needed to be able to create the domains that contain the active sites for the FT synthesis. On small cobalt particles the radial curvature is too high to be able to facilitate the formation of the islands of 1.75 nm. Concluding, we can state that CO-induced non-classical structure sensitivity explains our data very well and is of importance in the design of new generation FT catalysts.

Conclusions

Using different synthesis methods and different weight loadings a series of cobalt on carbon nanofiber catalysts with cobalt particle sizes varying from 2.6 to 27 nm was prepared. The catalytic performance in the Fischer-Tropsch reaction was independent of cobalt particle size for catalysts with sizes larger than 6 nm (1 bar) or 8 nm (35 bar) but both activity and selectivity were strongly affected for catalysts with smaller cobalt particles. At 35 bar the turn-over frequency decreased from $23 \cdot 10^{-3}$ s^{-1} to $1.4 \cdot 10^{-3}$ s^{-1}, while the C_{5+} selectivity decreased from 85 to 51 wt% when the particle size was decreased from 16 to 2.6 nm. It is interesting to note that the catalytic data obtained at 1 bar were in good agreement with data at high pressure, which shows the relevance of these measurements.

XAS data showed that both the reduced and the working catalysts were metallic and did not contain a measurable amount of cobalt carbides. The Co-Co coordination number decreased after exposure to synthesis gas, which points towards catalyst reconstruction. Therefore it was argued that the cobalt particle size effect has to be ascribed to CO-induced non-classical structure sensitivity. Cobalt based FT catalysts need a particle size of about 6 nm in order to create optimal active sites.

The presented data have a large consequence for the preparation of active cobalt-based Fischer-Tropsch catalysts. Synthesis should aim for catalysts with average cobalt particle sizes close to the optimum values of 6-8 nm, with a narrow cobalt particle size distribution, as both larger and smaller particles display a lower activity. Smaller particles exhibit also a lower C_{5+} selectivity, so an optimum should be sought between activity and chain growth probability.

References

1. S.E. Colley, R.G. Copperthwaite, G.J. Hutchings, S.P. Terblanche, M.M. Thackeray, Nature 339 (1989) 129.
2. H. Schulz, Appl. Catal. A 186 (1999) 3.
3. S.J. Jenkins, D.A. King, J. Am. Chem. Soc. 122 (2000) 10610.
4. M.E. Dry, Catal. Today 71 (2002) 227.
5. M.L. Turner, N. Marsih, B.E. Mann, R. Quyoum, H.C. Long, P.M. Maitlis, J. Am. Chem. Soc. 124 (2002) 10456.
6. Z.P. Liu, P. Hu, J. Am. Chem. Soc. 124 (2002) 11568.
7. R. Oukaci, A.H. Singleton, J.G. Goodwin, Appl. Catal. A 186 (1999) 129.
8. R.C. Reuel, C.H. Bartholomew, J. Catal. 85 (1984) 78.
9. A.S. Lisitsyn, A.V. Golovin, V.L. Kuznetsov, Y.I. Yermakov, C1 Mol. Chem. 1 (1984) 115.
10. A.S. Lisitsyn, A.V. Golovin, V.L. Kuznetsov, Y.I. Yermakov, J. Catal. 95 (1985) 527.
11. E. Iglesia, S.L. Soled, R.A. Fiato, J. Catal. 137 (1992) 212.
12. E. Iglesia, S.L. Soled, R.A. Fiato, G.H. Via, Stud. Surf. Sci. Catal. 81 (1994) 433.
13. E. Iglesia, Appl. Catal. A 161 (1997) 59.
14. G.L. Bezemer, A. van Laak, A.J. van Dillen, K.P. de Jong, Stud. Surf. Sci. Catal. (2004) 259.
15. A. Martinez, C. Lopez, F. Marquez, I. Diaz, J. Catal. 220 (2003) 486.
16. A. Barbier, A. Tuel, I. Arcon, A. Kodre, G.A. Martin, J. Catal. 200 (2001) 106.
17. L. Fu, C.H. Bartholomew, J. Catal. 92 (1985) 376.
18. J.H. Lee, D.K. Lee, S.K. Ihm, J. Catal. 113 (1988) 544.
19. S.W. Ho, M. Houalla, D.M. Hercules, J. Phys. Chem. 94 (1990) 6396.
20. A.M. Saib, M. Claeys, E. van Steen, Catal. Today 71 (2002) 395.
21. S.L. Soled, E. Iglesia, R.A. Fiato, J.E. Baumgartner, H. Vroman, S. Miseo, Top. Catal. 26 (2003) 101.
22. G. Jacobs, T.K. Das, Y.Q. Zhang, J.L. Li, G. Racoillet, B.H. Davis, Appl. Catal. A 233 (2002) 263.
23. I. Fernandez-Morales, A. Guerrero-Ruiz, F.J. Lopez-Garzon, I. Rodriguez-Ramos, C. Moreno-Castilla, Appl. Catal. 14 (1985) 159.
24. C.M. Lok, Stud. Surf. Sci. Catal. 147 (2004) 283.
25. B.G. Johnson, C.H. Bartholomew, D.W. Goodman, J. Catal. 128 (1991) 231.
26. C. Moreno-Castilla, F. Carrasco-Marin, J. Chem. Soc., Faraday Trans. 91 (1995) 3519.

27. A.Y. Khodakov, A. Griboval-Constant, R. Bechara, V.L. Zholobenko, J. Catal. 206 (2002) 230.
28. J.J.C. Geerlings, M.C. Zonnevylle, C.P.M. De Groot, Surf. Sci. 241 (1991) 315.
29. D. Schanke, A.M. Hilmen, E. Bergene, K. Kinnari, E. Rytter, E. Adnanes, A. Holmen, Energy Fuels 10 (1996) 867.
30. J.L. Li, G. Jacobs, T. Das, Y.Q. Zhang, B. Davis, Appl. Catal. A 236 (2002) 67.
31. P.J. van Berge, J. van de Loosdrecht, S. Barradas, A.M. van der Kraan, Catal. Today 58 (2000) 321.
32. G. Jacobs, P.M. Patterson, Y.Q. Zhang, T. Das, J.L. Li, B.H. Davis, Appl. Catal. A-Gen. 233 (2002) 215.
33. K.P. de Jong, J.W. Geus, Catal. Rev.-Sci. Eng. 42 (2000) 481.
34. P. Serp, M. Corrias, P. Kalck, Appl. Catal. A 253 (2003) 337.
35. G.L. Bezemer, U. Falke, A.J. van Dillen, K.P. de Jong, Chem. Commun. (2005) 701, chapter 4 of this thesis.
36. M.L. Toebes, J.H. Bitter, A.J. van Dillen, K.P. de Jong, Catal. Today 76 (2002) 33.
37. M.L. Toebes, J.M.P. van Heeswijk, J.H. Bitter, A.J. van Dillen, K.P. de Jong, Carbon 42 (2004) 307.
38. H.P.C.E. Kuipers, Solid State Ion. 16 (1985) 15.
39. H.P.C.E. Kuipers, H.C.E. Van Leuven, W.M. Visser, Surf. Interface Anal. 8 (1986) 235.
40. O.L.J. Gijzeman, XPS Analysis of Catalyst Surfaces, Utrecht University, The Netherlands, unpublished.
41. F. Winter, G.L. Bezemer, C. van der Spek, J.D. Meeldijk, A.J. van Dillen, J.W. Geus, K.P. de Jong, Carbon 43 (2005) 327, chapter 5 of this thesis.
42. R.C. Reuel, C.H. Bartholomew, J. Catal. 85 (1984) 63.
43. M. Vaarkamp, J.C. Linders, D.C. Koningsberger, Physica B 209 (1995) 159.
44. D.C. Koningsberger, B.L. Mojet, G.E. van Dorssen, D.E. Ramaker, Top. Catal. 10 (2000) 143.
45. A.J. van Dillen, R. Terorde, D.J. Lensveld, J.W. Geus, K.P. de Jong, J. Catal. 216 (2003) 257.
46. I. Arcon, A. Tuel, A. Kodre, G. Martin, A. Barbier, J. Synch. Rad. 8 (2001) 575.
47. J. de Graaf, A.J. van Dillen, K.P. de Jong, D.C. Koningsberger, J. Catal. 203 (2001) 307.
48. S. Sun, K. Fujimoto, Y. Yoneyama, N. Tsubaki, Fuel 81 (2002) 1583.
49. G.L. Zhang, Z.Y. Wu, A.G. Li, Y.S. Wang, J. Zhang, M.I. Abbas, R. Hu, X.B. Ni, Y.P. Tong, Y.K. Hwu, Phys. Rev. B 69 (2004)
50. F. Kapteijn, R.M. de Deugd, J.A. Moulijn, Catal. Today 105 (2005) 350.
51. E. Iglesia, S.L. Soled, J.E. Baumgartner, S.C. Reyes, Top. Catal. 2 (1995) 17.

52. G. Jacobs, T.K. Das, P.M. Patterson, J.L. Li, L. Sanchez, B.H. Davis, Appl. Catal. A 247 (2003) 335.
53. E. van Steen, M. Claeys, M.E. Dry, J. van de Loosdrecht, E.L. Viljoen, J.L. Visagie, J. Phys. Chem. B 109 (2005) 3575.
54. S. Weller, L.J.E. Hofer, R.B. Anderson, J. Am. Chem. Soc. 70 (1948) 799.
55. R.B. Anderson, W.K. Hall, A. Krieg, B. Seligman, J. Am. Chem. Soc. 71 (1949) 183.
56. R. Van Hardeveld, F. Hartog, Surf. Sci. 15 (1969) 189.
57. H. Schulz, Z.Q. Nie, F. Ousmanov, Catal. Today 71 (2002) 351.
58. J. Wilson, C. De Groot, J. Phys. Chem. 99 (1995) 7860.
59. J.D. Grunwaldt, A.M. Molenbroek, N.Y. Topsoe, H. Topsoe, B.S. Clausen, J. Catal. 194 (2000) 452.
60. P.L. Hansen, J.B. Wagner, S. Helveg, J.R. Rostrup-Nielsen, B.S. Clausen, H. Topsoe, Science 295 (2002) 2053.

IV

INVESTIGATION OF PROMOTING EFFECTS OF MANGANESE OXIDE ON CARBON NANOFIBERS SUPPORTED COBALT CATALYSTS FOR FISCHER-TROPSCH SYNTHESIS

The effects of the addition of MnO to a carbon nanofibers supported cobalt catalyst were studied. The original sample, cobalt loading 9.5 wt% and 8% cobalt dispersion, was promoted by impregnation with small amounts of MnO (0.03, 0.1, 0.3, 0.6 and 1.1 wt%). XPS and STEM-EELS showed MnO to be associated with Co both in the dried and in the reduced catalyst. In the drying step MnO was deposited on the passivated cobalt particles due to the tendency of both metals to form stable mixed compounds. After reduction the MnO remained close to the cobalt particles, as the support material lacked sites with significant interaction with MnO. The promoter suppressed both the hydrogen chemisorption uptake and the cobalt reducibility even with the lowest MnO loading. At 1 bar large improvements in the selectivity towards C_{5+} products (from 31 to 45 wt%) were found with MnO loadings of 0.3 wt% and higher. At 20 bar the addition of only 0.03 wt% MnO improved the C_{5+} selectivity from 74 to 78 wt%, but larger amounts decreased the selectivity to 52 wt% at 1.1 wt% MnO. The surface specific activity (TOF) first increased with MnO loading from 26 to $60 \cdot 10^{-3}$ s^{-1} for 0.3 wt% MnO while it decreased, probably as a consequence of too high coverage of the Co surface, at MnO loadings >0.3 wt%. From product analysis (paraffin-olefin ratio) it appears that a major role of MnO involves moderation of hydrogenation reactions.

Introduction

In the Fischer-Tropsch (FT) reaction synthesis gas (CO/H_2) is catalytically converted into hydrocarbons via surface polymerization. By using synthesis gas produced from natural gas, coal or biomass transportation fuels can be obtained from feedstocks other than crude oil. The quality of the products formed in combination with a non-crude oil feedstock support the FT process to play a crucial role in the energy supply to society in the coming decades.

Supported cobalt catalysts are well known for their activity and selectivity in the FT reaction [1]. The catalysts are often promoted with small amounts of noble metals to decrease the reduction temperature and to increase the activity [2-4]. To achieve better selectivities towards long chain products special metal oxides can be added [4-7]. In this chapter we investigate the influence of manganese oxide on carbon nanofibers supported cobalt catalysts. MnO is reported to be a promoter for cobalt-based FT catalysts in both academic and patent literature. Originally, most research was devoted to cobalt on MnO_2 supports and to systems with mixed oxides of cobalt and manganese [8-12]. All of these systems have relatively high manganese loadings. Recently, MnO promoter effects on cobalt catalysts supported on oxidic carriers have been investigated [13-20]. The promoting effect of MnO is suggested to originate from a lower degree of reduction of cobalt [12,13,20]. In all cases also a metal oxide was used as support material, which lowers the cobalt reducibility as well, thus complicating the analysis. Therefore, we decided to reduce support effects by using an inert carrier, *viz.* carbon nanofibers (CNF). This is a novel graphitic support material with promising applications, also as support for FT catalysts [21,22]. Recently, we showed with XPS and STEM-EELS that in Co/CNF catalysts promoted with MnO the promoter is present only in the vicinity of the cobalt particles and not elsewhere on the support [23]. The objective of this chapter is to provide comprehensive characterization and to investigate systematically at low and high pressure the catalytic effects of the manganese loading on Co/CNF catalysts. Catalysts with Co/Mn molar ratios varying from 11 to 431 were prepared and characterized by acid-base titration, H_2 chemisorption, STEM-EELS, TEM, TPR, XPS and XRD, while Fischer-Tropsch catalysis experiments were carried out in fixed bed reactors both at atmospheric pressure and at 20 bar.

Experimental session

Catalyst preparation

Carbon nanofibers of the fishbone-type with an average diameter of about 30 nm were grown from synthesis gas using an earlier described method [24]. Purification comprised refluxing in 1M KOH and adsorption sites were created by refluxing the CNF in concentrated HNO_3, as described by Toebes *et al.* [25]. After washing and drying at 120 ºC CNF with a BET surface area of 160 m^2/g and a bulk density of 0.50 g/ml were obtained.

Cobalt was loaded on the activated CNF by incipient-wetness impregnation (pore volume 0.56 ml/g) of a solution containing 0.97 g/ml $Co(NO_3)_2 \cdot 6H_2O$ (Acros *p.a.*) resulting in a loading of 9.5 wt% cobalt in the final catalyst. The catalyst precursor was dried in air at 120 ºC for 18 h and subsequently reduced at 350 ºC for 2 h in a flow of 10% H_2/He. After passivation in a 1 vol‰ oxygen flow at room temperature the sample coded Co/CNF was obtained.

Subsequently, manganese was loaded on six portions of Co/CNF using incipient wetness impregnation with aqueous solutions of $Mn(NO_3)_2 \cdot 4H_2O$ (Acros *p.a.*) with different concentrations. A reference sample coded CoH was prepared by impregnation with a diluted HNO_3 solution (pH 5) in order to reveal any effects caused by the new preparation step. The catalysts loaded with manganese are coded Co431Mn, Co95Mn, Co39Mn, Co19Mn and Co11Mn, the numbers indicating the cobalt to manganese atomic ratio (table 1). All catalyst precursors were dried in air at 120 ºC for 18 h.

Catalyst characterization

The number of acidic groups prior to loading the support with cobalt or manganese was determined by titration [25]. Amounts of 50 mg treated and untreated CNF were suspended in a 25 ml solution of 0.1 M NaCl and 0.1 M oxalic acid in demineralized water

Table 1. Composition, H_2 uptake and calculated cobalt dispersion of the samples under investigation.

Sample	Co (wt%)	MnO (wt%)	H_2 uptake (mmol/g)	Dispersion (%)
CoH	9.5	-	0.063	7.8
Co431Mn	9.5	0.028	0.063	7.8
Co95Mn	9.5	0.13	0.054	6.7
Co39Mn	9.5	0.30	0.051	6.4
Co19Mn	9.5	0.63	0.053	6.6
Co11Mn	9.4	1.1	0.052	6.5

(pH=3.0). Under continuous stirring 10 mM NaOH was added dropwise with a rate of 0.05 ml/min until the final pH of 10 was reached. During the titration the pH was monitored with a pH electrode. The difference in amount of NaOH needed to reach pH 7 with the blank and the sample is reported in mmol/g.

Powder X-ray diffraction (XRD) patterns were measured using an Enraf-Nonius CPS 120 powder diffraction apparatus with Co K_α radiation (λ = 1.789 Å).

Temperature programmed reductions were executed with an Autochem 2920 instrument from Micromeritics. Typically 0.1 g sample was after drying reduced in a flow of 50 ml/min 5%H_2/Ar, the temperature was increased with 5 ºC/min from room temperature to 750 ºC.

XPS measurements were performed on a Thermo VG Scientific XPS system using non-monochromatic Mg (K_α) radiation. The XPS apparatus was equipped with a reaction chamber where samples could be reduced *in situ*. The samples CoH and Co11Mn were measured both after drying and after *in situ* reduction at 350 ºC for 2 h, the other samples were only measured after drying. The pass energy of the analyser was set at 70 eV. Charging effects were minimal with shifts of at most 0.2 eV. The C peak at 284.2 eV was used as a reference to correct for the charging of the samples. The escape-depth of photoelectrons generated is small (~1.5 nm), which, if surface area of the support and metal loading are known, allows to evaluate particle sizes. From the quantitative Co/C and Mn/C ratios particle sizes for cobalt and manganese oxide were calculated using the model for hemi-spherical particle shapes [26-28].

Hydrogen chemisorption measurements were carried out using a Micromeritics ASAP 2010C. Before each measurement the sample was dried in vacuum at 120 ºC overnight and reduced for 2 h in flowing H_2 at 350 ºC with a heating rate of 5 ºC/min. After reduction the samples were evacuated at that temperature for 30 minutes. The H_2-adsorption isotherms were measured at 150 ºC [29]. The H/Co ratios at zero pressure were found by extrapolation of the linear part of the isotherm. Calculations were made using the total amount of hydrogen adsorbed assuming complete reduction and a stoichiometry of 1 hydrogen atom per cobalt surface atom [29].

The dried catalyst precursors and the reduced catalysts were examined with transmission electron microscopy (TEM) in a FEI Tecnai12 or in a FEI Technai20F. TEM samples were crushed and subsequently suspended in ethanol under ultrasonic vibration. A drop of this suspension was loaded onto a holey carbon film on a copper TEM grid.

The sample with the highest manganese loading was examined in a dedicated aberration corrected scanning transmission electron microscope (STEM), VG HB501, equipped with a Nion Mark II C_s corrector and a Gatan Enfina spectrometer to obtain energy electron loss spectroscopy (EELS) spectra. High Angle Annular Dark Field (HAADF) images were acquired at an acceptance angle of 70-210 mrad. A 2 s dwell time per spectrum was used, resulting for a 30*35 pixel image in an acquisition time of 45 min. We measured 14 full images and 8 line-scans, each taken on different parts of the specimen.

Catalytic testing

Catalysts were tested at atmospheric pressure and at high pressure. The measurements at 1 bar were carried out at 220 ºC using CO/H_2 (1/2 v/v) after a reduction treatment at 350 ºC for 2 h in hydrogen. Typically 30 mg of catalyst particles (0.5-1.0 mm) was diluted with 200 mg SiC particles (0.2 mm) to achieve isothermal plug-flow conditions. Selectivities of the catalysts were established at a CO-conversion of 2%, which was achieved by tailoring the space velocity. For the high-pressure measurements 0.25 g catalyst (150-212 μm) was diluted with 0.5-0.7 g SiC. Catalysts were also reduced in hydrogen at 350 ºC for 2 h and the catalytic data were obtained at 220 ºC and a pressure of 20 bar using a flow of $CO/H_2/N_2$ (33/66/6). The space velocity was adjusted to maximize CO conversions at around 60%. Reported catalytic data were obtained after three days of operation. Values for catalyst deactivation were based on the decrease of activity from day 1 to day 3 and are reported as percentage of activity per day.

Results and Discussion

Titration

The activated carbon nanofibers used as support contained initially 0.15 mmol acidic groups per gram. MnO was loaded on the Co/CNF after a reduction treatment at 350 ºC for 2 h. Unfortunately, the remaining amount of acidic groups on Co/CNF could not be measured directly as the presence of cobalt interfered. Therefore, a sample of the original oxidized, un-loaded CNF batch was reduced in H_2 at 350 ºC and was subsequently titrated. This sample contained only 0.06 mmol/g, which is an upper limit for the acid sites in Co/CNF that can serve as anchoring groups for the manganese. Despite of this decrease in acidic surface groups we noticed that the carbon nanofibers were still hydrophilic as wetting by water occurred smoothly.

XRD

XRD patterns of the unpromoted reduced and passivated Co/CNF together with dried CoH and dried Co11Mn are shown in figure 1. The starting material Co/CNF showed in addition to the graphite diffraction lines also contributions from CoO and metallic Co. The graphite diffraction lines are present at 30, 51, 63 and 95 º2θ while the diffractions at 43 and 77 º2θ are indicative for CoO. Line broadening analysis of the 43 º2θ diffraction resulted in a domain size of 3 nm for CoO. The main diffraction line for metallic cobalt is present at 52 º2θ and coincides with graphite contributions and three more metallic lines are found at 61, 91 and 114 º2θ, characteristic for fcc cobalt. Although hcp is the most stable structure for bulk cobalt up to the transition temperature of 416 ºC, small cobalt particles are reported to have the fcc structure [29,30]. The presence of CoO domains of 3 nm together with metallic Co in the sample demonstrates that reoxidation during the passivation treatment was not complete but probably resulted in the formation of a shell of cobalt oxide surrounding a metallic core.

Both the dried CoH sample and Co11Mn, as a representative example of the promoted catalysts, showed distinct diffractions typical for Co_3O_4. No diffraction lines other than those of CNF or Co_3O_4 were observed. Apparently during impregnation and drying cobalt originally present in Co/CNF as CoO and Co metal was oxidized to Co_3O_4. The formation of Co_3O_4 was also observed in the dried MnO promoted samples. For Co11Mn no additional diffractions originating from manganese compounds are observed, probably because the manganese loading was too small (figure 1).

TPR

Temperature programmed reduction profiles of the dried samples given in figure 2 show four distinct reduction peaks around 175, 240, 340 and 475 ºC. The first one at 175 ºC, which increases with the manganese loading, can be ascribed to reduction and

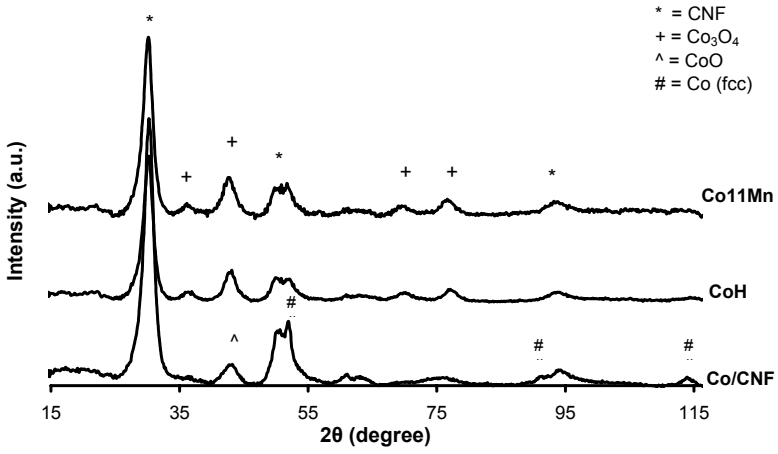

Figure 1. XRD patterns of original reduced and passivated Co/CNF together with the dried samples CoH and Co11Mn with strongest diffraction lines of main components indicated.

decomposition of nitrates [29]. The peak area of the second peak at 240 ºC is unaffected by the manganese loading. This peak is stemming from the reduction of Co^{3+} to Co^{2+} showing that Co_3O_4 is present in the dried catalyst precursors, as was found with XRD. We used peak fitting to get an estimation of the peak areas of the Co^{3+} reduction peak at 240 ºC and the Co^{2+} reduction peak at 340 ºC in CoH. From the ratio of the peaks it could be concluded that indeed in the dried samples all cobalt is present as Co_3O_4.

Interestingly, the Co^{2+} to Co^0 reduction found at 340 ºC is influenced by the presence of MnO. CoH and the catalysts with MnO loading up to 0.30 wt% MnO have similar peak areas, but going to higher manganese loadings the intensity of the peak for the CoO reduction decreases, which indicates a strong interaction between CoO and MnO. The run-up of the broad peak around 475 ºC makes quantitative identification difficult, but assuming similar peak shapes with peak fitting we obtained peak area ratios higher than 1:3 for CoH and the three catalysts with lowest manganese loading, suggesting complete reduction. However, the samples with higher manganese loading have a broadened reduction peak, which makes quantitative analysis impossible. Taking into account the shift of the CoO reduction peak to higher temperatures, it is possible that some cobalt will remain unreduced after the reduction treatment (350 ºC, 2 h) prior to H_2 chemisorption, *in situ* XPS, and catalytic testing.

The last broad reduction peak with a maximum around 475 ºC can be ascribed to some gasification of CNF to methane, as GC analysis demonstrated. The higher the manganese loading on the catalysts, the lower the gasification peak. The TPR pattern of the support (data not shown) has the support reduction peak around 600 ºC, which indicates that metallic cobalt acts as a catalyst probably by the spill-over of hydrogen atoms. Now from figure 2 it can be concluded that the addition of manganese to the catalyst lowers the gasification peak area. This indicates that either cobalt does not reduce

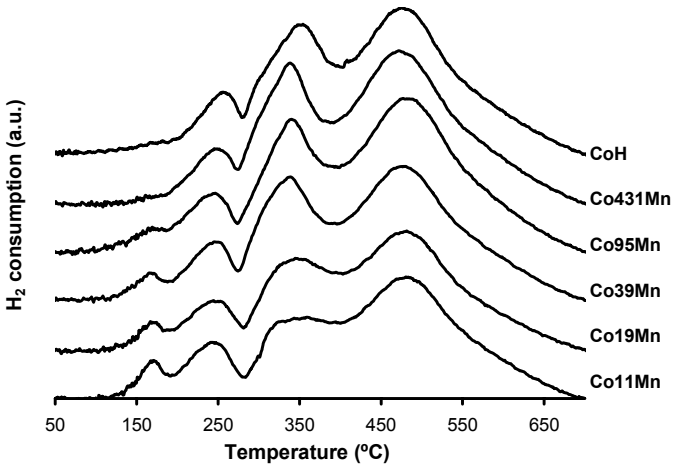

Figure 2. TPR profiles of the dried samples, normalized on cobalt intake.

completely at 475 ºC, which is rather unlikely, or that MnO remains associated with the metallic cobalt particles, thus reducing the cobalt surface area available for catalytic gasification of carbon.

XPS

The Co_{2p} spectra, normalized on the carbon 1s peak area are shown in figure 3 for the dried CoH and the three catalysts with the highest manganese loadings: Co39Mn, Co19Mn and Co11Mn. Distinct peaks stemming from $2p_{3/2}$ at 780.0 eV and $2p_{1/2}$ at 795.4 eV can be seen for CoH, characteristic for Co_3O_4. For the sample with the highest MnO loading, Co11Mn, both peaks are shifted to significantly higher binding energies, *i.e.* 780.9 and 797.2 eV, which indicates that a different cobalt compound is present at the surface of the cobalt particles. The mixed spinel of cobalt and manganese oxide and CoO both have a binding energy similar to the observed values [31]. In the samples Co19Mn and Co39Mn some broadening of the cobalt peak is observed but not the distinct shift to higher binding energy as observed for Co11Mn, which might be explained by the lower Mn loadings that were not sufficient to lead to mixed spinel formation.

In table 2 the Co/C, Mn/Co and Mn/C atomic ratios as measured by XPS are given. The cobalt particle size in CoH was calculated from the Co/C ratio to be 11 nm. The loading of MnO on the samples resulted in a small but distinct lowering of the Co/C atomic ratio, as we found before [23]. The atomic ratio of Co/C decreased from 0.022 to 0.018 going from CoH to Co11Mn (table 2). This decrease of the Co/C could be explained if the cobalt particle size would increase from 11 to 15 nm going from CoH to Co11Mn. In our TEM analysis, however, we did not find any indication of larger cobalt particle sizes related to the presence of MnO. An alternative explanation would be the coverage of cobalt(oxide) by MnO. From the STEM-EELS measurements (*vide infra*) we found that manganese and cobalt are super positioned. The mean escape depth of the

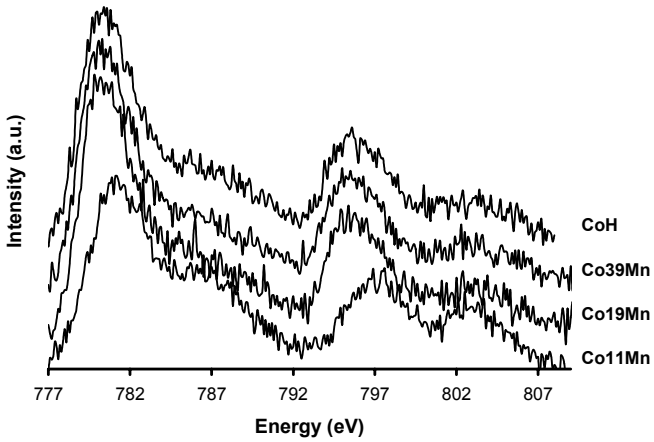

Figure 3. Co 2p XPS region of dried CoH and the three catalysts with highest MnO loading. Spectra have been normalized to carbon 1s.

Table 2. Atomic ratios of four dried catalysts as obtained with XPS.

Sample	Co/C	Mn/Co	Mn/C
CoH	0.022	-	-
Co39Mn	0.020	0.08	0.0017
Co19Mn	0.021	0.16	0.0036
Co11Mn	0.018	0.32	0.0059

generated photo-electrons through MnO is only 1.2 nm. This implies that the coverage of cobalt(oxide) by small amounts of MnO can significantly reduce the amount of photo-electrons that reach the detector. Consequently, the present decrease in Co/C ratio can be explained very well by coverage of the cobalt oxide particles with MnO.

The Mn/C atomic ratios obtained from XPS (table 2) were more than three times higher than the overall Mn/C ratio, which shows that MnO is highly dispersed on the samples. For Co11Mn we obtained from XPS a MnO particle size of 0.6 nm, assuming a hemi-spherical shape, or 0.4 nm for spherical particles. XPS is not able to discriminate between these options, but anyhow we can conclude from these data that MnO is highly dispersed in Co11Mn, and as discussed above, most likely (partly) located on top of the cobalt(oxide) particles. For Co19Mn and Co39Mn we found using the Mn/C ratios even smaller MnO particle sizes of 0.3-0.4 nm, which shows that the size of the MnO particles is affected by the loading.

The influence of manganese on the cobalt oxidation state after reduction was also investigated with XPS. The Co_{2p} spectra before and after reduction of CoH and Co11Mn are given in figure 4. For CoH the Co_{2p} binding energies shifted from 780.0 and 795.4 eV in the dried sample to 778.2 eV and 793.5 eV in the reduced sample, values that are indicative of metallic cobalt. After reduction a shoulder remained at the oxidic position showing that not all cobalt was reduced. For the promoted sample Co11Mn the peak

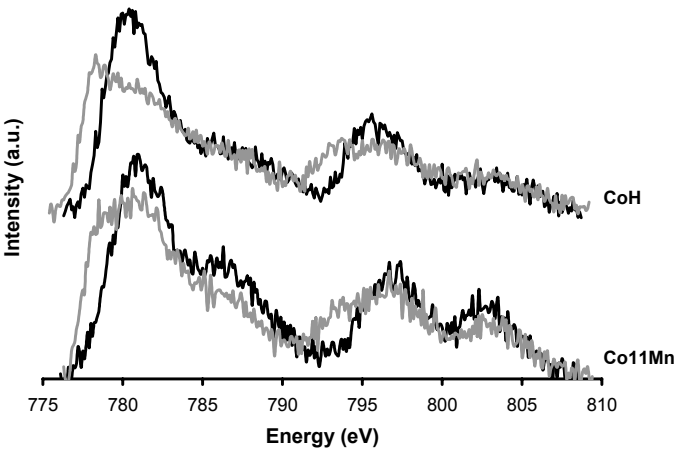

Figure 4. Co 2p XPS region before (black) and after reduction (grey) for CoH and Co11Mn, spectra have been normalized to carbon 1s.

maximums did not shift after reduction, although significant shoulders at the metallic cobalt positions were formed. This shows that the outer layer of the cobalt particles in Co11Mn was mainly oxidic, while in CoH the majority of cobalt atoms probed were reduced. The higher oxidation state of cobalt due to the presence of MnO, is in line with the TPR results where the influence of MnO on the cobalt reduction was pronounced. The atomic ratios between Co, C and Mn did not change upon reduction showing the absence of significant restructuring of the phases leading to changes in their dispersion. This makes it likely that Co and Mn remained closely associated after the reduction treatment.

H_2 chemisorption

The hydrogen uptake data and the calculated apparent dispersions of the catalysts are given in table 1. It was not possible to obtain the actual degree of reduction of cobalt as back titration with oxygen interfered with the oxidation of the support material. Therefore, we assumed complete reduction, which, as mentioned in the discussion on the TPR patterns, might not be valid for the two samples with the highest MnO loadings. Consequently, the actual dispersion of these samples could be higher than the values reported. For the unpromoted sample CoH we found a cobalt dispersion of 7.8%, which corresponds to an average cobalt particle size of 12 nm [29] that is close to the result of 11 nm found with XPS. The addition of 0.028 wt% MnO resulted in the same cobalt dispersion, but addition of higher amounts of manganese lowered the cobalt dispersion to the lowest value of 6.4%. The presence of manganese oxide on the cobalt surface may decrease the hydrogen chemisorption uptake in two different ways. The coverage of cobalt atoms at the surface by MnO decreases the amount of sites that are probed with chemisorption. It is also possible that MnO decreases the ultimate degree of reduction of cobalt, which also decreases the hydrogen uptake.

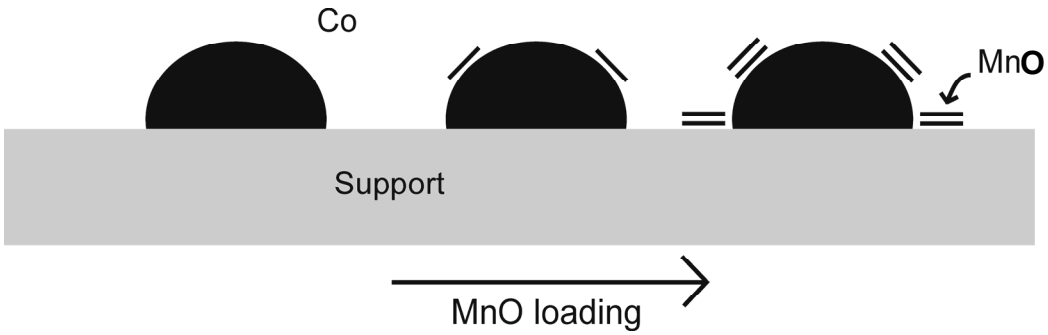

Figure 5. Schematic representation of the location of MnO on the cobalt catalysts. Until Co39Mn we find MnO mainly present as monolayers on Co, for higher loadings MnO forms multi-layers and is also found on the CNF support, still in close contact with the Co particles.

From table 1 it is clear that the exposed cobalt surface as probed by hydrogen chemisorption did not decrease further for MnO loadings higher than 0.30 wt%. The particle size for MnO calculated from quantitative XPS for Co39Mn was 0.3-0.4 nm, which is about the height of a monolayer of MnO. For low MnO loadings we therefore expect MnO to be mainly present as monolayer patches on the cobalt particles.

For higher MnO loadings monolayer coverage of the cobalt surface by MnO is unlikely. It was calculated that the Mn loading of Co11Mn is equivalent to an MnO-monolayer over the cobalt surface, which would block all the sites present for hydrogen chemisorption. But the amount of H_2 chemisorbed was still 80% of that of the unpromoted catalyst, from which we can conclude that for this loading of MnO the promoter is not exclusively present as a monolayer on the cobalt metal. From quantitative XPS for Co11Mn MnO particle sizes between 0.4 and 0.6 nm were obtained, which correspond to approximately two times the thickness of a monolayer. Therefore, we propose that at higher MnO loadings a significant part of MnO is located on the CNF surface in the close vicinity of the cobalt particles. The development of the MnO structure with increasing loading has been depicted in figure 5.

TEM

TEM was used to measure the particle size distribution in the original reduced and passivated Co/CNF sample. The majority of the particles observed had sizes around 8 nm. In figure 6 small cobalt(oxide) particles can be observed supported on the carbon nanofibers. The small particles displayed low contrast with the graphite support, which

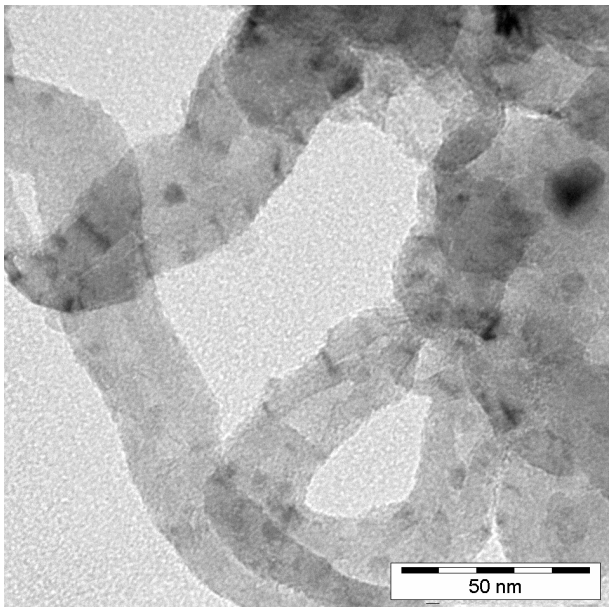

Figure 6. TEM image of original Co/CNF catalyst showing the interwoven carbon nanofibers structure of the support with small supported cobalt particles with low contrast.

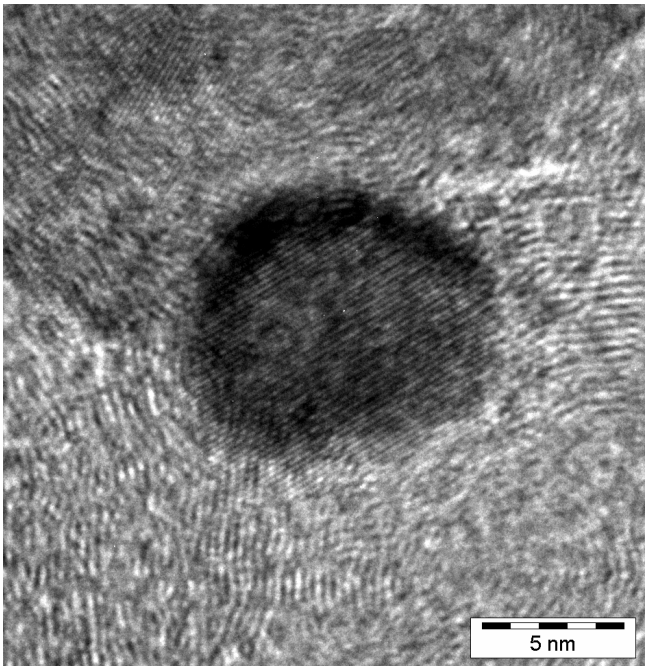

Figure 7. HRTEM image of original Co/CNF sample with d-spacing typical for CoO.

indicates that they have been oxidized. Indeed, in the high resolution image depicted in figure 7 the d-spacing (0.21 nm) confirms the presence of CoO. Also some larger particles were present with sizes up to 25 nm, thus shifting the average particle size towards the value (12 nm) obtained from H_2 chemisorption.

STEM-EELS

Scanning transmission electron microscopy (STEM) measurements combined with electron energy loss spectroscopy (EELS) were performed to gain more insight into the location of manganese and cobalt both before and after the reduction treatment. We studied the sample with the highest manganese loading, Co11Mn. In figure 8A a representative dark field image is shown together with the areal densities of carbon, cobalt, manganese and oxygen of the dried sample. In the dark field image an individual carbon nanofiber is depicted on which the several brighter spots are visible. By comparing the dark field image with the elemental mappings it can be concluded that these brighter spots in dark field, with sizes varying from 4-14 nm, comprise of both cobalt oxide and manganese oxide. Also the elemental mappings and the bright field image shown in figure 8B suggest that the particles contain both metals, however, the 8 nm-sized particle in the lower left corner does not appear in the manganese mapping. This indicates that although manganese is always associated with cobalt, the opposite is not true. Mixed particles, however, prevailed; in total we detected 54 mixed particles and only 2 monometallic cobalt oxide particles.

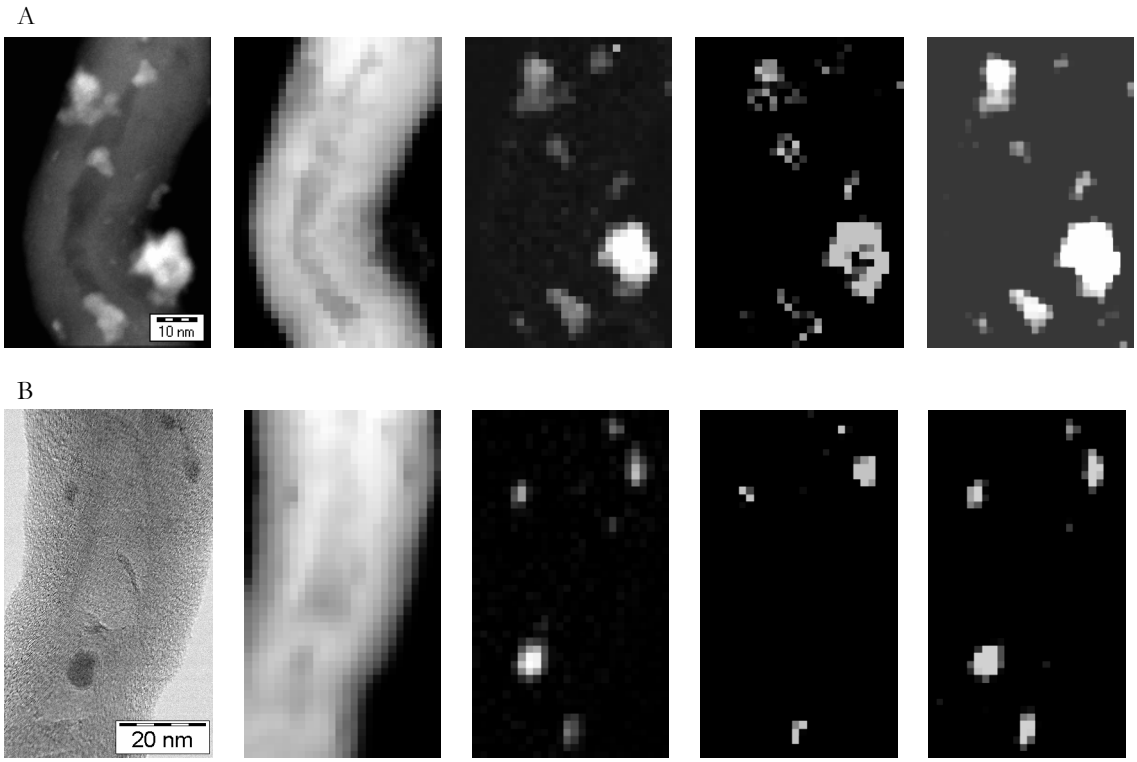

Figure 8. STEM-EELS images of dried Co11Mn, from left to right: the HAADF (A) or bright field image (B) and the C, Co, Mn and O areal densities, derived from the EELS signals for two parts (A,B) of the specimen.

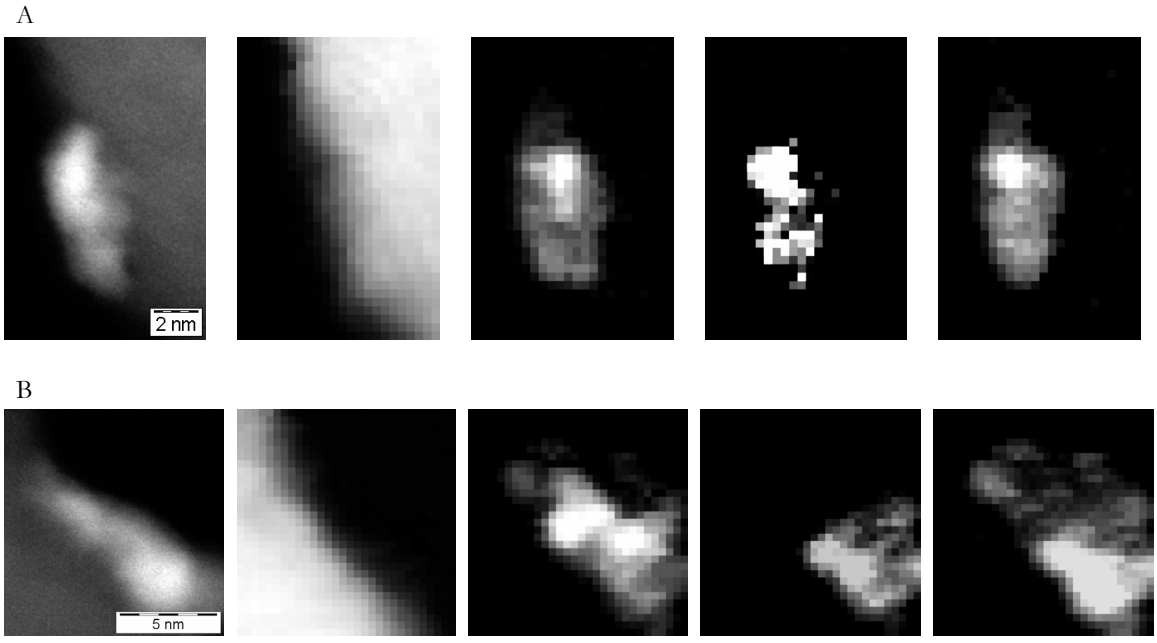

Figure 9. STEM-EELS of reduced Co11Mn, from left to right: the HAADF image and the C, Co, Mn and O areal densities as derived from the EELS signals for two parts (A,B) of the specimen.

The Mn patches have slightly different shapes than the Co particles, which suggests that Mn is covering Co, a conclusion that was also drawn from the presented XPS data. These findings are in line with literature results showing that mixed oxides of cobalt and manganese are sometimes found to be surface enriched in manganese [32]. Moreover, this larger size for the MnO particles strongly suggests that part of the promoter is present on the CNF support, although closely associated with Co.

Figure 9 shows the HAADF image and the elemental mappings with high resolution of two different single particles after reduction and passivation. The elemental mappings of cobalt, manganese and oxygen in figure 9A correlate, so it can be concluded that after the reduction treatment cobalt, manganese and oxygen remained associated. However, closer examination shows that cobalt matches with the particles imaged by HAADF, whereas the manganese mapping is non-continuous, pointing towards segregation on atomic scale. Segregation is also seen in figure 9B where the upper left part of the particle contains only cobalt oxide whereas the other parts consist of both cobalt- and manganese oxide. This indicates that during the reduction of cobalt oxide MnO was partly re-distributed over the cobalt metal surface. These findings agree with the results of XPS and H_2 chemisorption that indicate free metallic Co surface next to MnO coverage.

Catalysis

The steady state performance of the catalysts at 1 bar after 48 h is given in figure 10 and in table 3. The presence of MnO both influenced the activity and the selectivity of the catalysts. Upon manganese loading the C_{5+} selectivity increased from 31 to 45 wt% mainly at the expense of methane formation which decreased from 36 to 23 wt%. We note that C_{5+} selectivity increased markedly up to Co39Mn, but did not improve further

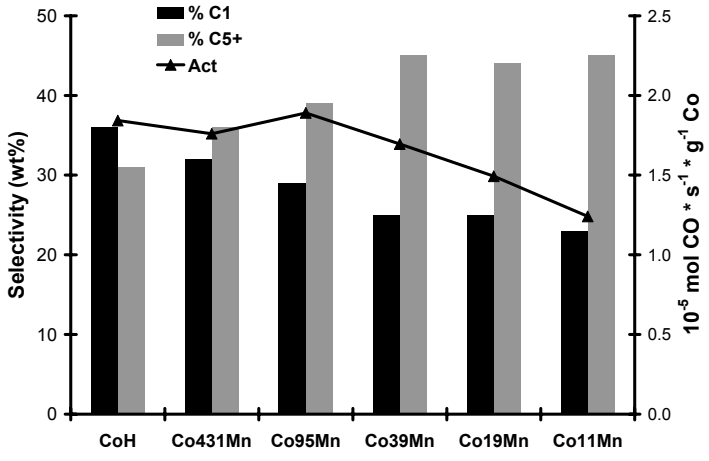

Figure 10. Influence of manganese loading on activity and selectivity in the FT reaction at 1 bar.

Table 3. FTS catalytic performances at 1 bar, 220 ºC.

Sample	Activity	TOF (10^{-3} s^{-1})	C_1 (wt%)	C_{5+}(wt%)	alpha
CoH	1.8	14	36	31	0.60
Co431Mn	1.7	13	32	36	0.63
Co95Mn	1.8	17	28	41	0.65
Co39Mn	1.6	16	25	45	0.67
Co19Mn	1.4	13	25	44	0.66
Co11Mn	1.2	11	23	45	0.67

Activity: 10^{-5} mol CO s^{-1} g^{-1} Co

with higher Mn loadings. Figure 11 plots the product distribution for CoH and Co11Mn is plotted. It is clear that the catalysts display ASF kinetics and the chain growth probabilities can be derived from the linear part of the plot. An increase of alpha from 0.60 to 0.67 was found going from the un-promoted to the highest loaded sample with a similar trend as with the methane and C_{5+} selectivities.

The activity of the catalysts at 1 bar decreased upon loading of MnO from 1.78 to 1.17 10^{-5} mol_{CO} g_{Co}^{-1} s^{-1} but the samples Co431Mn and Co95Mn showed no decrease in activity yet. This shows that small amounts of MnO on the catalyst improve the selectivity without hampering the activity. This is even more interesting as we found a decrease in the hydrogen chemisorption uptake for Co95Mn of 15% compared to the reference sample (CoH). The activity normalized on the cobalt surface area, the turn-over frequency (TOF), increased from 14 to $17 \cdot 10^{-3}$ s^{-1} going from CoH to Co95Mn. Also Co39Mn showed a higher TOF than the unpromoted sample. Minor amounts of MnO on the surface of cobalt therefore result in higher TOF values for the remaining sites. The TOF values mentioned are, however, based on the exposed cobalt surface area in the reduced samples prior to catalytic operation. As the actual cobalt catalyst is created *in situ*, the observed differences in TOF can also be related with changes to the catalyst under

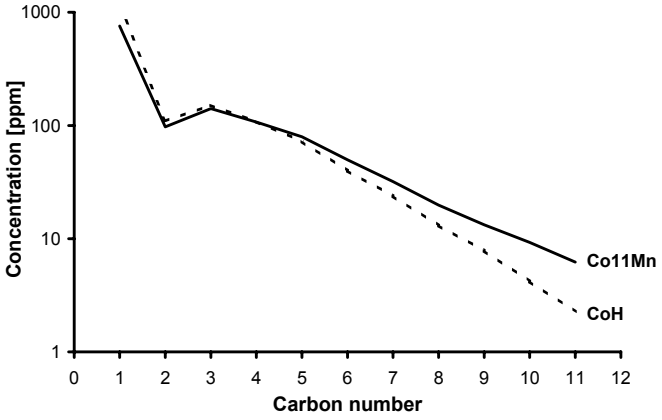

Figure 11. ASF plot for CoH and Co11Mn showing the influence of MnO on the chain growth probability and the product distribution at 1 bar.

reaction conditions [33]. We could not measure the hydrogen chemisorption after catalytic operation and consequently report these apparent TOF values.

Loading of higher amounts than 0.13 wt% MnO resulted in a decrease in activity. This decrease in activity showed the same trend as the decrease in dispersion obtained from H_2 chemisorption but was stronger. This resulted in a 35% lower TOF going from Co95Mn to Co11Mn. This clearly indicates that sites, which are present for H_2 chemisorption, are not one-to-one active for the FT reaction, but it rather shows that ensembles of cobalt sites are needed. This is comparable with our previous preliminary results on the cobalt particle size effect in FT catalysis where cobalt particles smaller than 12 nm were less active and exhibited far lower TOF values [22].

Another interesting feature of the MnO promoted catalysts is the change from paraffin-rich to olefin-rich products. In figure 12 the paraffin over olefin ratio is shown for the linear products for carbon numbers 2 to 8. The P/O ratio at all carbon numbers systematically decreased with the MnO loadings on the samples. The impact of addition of only 0.03 wt% MnO is again pronounced with a decrease of octane/octene ratio from 11 to 8. In the paraffin to olefin ratio the trade-off between the primary hydrogenation activity and the C-C coupling activity of the catalyst is manifested. As the hydrogenation activity of the catalysts decreases, more long-chain products will be formed as well as products that contain more olefins, which is the case for MnO promoted catalysts. A main role of the MnO promoter at 1 bar is therefore the moderation of the hydrogenation activity of the metallic cobalt.

Catalytic performances measured at 20 bar, which is a condition more relevant for industrial application, are reported in table 4. The loading of MnO on the catalysts influenced both the activity and the selectivity of the catalysts. The cobalt specific activity

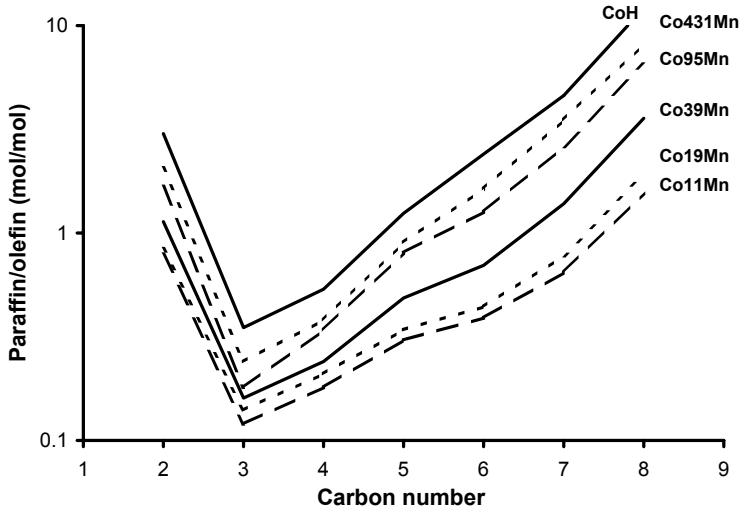

Figure 12. Influence of manganese loading on the ratio between paraffins and 1-olefins in the products at 1 bar.

Table 4. FTS catalytic performances at 20 bar, 220 ºC.

Sample	Activity	Deactivation (%/day)	TOF (10^{-3} s^{-1})	C_1 (wt%)	C_{5+}(wt%)	alpha
CoH	4.1	7	26	18	74	0.91
Co431Mn	5.1	6	37	14	78	0.89
Co95Mn	6.8	3	60	15	77	0.89
Co39Mn	5.8	3	54	20	66	0.86
Co11Mn	2.7	7	25	21	52	0.85

Activity: 10^{-5} mol CO $\cdot s^{-1} \cdot g^{-1}$ Co

increased from 4.1 to 6.8 $\cdot 10^{-5}$ $mol_{CO} \cdot g_{Co}^{-1} \cdot s^{-1}$ going from the unpromoted catalyst to Co95Mn. The addition of higher amounts of MnO caused a rapid decrease in activity to 2.7 $\cdot 10^{-5}$ $mol_{CO} \cdot g_{Co}^{-1} \cdot s^{-1}$ for Co11Mn. The differences in the TOF, also plotted in figure 13, were even larger and varied from 26 to 60 $\cdot 10^{-3}$ s^{-1} between CoH and Co95Mn. Interestingly similar TOF values were found for the un-promoted catalyst and the over-promoted catalyst. The catalysts deactivated with 4-7% of their activity per day, values that gradually declined in time. Meanwhile, stable selectivities were found. The addition of small amounts of MnO was beneficial for catalyst stability. The relative periods of time-on-stream in this study do not allow firm conclusions on the influence of MnO on the stability of the catalysts.

The methane selectivity of the catalysts varied from 14 to 21 wt%. Addition of only 0.03 wt% MnO resulted in a decrease in methane make from 18 to 14 wt%, but the addition of higher amounts of MnO caused progressively higher methane selectivities up to 21 wt%. Upon manganese loading the C_{5+} selectivity first increased from 74 to 78 wt% for Co431Mn, before it decreased to 52 wt% for Co11Mn. Also at 20 bar, the promoted catalysts contained more olefins, whilst the chain growth probability decreased continuously upon the addition of MnO from 0.91 to 0.85. It is known that the selectivity

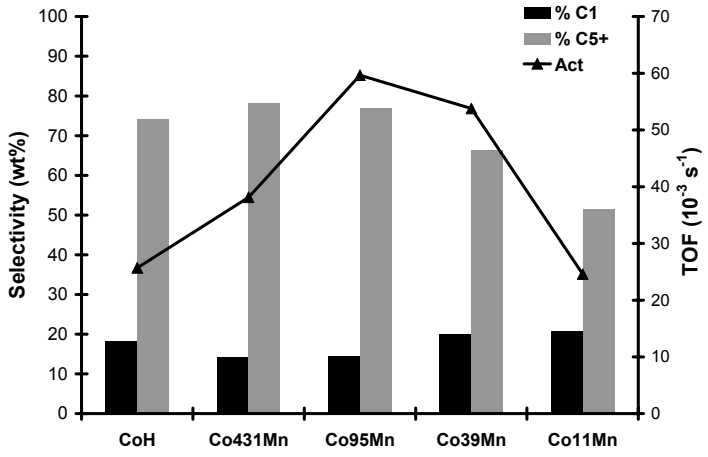

Figure 13. Influence of manganese loading on activity and selectivity in the FT reaction at 20 bar.

of catalysts in the FT reaction can vary largely with reaction conditions [33,34]. However, the presented data were measured at the same conditions and similar CO-conversions, which allows to study the influence of MnO as a promoter within this series.

Comparison of the catalytic data obtained at 1 bar and at 20 bar shows both similarities and large differences. At both conditions the TOF increased upon the loading of MnO, however, the 20% increase at 1 bar was modest compared to the 130% increase at 20 bar. From work on single crystals it is known that metal oxides can increase the specific activity for CO hydrogenation and that addition of too large amounts of the promoting element causes a decrease in TOF [35,36], confirming the trend in our data. Also operating at high pressures promoted catalysts can have higher turn-over rates with, for instance, a three-fold increase of TOF for Ru promoted cobalt catalysts [37]. The larger influence of MnO on the specific activity at 20 bar could be related to the more severe conditions at high pressure. For example, the presence of MnO in combination with cobalt surface reconstruction might create more sites on the catalyst that are active in chain growth. However, more research is needed to verify this hypothesis.

The trends in chain growth probability were completely different: an increase from 0.60 to 0.67 at 1 bar vs. a decrease from 0.91 to 0.85 at 20 bar. Related to these changes in chain growth probability we found a clear optimum in C_{5+} selectivity at 20 bar, while at 1 bar it remained high, also at high MnO loadings. The influence of MnO loading on selectivity at 1 bar is most probably related with the initially very low C_{5+} selectivity due to the high hydrogen coverage on the catalyst surface [38]. The addition of MnO may have decreased the hydrogen coverage on the catalyst, hereby increasing the C_{5+} selectivity. For the 20 bar experiments the catalyst surface is already largely covered with CO resulting in a high C_{5+} selectivity even for the un-promoted catalyst. The role of the promoter is now more delicate and over-promotion causes lower selectivity towards desired products [12].

Association of Mn with Co

The data presented so far show that small amounts of manganese have a significant influence on the cobalt reducibility and dispersion (TPR and H_2 chemisorption) and that MnO is present closely associated with the cobalt(oxide) particles in the dried and in the reduced samples (XPS and STEM-EELS). Now the question arises why manganese is only present associated with cobalt and is not located elsewhere on the CNF surface. Two explanations can be brought forward to answer the question. The first one addresses the number of available sites for anchoring the manganese during preparation, the second deals with the extent of interaction with sites on CoO and sites on carbon, respectively.

From the titration experiment we know that the reduction treatment of the support material diminishes the number of acidic groups to only 0.06 mmol per gram sample. The partly oxidized cobalt particles, however, account for a three times higher amount of oxygen surface groups in the sample. Assuming similar occupancies this would result in the majority of manganese located on top of cobalt oxide.

In the second explanation the presence of manganese oxide on top of the cobalt oxide particles is ascribed to the higher extent of interaction of MnO with CoO than with carbon. Co and Mn have similar ionic radii and readily form stable mixed oxides [32,39]. As we did not detect any manganese located on the CNF support, which is not expected with an equal distribution over the support oxygen groups and the cobalt oxide (*vide supra*), the most probable reason for the presence of manganese on top of cobalt in the dried catalyst is the high extent of interaction between cobalt and manganese oxide. However, during the reduction treatment the cobalt particles become metallic, which diminishes the interaction with MnO. In their study on MnO promotion in Co/TiO_2 catalysts, Morales *et al.* observed the migration of MnO away from the cobalt to the support during the reduction step [19]. In our case MnO did not interact with the inert graphite surface (*e.g.* Mn carbides were not observed in XPS), thus favoring the presence of the promoter close to the cobalt particles. This is the most important reason why CNF is our support of choice to study promoter effects in FT catalysis.

Conclusion

In this chapter we have shows that carbon nanofibers provide a suitable support to study the manganese oxide promotion effect in cobalt based FT catalysis, as interference of support effects is minimized. Cobalt properties can therefore be influenced by the addition of MnO loadings as low as 0.03 wt%. With XPS and STEM-EELS we show that manganese is present closely associated with cobalt both in the catalyst precursor and in the final catalyst. We demonstrate that manganese retarded the cobalt reduction and *in situ* XPS showed that the surface of the cobalt is more oxidic when MnO is added to the catalysts. Catalytic performances were affected differently at tests at 1 bar and at 20 bar. At 1 bar the chain growth probability increased and simultaneously the product distribution shifted towards olefinic products at increasing MnO loading. This shows that the presence of MnO moderates the hydrogenation activity of the catalysts. Interestingly, at 1 bar the TOF increased 20% upon loading with small amounts of manganese (0.13 wt% MnO). In the experiments at 20 bar C_{5+} selectivity first increased from 74 to 78 wt% at 0.03 wt% MnO, before it decreased to 52 wt% for 1.1 wt% MnO. The TOF increased

with at most 130% at 0.13 wt% MnO that nicely shows this promoter can favourably affect both activity and selectivity, depending on concentration and test conditions.

References

1. E. Iglesia, S.L. Soled, J.E. Baumgartner, S.C. Reyes, Top. Catal. 2 (1995) 17.
2. D. Schanke, S. Vada, E.A. Blekkan, A.M. Hilmen, A. Hoff, A. Holmen, J. Catal. 156 (1995) 85.
3. A. Kogelbauer, J.G. Goodwin, R. Oukaci, J. Catal. 160 (1996) 125.
4. G. Jacobs, T.K. Das, Y.Q. Zhang, J.L. Li, G. Racoillet, B.H. Davis, Appl. Catal. A 233 (2002) 263.
5. A. Guerrero-Ruiz, A. Sepulveda-Escribano, I. Rodriguez-Ramos, Appl. Catal. A 120 (1994) 71.
6. G.J. Haddad, B. Chen, J.G. Goodwin, J. Catal. 161 (1996) 274.
7. G.R. Moradi, M.M. Basir, A. Taeb, A. Kiennemann, Catal. Commun. 4 (2003) 27.
8. M. van der Riet, G.J. Hutchings, R.G. Copperthwaite, J. Chem. Soc., Chem. Commun. (1986) 798.
9. K. Guse, H. Papp, Fresenius J. Anal. Chem. 346 (1993) 84.
10. M.J. Keyser, R.C. Everson, R.L. Espinoza, Appl. Catal. A 171 (1998) 99.
11. S.E. Colley, R.G. Copperthwaite, G.J. Hutchings, S.P. Terblanche, M.M. Thackeray, Nature 339 (1989) 129.
12. S. Colley, R.G. Copperthwaite, G.J. Hutchings, M. Van der Riet, Ind. Eng. Chem. Res. 27 (1988) 1339.
13. F. Morales, F.M.F. de Groot, P. Glatzel, E. Kleimenov, H. Bluhm, M. Havecker, A. Knop-Gericke, B.M. Weckhuysen, J. Phys. Chem. B 108 (2004) 16201.
14. F.M. Cano, O.L.J. Gijzeman, F.M.F. de Groot, B.M. Weckhuysen, Stud. Surf. Sci. Catal. 147 (2004) 271.
15. Y.-Q. Zhang, B. Zhong, Q. Wang, J. Nat. Gas Chem. 6 (1997) 275.
16. M. Johns, P. Landon, T. Alderson, G.J. Hutchings, Chem. Commun. (2001) 2454.
17. J.J.C. Geerlings, M.F. Goes, H.M. Huisman, J.-P. Lange, H. Oosterbeek, P.J.M. Rek, D. Schadenhorst, WO Patent 9700231 (1997), to Royal Dutch Shell.
18. M. Jiang, N. Koizumi, T. Ozaki, M. Yamada, Appl. Catal. A 209 (2001) 59.
19. F. Morales, D. Grandjean, F.M.F. de Groot, O. Stephan, B.M. Weckhuysen, Phys. Chem. Chem. Phys. 7 (2005) 568.
20. F. Morales, F.M.F. de Groot, O.L.J. Gijzeman, A. Mens, O. Stephan, B.M. Weckhuysen, J. Catal. 230 (2005) 301.

21. K.P. de Jong, J.W. Geus, Catal. Rev.-Sci. Eng. 42 (2000) 481.
22. G.L. Bezemer, A. van Laak, A.J. van Dillen, K.P. de Jong, Stud. Surf. Sci. Catal. (2004) 259.
23. G.L. Bezemer, U. Falke, A.J. van Dillen, K.P. de Jong, Chem. Commun. (2005) 701.
24. M.L. Toebes, J.H. Bitter, A.J. van Dillen, K.P. de Jong, Catal. Today 76 (2002) 33.
25. M.L. Toebes, J.M.P. van Heeswijk, J.H. Bitter, A.J. van Dillen, K.P. de Jong, Carbon 42 (2004) 307.
26. H.P.C.E. Kuipers, Solid State Ion. 16 (1985) 15.
27. H.P.C.E. Kuipers, H.C.E. Van Leuven, W.M. Visser, Surf. Interface Anal. 8 (1986) 235.
28. F. Winter, G.L. Bezemer, C. van der Spek, J.D. Meeldijk, A.J. van Dillen, J.W. Geus, K.P. de Jong, Carbon 43 (2005) 327, chapter 5 of this thesis.
29. R.C. Reuel, C.H. Bartholomew, J. Catal. 85 (1984) 63.
30. V. Dureuil, C. Ricolleau, M. Gandais, C. Grigis, Eur. Phys. J. D 14 (2001) 83.
31. M. Oku, K. Hirokawa, J. Electron. Spectrosc. Relat. Phenom. 8 (1976) 475.
32. M.A. Langell, F. Gevrey, M.W. Nydegger, Appl. Surf. Sci. 153 (2000) 114.
33. C.J. Bertole, C.A. Mims, G. Kiss, J. Catal. 221 (2004) 191.
34. E. Iglesia, Appl. Catal. A 161 (1997) 59.
35. M.E. Levin, K.J. Williams, M. Salmeron, A.T. Bell, G.A. Somorjai, Surf. Sci. 195 (1988) 341.
36. M.E. Levin, M. Salmeron, A.T. Bell, G.A. Somorjai, J. Catal. 106 (1987) 401.
37. E. Iglesia, S.L. Soled, R.A. Fiato, G.H. Via, Stud. Surf. Sci. Catal. 81 (1994) 433.
38. C.J. Bertole, C.A. Mims, G. Kiss, J. Catal. 210 (2002) 84.
39. J.L. Martin de Vidales, E. Vila, R.M. Rojas, O. Garcia-Martinez, Chem. Mat. 7 (1995) 1716.

V

TEM AND XPS STUDIES TO REVEAL THE PRESENCE OF COBALT AND PALLADIUM PARTICLES IN THE INNER CORE OF CARBON NANOFIBERS

The presence of a considerable number of Co and Pd particles in the inner tube (4-9 nm inner diameter) of carbon nanofibers is demonstrated with TEM and XPS. Oxidation of freshly grown carbon nanofibers in nitric acid resulted in the opening of the inner tube of the fibers and in the creation of adsorption sites on the internal and external surface of the fibers, which are needed for anchoring of the metal precursors. It is demonstrated that analysis with TEM tilt series is a very powerful tool to locate the actual position of the metal particles, *i.e.* on the external or internal surface of the fibers. The fraction of metal present in the inner core of the fibers varied from 10-15% for Pd to 28-34% for Co, depending on the synthesis method.

Introduction

Carbon nanofibers (CNF) and carbon nanotubes (CNT) receive growing attention as support material for heterogeneous catalysts because of their purity, high mechanical strength, tunable surface properties, high surface area and accessibility and the absence of micropores [1,2]. The fibers consist of stacks of graphene sheets and, depending on the growth conditions and/or the type of metal used as growth catalyst, different structures can be obtained [3].

CNT, built up of coaxial cylindrical sheets, have a straight hollow core throughout the entire length of the fiber, which can be opened by careful oxidation in air [4] or carbon dioxide [5], or by treatment in nitric acid [6]. The diameter of the inner tubes of CNT is variable in the range of a few nanometers up to 100 nm. With the fishbone-type CNF the graphitic layers are cone-shaped and stacked on top of each other. The macroscopic CNF bodies consist of skeins of interwoven fibers [1,3,7]. The core of an individual fiber most probably consists of highly disordered graphene sheets or an amorphous carbon phase, which is removed upon HNO_3 treatment [1,8]. Only recently, it has been shown that it is also possible to grow in a single step fishbone-type carbon nanofibers with a hollow core throughout the length of the fiber [9-11]. In general, we can differentiate into three types of CNT/CNF (figure 1), wherein the main difference between CNF of type 1 and type 2 is the absence or presence, respectively, of a hollow core throughout the length of the fiber.

The deposition of metals and metal oxides inside CNT pretreated as indicated has been reported by several authors [12-16]. After removing the caps of the tubes, it appeared to be possible to fill these tubes with the metal(oxide) precursor solution.

The preparation, via impregnation and ion adsorption, of noble metal catalysts

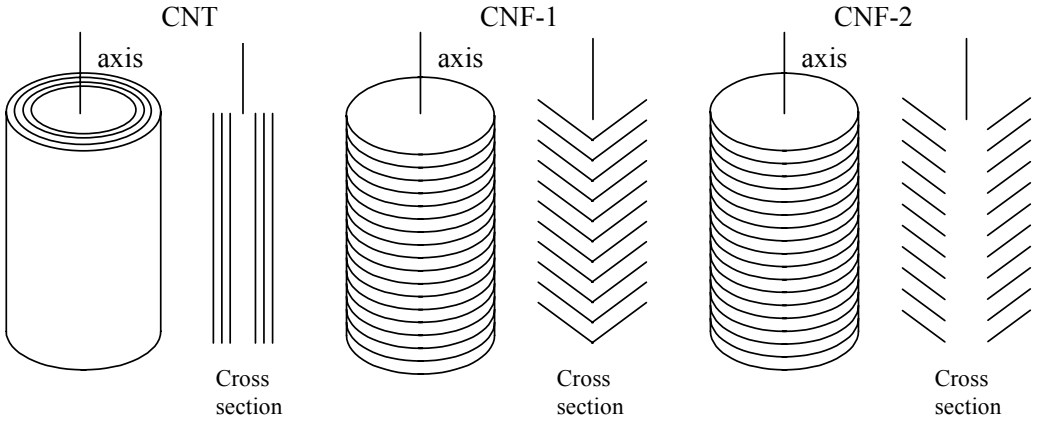

Figure 1. Schematic representation of CNT and CNF of different types.

supported on CNF/CNT has been studied extensively [*e.g.* 3,7,17-26]. In this chapter we report on the synthesis of Co and Pd catalysts on CNF using wet-impregnation/ion-adsorption techniques. The CNF were pretreated in concentrated nitric acid, which is necessary to introduce adsorption sites for the polar catalyst precursor on the originally hydrophobic surface of the fibers. It also makes the inner tube accessible. To our best knowledge we are the first to establish unambiguously the presence of a considerable fraction of metal particles at the internal surface of fishbone-type fibers in the ultimate catalyst. It is demonstrated that TEM imaging of samples tilted over a sequence of angles with respect to the electron beam is a powerful tool to discriminate between particles at the external and internal fiber surface.

Experimental session

Synthesis of carbon nanofibers

CNF were grown out of synthesis gas (H_2/CO) using either a commercial 57 wt% Ni/SiO_2 catalyst (Engelhard Ni5270P) or a 20 wt% Ni/SiO_2 catalyst, prepared as described elsewhere [1,20,27-29] at a growth temperature of 500 ºC and 550 ºC, respectively. After growth, the reactor content (further denoted as CNF a.s.) was refluxed for 1.5 h in a 1 M KOH solution, for removal of the silica support, and after thoroughly washing treated in boiling concentrated nitric acid for 2 h.

Synthesis of catalysts

The Pd/CNF catalyst (1 wt% Pd) was obtained by ion adsorption [3,30]. Typically, 5 g of CNF was suspended in 100 ml demineralized water. The pH of the suspension was adjusted to a value between 5 and 6 by adding drops of ammonia (25 wt%, Merck pure). Subsequently, an aqueous solution of $Pd(NH_3)_4(NO_3)_2$ (Alfa Aesar) was added and the resulting suspension was stirred for 20 h at room temperature under N_2 atmosphere. The catalyst precursor was filtered off under N_2 flow, washed and dried at 80 ºC for 20 h in N_2 flow. The Pd catalyst precursors were reduced in hydrogen flow at 250 ºC for 2 h.

The Co/CNF sample (5 wt% Co) was prepared using a wet-impregnation method [31]. In a flask 0.26 g $Co(NO_3)_2{\cdot}6H_2O$ (Acros *p.a.*) dissolved in 10 ml toluene/ethanol (2:1 v/v) was added to 1.0 g of CNF. Under continuous stirring the solvent was evaporated at ambient temperature applying a dynamic vacuum. The catalyst precursors were dried for 20 h at 60 ºC in air and subsequently reduced in a pure hydrogen flow at 300 ºC for 2 h. The samples were carefully passivated at 150 ºC using a CO_2/N_2 flow (1:5 v/v).

Characterization

TEM images were obtained with a Fei Technai 20 FEG TEM. TEM samples were, after ultrasonic treatment in butanol, dispersed on a holey carbon film. From a representative fiber a tilt series was taken from about -60º to +45º with 15º intervals. The tilt axis was chosen parallel to the length of the fiber.

N_2 physisorption measurements were performed using a Micromeritics ASAP 2400 analyzer. Before characterization measurements were performed, the samples were out gassed in vacuum at 120 ºC.

Powder X-ray diffraction (XRD) was performed using an Enraf-Nonius CPS 120 powder diffraction apparatus with Co K_α radiation (λ= 1.789 Å).

X-ray Photoelectron Spectroscopy (XPS) measurements were performed on a Thermo VG Scientific XPS system using non-monochromatic Mg (Kα) radiation. The pass energy of the analyzer was set at 70 eV. Calculations to determine the percentage of metal situated on the inner surface of CNF were performed with XPSCAT [32], a dispersion analysis program based on the original idea by Kuipers *et al.* [33,34]. In this model, and based on the TEM images Pd particles were assumed to have hemi-spherical shapes, whereas for Co spherical particles were used. Surface areas as determined with N_2 physisorption were used in the calculations.

Results and discussion

The CNF have a length of several hundreds of nanometers and diameters of around 30 nm for Co/CNF (not shown) and of 20-80 nm for Pd/CNF (figure 2). It appears that

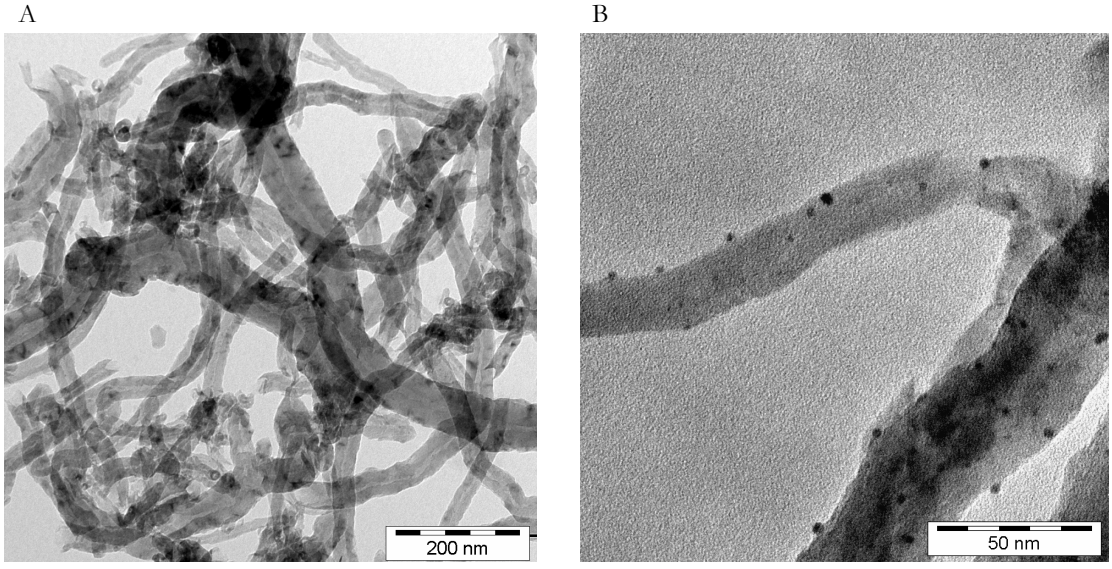

Figure 2. TEM images of Pd/CNF at (A) medium resolution and (B) high resolution.

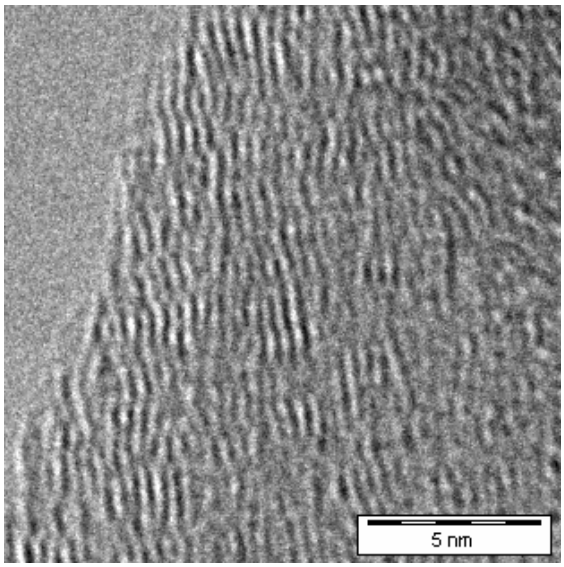

Figure 3. High resolution TEM image of CNF showing the typical fishbone structure.

most of the fibers contain an inner core, present over the whole length of the fiber, with diameters ranging from 4 to 9 nm. This variation is dependent on the diameter of the fiber itself. High resolution TEM (figure 3) shows that the fibers are indeed of the fishbone type, however, with irregularities in the graphene sheets. The distance between the graphene sheets is about 3.4 Å, a value which corresponds well with values that were obtained with XRD and are similar to values reported by other authors [3,8,35]. The core in the 'as synthesized' (a.s.) CNF is either empty or filled by an amorphous carbon phase of highly disordered graphene sheets.

Nitrogen physisorption was performed on the CNF materials in the different synthesis stages. In figure 4 the adsorption and desorption isotherms of CNF after KOH treatment and after treatment in HNO_3 are depicted. BET surface area and pore volume of the CNF materials are summarized in table 1. The isotherms are characteristic for multilayer adsorption/desorption and capillary condensation in mesopores, which

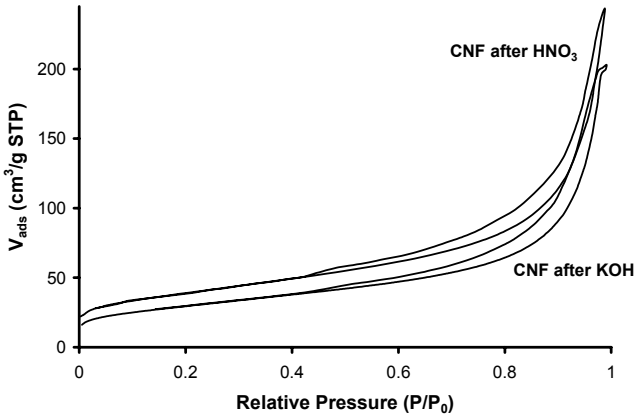

Figure 4. Nitrogen adsorption and desorption isotherms of CNF after treatments in KOH and HNO_3.

Table 1. N_2 physisorption on the CNF materials during different stages of preparation.

Samples	BET surface area ($m^2 \cdot g^{-1}$)	Total pore volume ($ml \cdot g^{-1}$)	Micropore volume ($ml \cdot g^{-1}$)
CNF a.s.	113[a]	0.32	0.002
CNF after KOH	106	0.26	0.003
CNF after HNO_3	137	0.38	0.004
Pd/CNF	138	0.40	0.003

causes the hysteresis loop. The shape of the hysteresis loops is characteristic for the presence of cylindrical mesopores with open ends at both sides can be derived. The micropore volume, calculated with the *t*-method, is very low in all samples, below 0.004 $ml \cdot g^{-1}$. CNF after KOH treatment exhibits, after correction for the silica support, a BET surface area similar to CNF a.s., *i.e.* 106 $m^2 \cdot g^{-1}$. Treatment in nitric acid increases the specific surface considerably, mainly due to the opening of the inner tubes, as was earlier suggested by Toebes *et al.* [36].

After applying the metal on the fibers, metal particles of 1-4 nm for Pd/CNF (figures 2 and 5) and 3-4 nm for Co/CNF (figure 6) were found by TEM, imaged by small black dots. These particles are randomly distributed as well as ordered to a great extent over the cores of the fibers. It is emphasized that TEM gives a two-dimensional projection, which makes a decision regarding the actual location of the metal particles, *i.e.* inside the core or at the external surface, difficult. Recently, electron tomography has been used to analyze porous catalysts [37-39]. TEM images taken over an angular tilt range give more detailed information about the actual position of the metal particles in the catalyst. In figure 5 a series of TEM images of Pd/CNF is depicted wherein the tilt axis, which was chosen parallel to the length of the fiber, is varied over a large angular range. In this series the displacement of four marked particles is key. When a metal particle is situated on the external surface of the fiber along with tilting the position of the particle should be largely determined by the tilt angle. In contrast to this, no or hardly any translation should occur upon tilting when a particle is situated inside the core of the fiber. From the sequence of the images it can be concluded that the particles denoted with a circle appear to be on the external surface of the fiber. The particles denoted by a square are located inside the fiber. Clearly, Pd particles are present both on the internal surface and on the external surface over the entire length of these fishbone fibers. Similar results were found with the Co/CNF samples (figure 6).

The presence of metal particles in the inner tubes strongly suggests that the required adsorption sites brought about by treatment in boiling HNO_3 are also present on the internal surface and that this inner tube is accessible for the metal precursor solutions and

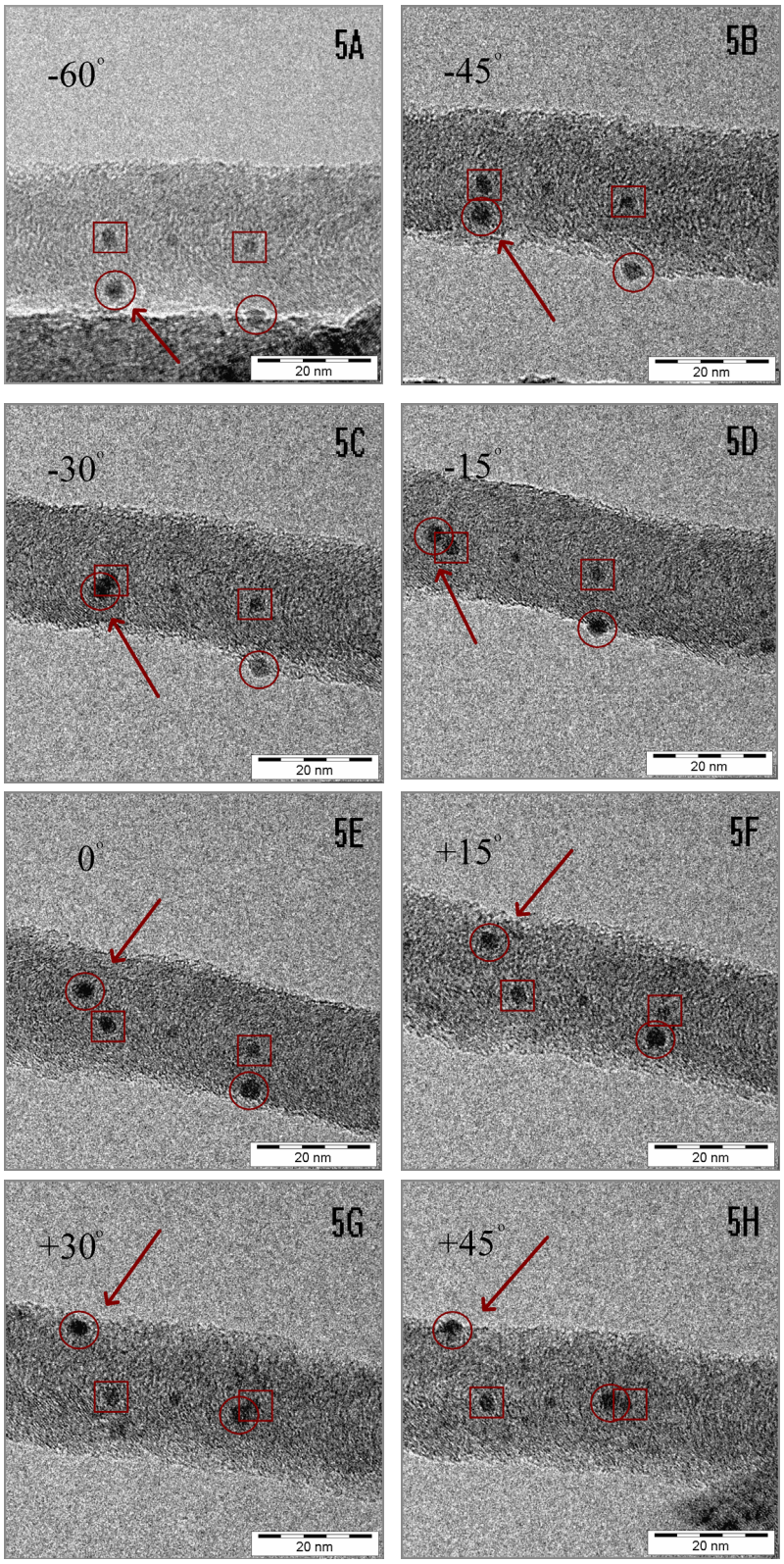

Figure 5. TEM tilt series over an angular tilt range with palladium particles on the inside (□) as well as on the outside (○) of the fiber. The tilt axis was chosen parallel to the length of the fiber. Arrows show a particle that appears to have a hemi-spherical shape when observed from the side.

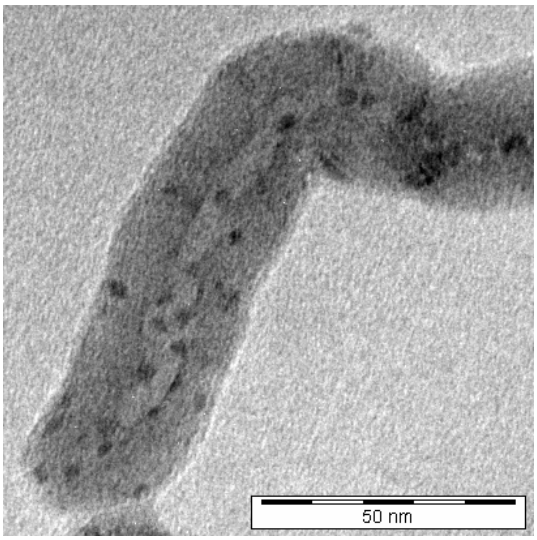

Figure 6. TEM image of Co/CNF showing particles both on the inside and the outside of the fiber.

later on for H_2 to make reduction of the precursor possible. Moreover, with Co/CNF we found that treatment of CNF with nitric acid is necessary to effectuate catalysts with high metal dispersions. Without this oxidative pre-treatment cobalt clusters as large as 300 nm were obtained on the surface of the macroscopic CNF bodies, while no cobalt particles on the internal surface of the fibers were found. Earlier studies on the deposition of Ni, Pt and Ru on CNF showed that deposition of metals using similar preparation methods is only possible when the surface of the fibers is oxidized [40,41].

To get an impression of the distribution ratio of the metal phase between internal and external surface we localized over 720 Pd particles distributed over 100 different fibers (table 2). In the 2D TEM images about 28% of the Pd particles measured appears to overlap with the 2D-projection of the fiber core. By calculation we found that the percentage of external surface area of the fiber overlapping with the 2D-projection of the fiber core is about 13% of the total external surface area, with the assumption that the fibers have an average diameter of 35 nm with an average inner core of 7 nm. Therefore, in case of a homogeneous distribution exclusively over the external surface of the fibers, the percentage of Pd overlapping with the fiber core should be about 13%, which is considerably lower than the percentage observed. These results give an indication of the percentage of Pd inside the fibers, *i.e.* 15%. The ratio between the surface area of the

Table 2. Percentage of metal particles situated in the inner tube of the fibers for Pd/CNF and Co/CNF as determined with TEM and XPS.

Sample	**% metal in inner tube (TEM)**	**% metal in inner tube (XPS)**
Pd/CNF	15	10
Co/CNF	34	28

inner tube and the total surface area is of about the same order (17%) as the percentage of Pd on the internal surface. This indicates that the distribution over the fibers is rather homogeneous over the internal as well as the external surface and that the inner tubes are completely accessible for metal deposition using the ion-adsorption method. Furthermore, no significant differences in metal particle size between particles situated on the internal or external surface were observed.

With the Co/CNF catalyst over 410 particles distributed on 80 fibers were examined. The mean Co particle size turned out to be 4 nm, which corresponds nicely to the particle size found with XRD. Nearly 47% of the particles seemed to overlap in 2D-TEM micrographs with the inner tubes of the fibers, whereas a homogeneous coverage of internal and external surface should have given the value of 28%, as argued above. This indicates that about 34% of Co particles is present in the inner tubes of the fibers.

With XPS analysis metal particles located in the inner tubes of the fibers give no contribution to the signal, due to the short mean free path of excitated electrons in graphite (2.6 nm) and the relatively large thickness of the fibers (14 nm). This loss in signal gives valuable information about the percentage of metal particles situated at the inner surface of the fibers (table 2). In the calculation we assumed that the Pd particles in Pd/CNF have hemi-spherical shapes. The shape of the particles can be inferred from the TEM tilt series if a particle is situated on the edge of the fiber in the TEM micrograph as indicated by the arrows in figure 5. For Co/CNF, also in line with our TEM results, a spherical particle shape was used. The weight percentage of metal situated in the inner tubes of CNF was determined by calculating from the XPS data the metal loading at the averaged metal particle sizes (as determined with TEM). The calculated metal loading reflects the weight percentage of metal situated at the external surface of the fibers. With this information we calculated that according to XPS analysis, about 10% of the metal particles of Pd/CNF and 28% of the metal particles of Co/CNF appears to be at the internal surface, which is readily in line with the observations from TEM analysis.

The relative high percentage of Co inside the tubes for the Co/CNF catalyst, which was prepared by wet impregnation, compared to the nominal fraction of Pd present inside the Pd/CNF catalyst, prepared using ion-adsorption, points out that different loading processes result in different distributions. On basis of the increase in pore volume due to the treatment of the fibers in nitric acid we would expect 32% of metal to be present on the internal surface when applying the wet-impregnation method. When ion-adsorption is used the surface ratio between inner and outer tube (17%) should govern the fraction of metal particles located inside the fibers. Above values are close to the fractions of metal particles present in the inner tube of the samples.

Conclusions

We have demonstrated that treatment of fishbone-type CNF in nitric acid results in opening of the inner tubes of the fibers and the creation of anchoring sites for the metal precursors. Results show that, depending on the synthesis method, 28-34% of Co and 10-15% Pd end up in the inner cores of these fibers. It is demonstrated that tilting the axis during TEM analysis gives very valuable information about the location of metal particles in CNF supported catalysts. Location of the metal particles on the internal surface of the fibers can be disadvantageous from a catalytic perspective, because mass transfer limitations in the narrow tubes of the fibers may arise, especially in liquid phase processes.

References

1. K.P. de Jong, J.W. Geus, Catal. Rev. -Sci. Eng. 42 (2000) 481.
2. P. Serp, M. Corrias, P. Kalck, Appl. Catal. A: Gen. 253 (2003) 337.
3. M.S. Hoogenraad. Utrecht University, The Netherlands (1995).
4. S.C. Tsang, Y.K. Chen, P.J.F. Harris, M.L.H. Green, Nature 372 (1994) 159.
5. S.C. Tsang, P.J.F. Harris, M.L.H. Green, Nature 362 (1993) 520.
6. P.M. Ajayan, T.W. Ebbesen, T. Ichihashi, S. Iijima, K. Tanigaki, H. Hiura, Nature 362 (1993) 522.
7. W. Teunissen. Utrecht University, The Netherlands (2000).
8. T.G. Ros, A.J. van Dillen, J.W. Geus, D.C. Koningsberger, ChemPhysChem 3 (2002) 209.
9. W.C. Ren, H.M. Cheng, Carbon 41 (2002) 1657.
10. M. Endo, Y.A. Kim, T. Hayashi, Y. Fukai, K. Oshida, M. Terrones, T. Yanagisawa, S. Higaki, M.S. Dresselhaus, Appl. Phys. Lett. 80 (2002) 1267.
11. K. Otsuka, Y. Abe, N. Kanai, Y. Kobayashi, S. Takenaka, E. Tanabe, Carbon 42 (2004) 727.
12. P.M. Ajayan, S. Iijima, Nature 361 (1993) 333.
13. P.M. Ajayan, O. Stephan, P. Redlich, C. Colliex, Nature 375 (1995) 564.
14. P.M. Ajayan, C. Colliex, J.M. Lambert, P. Bernier, L. Barbedette, M. Tence, O. Stephan, Phys. Rev. Lett. 72 (1994) 1722.
15. R.M. Lago, S.C. Tsang, K.L. Lu, Y.K. Chen, M.L.H. Green, J. Chem. Soc., Chem. Commun. 13 (1995) 1355.
16. J.-P. Tessonier, L. Pesant, C. Pham-Huu, G. Ehret, M.J. Ledoux, Stud. Surf. Sci. Catal. 143 (2002) 697.
17. C. Pham-Huu, N. Keller, G. Ehret, L.J. Charbonnierre, R. Ziessel, M.J. Ledoux, J. Mol. Catal. A: Chem. 170 (2001) 155.

18. C. Pham-Huu, N. Keller, L.J. Charbonnierre, R. Ziessel, M.J. Ledoux, Chem. Commun. (2000) 1871.
19. C. Park, M.A. Keane, J. Colloids Interface Sci. 266 (2003) 183.
20. M.S. Hoogenraad, R.A.G.M.M. van Leeuwarden, G.J.B. van Breda Vriesman, A. Broersma, A.J. van Dillen, J.W. Geus, Stud. Surf. Sci. Catal. 91 (1995) 263.
21. Hoogenraad, M.F. Onwezen, A.J. van Dillen, J.W. Geus, Stud. Surf. Sci. Catal. 101 (1996) 1331.
22. Z.-J. Liu, Z.-Y. Yuan, W. Zhou, L.-M. Peng, Z. Xu, Phys. Chem. Chem. Phys. 3 (2001) 2518.
23. A. Chambers, T. Nemes, N.M. Rodriguez, R.T.K. Baker, J. Phys. Chem. B 102 (1998) 2251.
24. R.T.K. Baker, K. Laubernds, A. Wootsch, Z. Paál, J. Catal. 193 (2000) 165.
25. J.M. Planeix, N. Coustel, B. Coq, V. Brotons, P.S. Kumbhar, R. Dutartre, P. Geneste, P. Bernier, P.M. Ajayan, J. Am. Chem. Soc. 116 (1994) 7935.
26. E.S. Steigerwalt, G.A. Deluga, D.E. Cliffel, C.M. Lukehart, J. Phys. Chem. B 105 (2001) 8097.
27. N.M. Rodriguez, J. Mater. Res. 8 (1993) 3233.
28. M.L. Toebes, J.H. Bitter, A.J. van Dillen, K.P. de Jong, Catal. Today 76 (2002) 33.
29. M.L. Toebes, F.F. Prinsloo, J.H. Bitter, A.J. van Dillen, K.P. de Jong, J. Catal. 214 (2003) 78.
30. F. Winter, A.J. van Dillen, K.P. de Jong, J. Mol. Catal. A: Chem. 219 (2004) 273.
31. G.L. Bezemer, A. van Laak, A.J. van Dillen, K.P. de Jong, Stud. Surf. Sci .Catal. 147 (2004) 259.
32. O.L.J. Gijzeman, XPS Analysis of Catalyst Surfaces, Utrecht University, Utrecht, The Netherlands (unpublished).
33. H.P.C.E. Kuipers, Solid State Ionics 16 (1985) 15.
34. H.P.C.E. Kuipers, H.C.E.v. Leuven, W.M. Visser, Surf. Interface Anal. 8 (1986) 235.
35. M. Nijkamp, Utrecht University, The Netherlands (2002).
36. M.L. Toebes, J.M.P. van Heeswijk, J.H. Bitter, A.J. van Dillen, K.P. de Jong, Carbon 42 (2004) 307.
37. A.J. Koster, U. Ziese, A.J. Verkleij, A.H. Janssen, K.P. de Jong, J. Phys. Chem. B 104 (2000) 9368.
38. A.H. Janssen, P. van der Voort, A.J. Koster, K.P. de Jong, Chem. Commun. 15 (2002) 1632.
39. A.H. Janssen, P. van der Voort, A.J. Koster, K.P. de Jong, Angew. Chem.-Int. Edit. 40 (2002) 1102.
40. J.H. Bitter, M.K. van der Lee, A.G.T. Slotboom, A.J. van Dillen, K.P. de Jong, Catal. Lett. 89 (2003) 139.
41. M.L. Toebes, M.K. van der Lee, L.M. Tang, M.H. Huis in 't Veld, J.H. Bitter, A.J. van Dillen, K.P. de Jong, J. Phys. Chem. B 108 (2004) 11611.

VI

SUMMARY AND CONCLUDING REMARKS

The Fischer-Tropsch (FT) process converts synthesis gas (H_2/CO) over a heterogeneous catalyst into hydrocarbons. This enables the production of transportation fuels from other carbon sources than crude oil. Generally, cobalt catalysts supported on oxidic carriers are used for the FT process. On these oxidic support materials it appears to be difficult to obtain and maintain fully reduced cobalt particles as stable cobalt-support compounds can be formed during preparation and treatments, especially with small precursor particles. To overcome these problems we started to use carbon nanofibers (CNF), a novel support material on which cobalt-support compounds are not expected to form. CNF consists of interwoven fibers of graphitic carbon with a high purity, a high mechanical strength and a high chemical inertness. This latter feature, however, makes the application of a dispersed cobalt phase a challenging task. Therefore, we concentrated on the design of well-defined CNF-supported cobalt catalysts.

Homogeneous deposition-precipitation (HDP) is a synthesis procedure often applied for the preparation of dispersed metal(oxide) catalysts on oxidic supports. In **chapter 2** we describe our research on the preparation of catalysts with an intended loading of 15 wt% cobalt on CNF and on silica using the HDP method. Besides the conventional deposition starting from acidic solution we also performed experiments starting from basic solution. Urea hydrolysis was used to achieve a slow and homogeneous pH increase for experiments starting at low pH, while ammonia evaporation was used to slowly decrease the hydroxyl concentration for experiments starting at high pH. Analysis of the pH curves and the corresponding cobalt concentration revealed a very high interaction between silica and cobalt with the low pH procedure. The obtained cobalt hydrosilicate precursor required a reduction temperature of at least 600 ºC, resulting in large metallic cobalt particles (40 nm).

Desired lower interaction between silica and cobalt was achieved in preparations from basic solution. Now a dispersed Co_3O_4 precursor was obtained after drying that could be reduced at 500 ºC, resulting in a catalyst with cobalt particles of only 13 nm. Too low an interaction between support and precipitate was found with the low pH experiments using activated CNF as the support material. The adsorption of Co species on the carboxylic surface groups appeared too small to achieve nucleation selectively on CNF. Consequently, a catalyst with a cobalt metal dispersion of only 3.9% was obtained after reduction. A stronger interaction and a 2.3 times higher adsorption of cobalt ions was found with the sample prepared using the high pH method. In the dried sample small Co_3O_4 clusters were found on the CNF, that after reduction at 350 ºC resulted in a catalyst with an average cobalt particle size of 8 nm.

The inert nature of CNF made application of a dispersed cobalt precursor difficult, but also enabled complete reduction at low temperatures, thus avoiding cobalt sintering. Presented results demonstrate that the newly developed, high pH method yields better-dispersed Co catalysts on both supports compared to the conventional low pH method. Due to the larger cobalt surface area we found 2-4 times higher FT activities for samples prepared from basic environment, with similar or better catalyst selectivities. Homogeneous deposition-precipitation starting from basic environment might be also useful for the preparation of other metal(oxide) catalysts.

The preparation of Co/CNF catalysts was further studied in **chapter 3** where besides the two ways of performing HDP also incipient-wetness impregnation and ion adsorption were used to synthesize catalysts with different dispersions. The average cobalt particle size in the catalysts varied from 2.7 to 27 nm with narrow size distributions. Using these catalysts we investigated the influence of cobalt particle size on the Fischer-Tropsch reaction. X-ray Absorption Spectroscopy measurements proved that the cobalt phase was metallic after an *in situ* reduction treatment, which is an prerequisite for catalytic operation and is difficult on oxidic supports.

In the catalytic tests we observed that the turn-over frequency (TOF) was independent of cobalt particle size for catalysts with sizes larger than 6 nm (1 bar) or 8 nm (35 bar), while both the selectivity and the activity changed for catalysts with smaller particles. At 35 bar the TOF decreased from 23 $\cdot 10^{-3}$ s^{-1} to 1.4 $\cdot 10^{-3}$ s^{-1} while the C_{5+} selectivity decreased from 85 to 51 wt% when the cobalt particle size was reduced from 16 to 2.6 nm. This demonstrates that the minimal required cobalt particle size for Fischer-Tropsch catalysis is larger (6-8 nm) than can be explained by classical structure sensitivity. Other explanations raised in literature, *viz.* formation of CoO or Co carbide species on small particles during catalytic testing, were not substantiated by experimental evidence with X-ray Absorption Spectroscopy. Interestingly we found with EXAFS a decrease of the cobalt coordination number under reaction conditions, which points to reconstruction of the cobalt surface. Consequently, it is argued that the cobalt particle size effects can be attributed to CO-induced non-classical structure sensitivity. The profound influence of cobalt dispersion on FT performance found in our work is very relevant for the design of economic Fischer-Tropsch catalysts that should have narrow particle size distributions with average values close to the optimum value which depends on pressure.

Another way to influence the performance of cobalt-based Fischer-Tropsch catalysts is the addition of promoter elements. On oxidic support materials noble metals are generally added to decrease the reduction temperature and to increase the

activity. To achieve better selectivities towards heavier hydrocarbons metal oxides are generally added. An example of such a promoter system is MnO, which is mentioned in patent literature although not much has been published in open literature. **Chapter 4** deals with the preparation and testing of MnO-promoted cobalt catalysts supported on carbon nanofibers. We demonstrated with XPS and STEM-EELS that in the dried samples the promoter was only present associated with the cobalt particles, probably due to the tendency of cobalt and manganese to form stable mixed compounds. After reduction at 350 ºC the manganese phase remained in the oxidized state, localized close to the cobalt particles, as the inert support material lacked sites with significant interaction with metal oxides.

This close association between cobalt and MnO resulted in significant changes in catalytic performances even with very low concentrations of promoter present. At 1 bar large improvements in C_{5+} selectivity were found with MnO loadings of 0.03 wt% and higher, with only slightly lower TOF values. From product analysis (paraffin-olefin ratio) it appears that a major role of MnO involves moderation of hydrogenation reactions. At 20 bar the addition of 0.03 wt% MnO improved the C_{5+} selectivity, while larger amounts decreased the selectivity. The TOF increased 130% upon addition of 0.3 wt% MnO while it decreased when higher loadings were applied. Presented data show that the addition of small amounts of MnO on cobalt on carbon nanofibers catalysts has a large influence on both selectivity and activity, depending on test conditions and promoter concentration. The relatively inert nature of carbon nanofibers directs the promoter towards the cobalt precursor, thus causing large influences on catalytic performances, even for very low MnO loadings. It is speculated that the study of other promoters could also benefit from the use of CNF as support material.

It has been mentioned before that CNF consists of interwoven fibers. In **chapter 5** it is shown that these individual fibers have an inner tube that is opened during the activation treatment in nitric acid. The preparation of cobalt and palladium catalysts with impregnation and ion exchange, respectively, resulted in the deposition of metal particles inside the fibers. Using TEM tilt series and quantitative XPS we showed that the weight fraction of metal deposited in the inner tube is related to the fraction of surface area or pore volume related with this tube. The location of the metal particles on the internal surface of the fibers can be disadvantageous from a catalytic perspective, because mass transfer limitations in the narrow tubes of the fibers may arise, especially in liquid-phase processes.

Presented results demonstrate that the use of CNF helped to solve fundamental issues related with Fischer-Tropsch synthesis. Moreover, we discovered ways to enhance both activity and selectivity of these catalysts, which is very interesting for the development of new Fischer-Tropsch catalysts.

VII

NEDERLANDSE SAMENVATTING

Het Fischer-Tropsch (FT) proces is genoemd naar Franz Fischer en Hans Tropsch die in 1923 publiceerden dat er koolwaterstoffen kunnen worden gevormd wanneer synthesegas (H_2/CO) over een katalysator wordt geleid. Door gebruik te maken van dit proces kunnen schone, vloeibare brandstoffen worden verkregen uit aardgas, biomassa of steenkool. Momenteel is er veel belangstelling voor het FT-proces en de grootschalige toepassing hiervan komt steeds dichterbij. Een typische FT-katalysator bestaat uit kleine kobaltdeeltjes op een oxidisch dragermateriaal. Nadeel van deze traditionele dragermaterialen is hun reactiviteit, waardoor tijdens bereiding en gebruik stabiele mengverbindingen tussen kobalt en drager kunnen ontstaan die slechts moeilijk gereduceerd kunnen worden. Om deze problemen te vermijden hebben we de mogelijkheden van het gebruik van koolstofvezels bestudeerd. Koolstofvezels, ofwel carbon nanofibers (CNF), vormen een nieuw en inert dragermateriaal dat bestaat uit draden van grafitische koolstof die verweven zijn tot een sterke driedimensionale structuur. Door de inertheid van koolstofvezels is een mengverbinding met kobalt niet te verwachten, echter dit maakt het ook moeilijker om katalysatoren met kleine kobaltdeeltjes te synthetiseren. Daarom hebben we veel aandacht besteed aan de bereiding van goed gedefinieerde systemen van kobalt op koolstofvezels.

Voor de bereiding van katalysatoren met fijn verdeelde metaal(oxide)deeltjes op oxidische dragers wordt vaak gebruik gemaakt van homogene depositie-precipitatie (HDP). De mogelijkheden van deze methode voor de bereiding van kobaltkatalysatoren op koolstofvezels en op silica worden onderzocht in **hoofdstuk 2**. Hierbij hebben we de traditionele methode uit zuur milieu vergeleken met een nieuwe methode uit basisch milieu. De bereidingen vanuit zuur milieu gebruikten de hydrolyse van ureum voor een graduele en homogene stijging van de pH, terwijl voor de bereidingen vanuit basisch milieu de gecontroleerde verdamping van ammoniak gebruikt werd om de pH langzaam te verlagen. Tijdens de precipitatie werd het verloop van de pH gevolgd en ook werd de kobaltconcentratie periodiek bepaald. Analyse hiervan liet een te sterke interactie tussen kobalt en silica zien voor experiment bij lage pH. Het kobalt bleek gereageerd te hebben met silica tot kobalthydrosilicaat dat pas bij 600 °C gereduceerd kon worden, wat resulteerde in grote metallische kobaltdeeltjes van zo'n 40 nm.

Een verminderde interactie tussen kobalt en silica werd bereikt met experimenten uit basisch milieu, waarbij het verkregen Co_3O_4 al bij 500 °C gereduceerd kon worden tot een katalysator met kobaltdeeltjes van 13 nm. Bij het experiment vanuit zuur milieu met koolstofvezels als dragermateriaal bleek de interactie tussen het neerslag en de drager juist te gering te zijn. De adsorptie van kobalt op de zure groepen was

onvoldoende om selectieve kiemvorming op het oppervlak te bewerkstelligen, resulterend in kobaltdeeltjes van 25 nm in de uiteindelijke katalysator. Een sterkere interactie en een 2,3 keer hogere adsorptie van kobaltionen werd gevonden met het monster bereid met de hoge pH methode. Ook hier werden kleine gedragen Co_3O_4 clusters gevonden, die na reductie bij 350 ºC een katalysator met 8 nm grote kobaltdeeltjes opleverden. De inertheid van de koolstofvezels bemoeilijkte het afzetten van fijnverdeeld kobaltoxide maar had ook tot gevolg dat volstaan kon worden met lage reductietemperaturen waardoor sintering van kobalt kon worden voorkomen. De resultaten laten verder zien dat de nieuwe bereidingsmethode vanuit basisch milieu katalysatoren met betere dispersies en hierdoor 2-4 maal hogere activiteiten oplevert dan de traditionele methode in zuur milieu.

In **hoofdstuk 3** werden behalve de twee genoemde HDP-methoden ook impregnatie en ionenuitwisseling gebruikt om katalysatoren met uiteenlopende kobaltdispersies te maken. De gemiddelde kobaltdeeltjesgrootte in de katalysatoren varieerde van 2,6 tot 27 nm met een smalle deeltjesgrootteverdeling. Met deze katalysatoren hebben we de invloed van de grootte van kobaltdeeltjes op de prestaties in de Fischer-Tropsch reactie bestudeerd. XAS metingen op de katalysatoren met de kleinste kobaltdeeltjes na *in situ* reductie lieten metallisch kobalt zien, iets wat noodzakelijk is voor het functioneren van de katalysatoren. In de katalytische metingen bleek de activiteit per kobaltatoom aan het oppervlak (TOF) onafhankelijk te zijn van de deeltjesgrootte voor katalysatoren met kobaltdeeltjes groter dan 6 nm (1 bar) of 8 nm (35 bar). Echter, voor katalysatoren met kleinere deeltjes werd een tot vijftien keer lagere waarde voor de TOF gevonden en ook de C_{5+}-selectiviteit was substantieel lager. Deze resultaten laten zien dat de minimaal benodigde kobaltdeeltjesgrootte voor Fischer-Tropsch katalyse ongeveer 6-8 nm is, dit is veel groter dan verwacht op basis van klassieke structuurgevoeligheid. Om de oorzaak van het deeltjesgrootte-effect te bepalen werden XAS metingen uitgevoerd op katalysatoren onder reactiecondities. Hierbij werd geen bewijs gevonden voor de vorming van CoO of CoC, noch voor het optreden van sintering, welke allemaal in de literatuur genoemde verklaringen zijn voor de geringere prestaties van kleine deeltjes. Wel was er een duidelijke aanwijzing voor het optreden van reconstructie van het kobaltoppervlak onder reactiecondities. Daarom wordt betoogd dat deeltjesgrootte-effecten van kobalt samenhangen met door koolmonoxide geïnduceerde structuurgevoeligheid. De duidelijke invloed van kobaltdispersie op activiteit en selectiviteit van FT katalysatoren is ook van belang voor de bereiding van goede

katalysatoren die een smalle deeltjesgrootteverdeling zullen moeten hebben rond een gemiddelde dicht bij de drukafhankelijke optimale waarde.

Behalve het variëren van de kobaltdispersie is een andere mogelijkheid om de prestaties van kobaltkatalysatoren in de FT reactie te veranderen het toevoegen van promoters. Op oxidische dragermaterialen worden vaak edelmetalen toegevoegd om reductie bij lagere temperaturen mogelijk te maken en de activiteit te verhogen. Om de selectiviteit te verbeteren worden veelal metaaloxides toegevoegd, zoals bijvoorbeeld MnO. In **hoofdstuk 4** wordt de bereiding, karakterisering en het testen van MnO-gepromoteerde kobaltkatalysatoren op koolstofvezels beschreven . Met XPS en STEM-EELS werd aangetoond dat de promoter selectief aanwezig was bij de kobaltdeeltjes in de gedroogde katalysator wat verklaard kan worden door de neiging van deze elementen om stabiele mengverbindingen te vormen. Ook na de reductiestap was mangaanoxide te vinden bij kobalt waarschijnlijk ten gevolge van de afwezigheid van groepen met voldoende interactie met het oxide op de drager. Dit verklaart waarom het toevoegen van geringe hoeveelheden MnO de eigenschappen van de katalysator kan veranderen. De C_{5+}-selectiviteit verbeterde sterk door toevoeging van MnO terwijl de TOF nauwelijks veranderde. Productanalyse liet zien dat een belangrijke rol van MnO het onderdrukken van de hydrogeneringsactiviteit betreft. Bij 20 bar werd de C_{5+}-selectiviteit alleen vergroot bij een MnO-belading van 0,03 wt%, terwijl hogere beladingen juist een lagere selectiviteit lieten zien. De TOF steeg met maximaal 130% voor het monster met 0,3 wt% MnO, met kleinere stijgingen voor zowel grotere als kleinere hoeveelheden promoter. De grote verandering van de katalytische eigenschappen door het toevoegen van geringe hoeveelheden MnO, maakt koolstofvezels een potentieel interessant dragermateriaal voor onderzoek naar andere promoters.

In **hoofdstuk 5** wordt in meer detail ingegaan op een interessant aspect van het dragermateriaal. Het blijkt dat de behandeling met salpeterzuur, nodig om de koolstofvezels te activeren, ook een binnenbuis opent in de draden. Tijdens de bereiding van kobalt- en palladiumkatalysatoren met respectievelijk impregnatie en ionenuitwisseling werden metaaldeeltjes in deze binnenbuis afgezet. Met behulp van TEM en kwantitatieve XPS werd aangetoond dat het percentage metaaldeeltjes in de binnenbuis gerelateerd is aan het aandeel van de binnenbuis in het totale oppervlak dan wel in het totale porievolume. De aanwezigheid van metaaldeeltjes in de binnenbuis kan nadelig zijn aangezien stoftransport te langzaam kan zijn in de nauwe buizen, in het bijzonder bij vloeistoffaseprocessen.

De in dit proefschrift beschreven resultaten laten zien dat het gebruik van koolstofvezels als dragermateriaal behulpzaam was voor het oplossen van fundamentele problemen in de Fischer-Tropsch synthese. Verder hebben we mogelijkheden laten zien waarmee zowel de activiteit als de selectiviteit van deze katalysatoren verhoogd kunnen worden, wat interessant kan zijn voor de ontwikkeling van nieuwe Fischer-Tropsch katalysatoren.

LIST OF PUBLICATIONS AND PRESENTATIONS

Publications

G.L. Bezemer, A. van Laak, A.J. van Dillen, K.P. de Jong: Cobalt supported on carbon nanofibers - a promising novel Fischer-Tropsch catalyst.
Stud. Surf. Sci. Catal. (2004) 259-264.

G.L. Bezemer, U. Falke, A.J. van Dillen, K.P. de Jong: Cobalt on carbon nanofiber catalysts: auspicious system for study of manganese promotion in Fischer-Tropsch catalysis.
Chemical Communications (2005) 701-703.

F. Winter, G.L. Bezemer, C. van der Spek, J.D. Meeldijk, A.J. van Dillen, J.W. Geus, K.P. de Jong: TEM and XPS studies to reveal the presence of cobalt and palladium particles in the inner core of carbon nanofibers.
Carbon 43 (2005) 327-332.

G.L. Bezemer, P.B. Radstake, U. Falke, H.Oosterbeek, A.J. van Dillen and K.P. de Jong: Investigation of promoter effects of manganese oxide on carbon nanofibers supported cobalt catalysts for Fischer-Tropsch synthesis
Accepted in J. Catal.

G.L. Bezemer, P.B. Radstake, V. Koot, A.J van Dillen, J.W. Geus and K.P. de Jong: Preparation of Fischer-Tropsch cobalt catalysts supported on carbon nanofibers and silica using homogeneous deposition-precipitation
Accepted in J. Catal.

G.L. Bezemer, J.H. Bitter, H.P.C.E. Kuipers, H. Oosterbeek, H. Holewijn, X. Xu, F. Kapteijn, A.J van Dillen, and K.P. de Jong: Cobalt particle size effects in Fischer-Tropsch catalysis studied with carbon nanofibers supported cobalt catalysts
Submitted.

L.G.A. van de Water, G.L. Bezemer, J.A. Bergwerff, B.M. Weckhuysen and K.P. de Jong: Studying the Preparation Process of Co-γ-Al_2O_3 Fischer-Tropsch catalysts by spatially resolved UV-Vis (DRS) Microspectroscopy
In preparation

Keynote lecture

G.L. Bezemer, A. van Laak, A.J. van Dillen and K.P. de Jong: Fischer-Tropsch synthesis using cobalt on carbon nanofibers
7th Natural Gas Conversion Symposium, Dalian, China, June 2004.

Oral presentations

G.L. Bezemer, A.J. van Dillen and K.P. de Jong: Cobalt supported on carbon nanofibers – a novel Fischer-Tropsch catalyst
5th Netherlands' Catalysis and Chemistry Conference, Noordwijkerhout, The Netherlands, March 2004.

G.L. Bezemer, J.H. Bitter, A.J.van Dillen, K.P. de Jong: Cobalt supported on carbon nanofibers – a novel Fischer-Tropsch catalyst
Carbon 2004, Providence, USA, July 2004

G.L. Bezemer, A.J. van Dillen and K.P. de Jong: Cobalt supported on carbon nanofibers
NIOK Fischer-Tropsch workshop, Utrecht, The Netherlands, October 2004

G.L. Bezemer, P.B. Radstake, A.J. van Dillen and K.P. de Jong: Cobalt on CNF catalysts for fundamental studies in Fischer-Tropsch synthesis
6th Netherlands' Catalysis and Chemistry Conference, Noordwijkerhout, The Netherlands, March 2005

G.L. Bezemer, A.J. van Dillen and K.P. de Jong : Cobalt on carbon nanofibers catalysts for the study of cobalt particle-size effects in Fischer-Tropsch catalysis
19th North American Catalysis Society Meeting, Philadelphia, May 2005

G.L. Bezemer, P.B. Radstake, A.J. van Dillen and K.P. de Jong: New insights into manganese promotion effects in Fischer-Tropsch synthesis
Europacat VII, Sofia, Bulgaria, August 2005

Poster presentations

G.L. Bezemer, A.A. Battiston, J.H. Bitter and D.C. Koningsberger: Catalytic reduction of NO via Pt/ZSM5 and overexchanged Fe/ZSM5: dual bed configuration
3rd Netherlands' Catalysis and Chemistry Conference, Noordwijkerhout, The Netherlands, March 2002

G.L. Bezemer, J.H. Bitter, A.J. van Dillen and K.P. de Jong: Fischer-Tropsch synthesis using cobalt on carbon nanofibers
4th Netherlands' Catalysis and Chemistry Conference, Noordwijkerhout, The Netherlands, March 2003

G.L. Bezemer, A.J. van Dillen and K.P. de Jong: Cobalt supported on carbon nanofibers – a novel Fischer-Tropsch catalyst
Scope 2004, Florence, Italy, June 2004

G.L. Bezemer, A.J. van Dillen and K.P. de Jong: Cobalt supported on Carbon Nanofibers – A promising novel Fischer-Tropsch Catalyst for the production of clean Fuels
13th International Catalysis Conference, Paris, France, July 2004

P.B. Radstake, G.L. Bezemer, A.J. van Dillen and K.P. de Jong: Promoting effects of manganese oxide on cobalt in Fischer-Tropsch catalysis
6th Netherlands' Catalysis and Chemistry Conference, Noordwijkerhout, The Netherlands, March 2005

DANKWOORD

Tja, het zit er bijna op. Na bijna vier jaar promotieonderzoek is het nu tijd voor het schrijven van dit dankwoord. Ik heb het goed naar mijn zin gehad in mijn tijd als AIO en ik wil iedereen bedanken die daaraan heeft bijgedragen. Hoewel ik nu in feite dit dankwoord kan afsluiten met mijn naam, wil ik toch nog een aantal lieden specifieker aanspreken, terwijl ik tegelijkertijd niet bang hoef te zijn iemand niet genoemd te hebben.

Krijn, ik wil je hartelijk bedanken voor de kans die je me hebt geboden om te promoveren. Toen we destijds de mogelijke projecten bij jou langs liepen, sprak de combinatie van het doen van fundamenteel onderzoek met een praktische relevantie me erg aan. Vandaar dat mijn keus viel op het project in samenwerking met Shell waar de vraag naar de invloed van de grootte van kobaltdeeltjes op Fischer-Tropsch katalysatoren centraal stond. Ik heb gelukkig geen spijt gekregen van mijn keuze, al was het maar goed dat er gaandeweg nog wat andere onderwerpen bijkwamen, anders had dit proefschrift slechts één wetenschappelijk hoofdstuk geteld. Krijn, de samenwerking met jou heb ik als heel plezierig ervaren. Hartelijk dank voor alles wat je me leerde. Gelukkig hierbij was dat je vaak tijd had voor een 'korte vraag', waarbij het natuurlijk zo was dat de lengte van de vraag niet indicatief hoeft te zijn voor de lengte van het antwoord.

Jos, zeer gewaardeerde co-promoter, hartelijk dank voor al je inzet. De open deur van je kamer was altijd gemakkelijk, behalve dan wanneer iemand anders daar al gebruik van gemaakt had. Het corrigeren van de verschillende artikelen heb je altijd zeer consciëntieus gedaan, waarbij met name het HDP-verhaal een moeilijke geboorte was. Dank ook voor je voortdurende optimisme.

Harry, jou wil ik bedanken voor je hulp bij het aanvragen van meettijd in Hasylab en voor je hulp bij het uitvoeren en uitwerken van de metingen. De resultaten van de EXAFS metingen hebben een tamelijk prominente plaats gekregen in hoofdstuk 3, iets wat zonder jou niet was gelukt. John, het was me altijd weer een genoegen met je achter de microscoop te zitten. Hartelijk dank voor alle mooie plaatjes en je goede commentaar.

Tijdens mijn AIO-periode heb ik het geluk gehad tweemaal een afstudeerder te kunnen begeleiden, iets wat met de teruglopende studentenaantallen niet voor iedereen is weggelegd. Adri, jij kwam toen ik nog geen jaar bezig was en veel zaken nog uitgevogeld moesten worden, terwijl jij, Paul, in de eindfase het onderzoek inrolde. Hartelijk dank voor jullie enthousiaste bijdrage en veel succes met jullie eigen promotieonderzoek..

Heiko Oosterbeek, jij was onze Shell Monitor, zoals dat volgens het contract heette en met regelmatig contact in Utrecht of Amsterdam nam je die taak heel serieus. Het was me

een genoegen met je samen te werken en ik heb goed kunnen profiteren van je grote kennis van het Fischer-Tropsch proces. Hoewel jij vaak moest manoeuvreren tussen wetenschappelijke en Koninklijke belangen, is het uiteindelijk mede dankzij jou toch goed gekomen met de metingen op relevante condities, iets wat het belang van hoofdstuk 3 en 4 ten goede is gekomen. Herman Kuipers en Carl Mesters dank ik voor het plezierige overleg en de discussies die we hadden. Kees de Kloe, de macro die je voor mij hebt geschreven voor het uitwerken van data gebruik ik al jaren met veel genoegen. Verder ben ik de volgende personen erkentelijk voor het uitvoeren van metingen: Ralph Haswell (TEM), Hans Holewijn (hoge-druk FT) en Gert-Jan Jonkers (XPS).

Freek Kapteijn wil ik hartelijk bedanken voor de mogelijkheid katalytische metingen bij hoge druk uit te voeren op de TUD en aan jou, Xiaoding, heeft het niet gelegen dat die metingen uiteindelijk niet opleverden wat we ervan verwachten. Je was steeds erg ijverig en behulpzaam, hartelijk dank daarvoor.

I want to express my thanks to Andrew Bleloch from the SuperSTEM facility in Daresbury for the possibility to investigate my MnO promoted Co/CNF catalysts. I thank you, Uwe Falke, for our nice collaboration that proved to be very fruitful.

Zo langzamerhand is het tijd om weer wat dichter naar huis te gaan. Ferry, we zijn niet alleen op dezelfde dag met de studie scheikunde begonnen, maar ook nog eens tegelijkertijd als AIO bij anorganisch begonnen. Dit gaf toch wel een speciale band. Ik kijk met genoegen terug op de samenwerking met jou rond onze gezamenlijke ontdekking dat kooldraden meer op rietjes lijken dan altijd was gedacht. Leon, ook jij bedankt voor de goede samenwerking, veel geluk daar in het verre oosten. Fernando, (nu je plannen maakt je toch in dit houtland te vestigen moet het in het Nederlands kunnen, dunkt me), door ons vergelijkbare project hebben we veel met elkaar te maken gehad, wat me ook meer inzicht in de Spaanse cultuur heeft geboden. Hartelijk dank voor wat je hebt betekend, hierbij zie ik onze trip naar het prachtig verzorgde congres in Dalian als hoogtepunt.

Bij de EXAFS metingen die ik al even noemde heb ik behalve van Harry ook hulp van Ad, Didier, Fernando, Kees en Yihua gehad. Allemaal hartelijk bedankt voor jullie inzet tijdens deze soms saaie en slopende dagen. Echter, ook nu was driemaal scheepsrecht.

Tijdens mijn promotieperiode heb ik niet alleen erg genoten van de mooiste AIO-kamer van de vakgroep, maar ook van heel plezierige kamergenoten. Marjolein, jij was een gezellige kletstante, die altijd in was voor het uitzoeken van semi-wetenschappelijke feiten op internet. Terwijl jouw grafische kijk, Stefan, vaak buitengewoon van pas kwam bij het maken van posters en mooie figuren. Erg leuk vond ik het ook dat we het laatste jaar regelmatig (pré)vaderlijke praatjes met elkaar hadden. Kaisa, met jouw komst werd er voortaan koffie gezet op onze kamer (lijkt me trouwens in je huidige baan helemaal

nodig), maar je opvolger Heiner veranderde dat weer terug naar thee. Iedereen erg bedankt voor de afgelopen jaren en alle goeds voor de toekomst gewenst.

Mijn (oud)collega's van de vakgroep dank ik voor de ontspannende koffiepauzes, lunches, borrels etc. Het was altijd weer een goede gelegenheid de gedachten te verzetten om daarna weer aan de slag te gaan. Overigens ben ik, net als een van mijn voorgangers, van mening dat het niveau van de gesprekken zeer ten goede gekeerd is de afgelopen tijd.

Weinig van de resultaten in mijn proefschrift zijn er gekomen zonder assistentie van de technische staf. Dankzij Ad^{M} kwam de fraaie meetopstelling tot stand en kreeg ik bovendien mijn XPS data. Vincent, dank voor de bijdrage aan de HDP en TPR en H_2-sorptie metingen. Verder dank ik Ad met de E (XRF), Cor (TEM), Fred (TGA-MS), Hans (TEM), Marjan (last minute SEM) en Onno (XPS). Ook dank ik Dymph, Monique voor de (secretariële) ondersteuning en Thea voor de snelle afhandeling van declaraties. De medewerkers van de glasblazerij, de AV-dienst en de werkplaats ben ik ook erkentelijk.

De mede-kringleden van de illustere Natuurwetenschappenstudiekring op *Depositum Custodi* dank ik voor het aanscherpen van mijn wetenschappelijke belangstelling (niet gek met zeven aankomende *doctores*) en de bezinning op wetenschap *an sich*. Vrienden van het Oudledengezelschap, de Reünistenkring en de Vriendendagen, bedankt dat jullie er steeds weer voor zorgen dat mijn blik zich niet verengt.

Papa en mama, jullie wil ik hartelijk bedanken voor jullie voortdurende steun en liefde. Het moge dan zijn dan jullie geen verstand hebben van Fischer-Tropsch (maar wie heeft dat nu eigenlijk wel?), het verhinderde jullie niet steeds belangstellend naar mijn vorderingen te informeren. Leuk ook dat u, papa, mijn paranimf wil zijn. Broers, zussen zwager, het is me altijd weer een groot genoegen bij jullie te zijn en straks heb ik weer tijd… Ook de Polletjes dank ik voor hun belangstelling naar 'nieuws van de Shell'.

Martineke, mijn lieve vrouw, ik ben erg dankbaar dat we bij elkaar horen. Je hebt me steeds gesteund de afgelopen vier jaar en zult dat de 23ste weer doen. Erg leuk ook dat je de opmaak voor je rekening hebt genomen. En jij, kleine Hannah, ik hoop dat je, als je tot je verstand gekomen zult zijn, dit boekwerk met plezier zult doornemen.

Maar wat is een dankwoord, zonder de dank aan Hem, die in leven riep en nog regeert, die mijn leven steeds leidt en mij van moment tot moment hielp?

Nun danket alle Gott
Mit Herzen, Mund und Händen.

LEENDERT

CURRICULUM VITAE

Gerrit Leendert Bezemer werd op 4 mei 1979 geboren in Bleskensgraaf en Hofwegen. In 1996 behaalde hij het HAVO diploma aan de Gomarus Scholengemeenschap in Gorinchem. Na het behalen van het VWO diploma aan het Rotterdamse Wartburg college in 1997, ging hij Scheikunde studeren aan de Universiteit Utrecht. December 2001 studeerde hij met genoegen af bij de sectie Anorganische Chemie en Katalyse (dr. A.A. Battiston en prof. dr. ir. D.C. Koningsberger). Vanaf begin 2002 was hij werkzaam als Assistent in Opleiding (AIO) in dezelfde vakgroep, maar nu onder begeleiding van prof. dr. ir. K.P. de Jong en dr. A.J. van Dillen. Het onderzoek werd gefinancierd door Shell Global Solutions en een deel van de verkregen onderzoeksresultaten staan beschreven in dit proefschrift. Vanaf begin 2006 zal hij werkzaam zijn als onderzoeker bij Shell Global Solutions in Amsterdam.